Cell

Genomic surveillance as a scalable framework for precision phage therapy against antibiotic-resistant pathogens

Graphical abstract

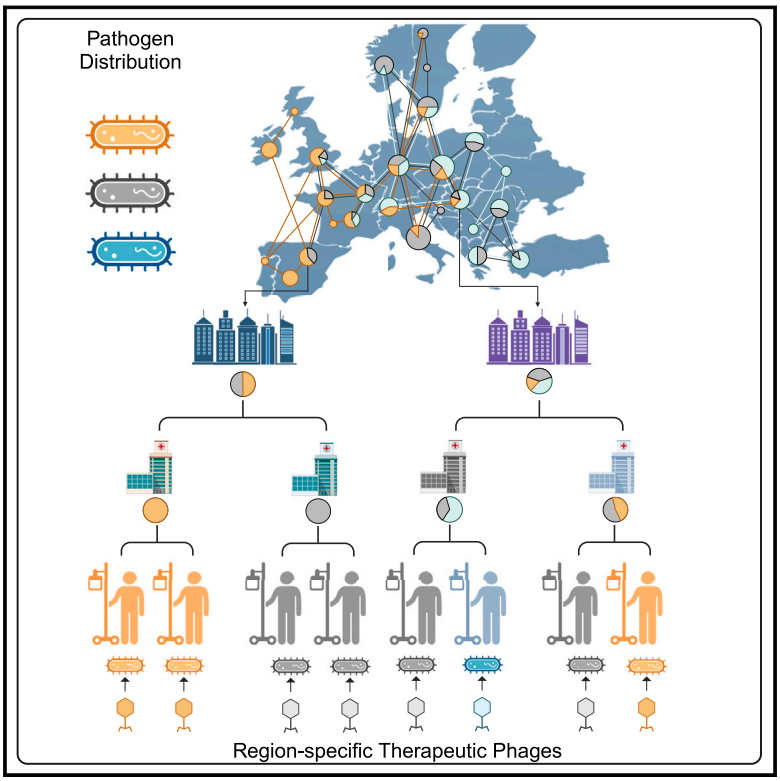

Authors

Mihály Koncz, Tamás Stirling, Hiba Hadj Mehdi, Orsolya Méhi, ..., Balázs Papp, Bálint Kintses

Correspondence

papp.balazs@brc.hu (B.P.), kintses.balint@brc.hu (B.K.)

In brief

By mapping the genetic diversity and geographic distribution of carbapenem-resistant *Acinetobacter baumannii*, bacteriophage cocktails were developed and designed to treat the maximum number of patients within a specific geographic region.

Highlights

- A few CRAB types dominate infections in individual world regions
- Phylogeography reveals stable strain composition for countries over 6 years
- Spatiotemporal distribution informs the development of region-specific phage collections
- Phage cocktails are effective against the most prevalent strain types in Eastern Europe

Koncz et al., 2024, Cell *187*, 1–18
October 17, 2024
https://doi.org/10.1016/j.cell.2024.09.009

CellPress

Please cite this article in press as: Koncz et al., Genomic surveillance as a scalable framework for precision phage therapy against antibiotic-resistant pathogens, Cell (2024), https://doi.org/10.1016/j.cell.2024.09.009

Cell

CellPress
OPEN ACCESS

Article

Genomic surveillance as a scalable framework for precision phage therapy against antibiotic-resistant pathogens

Mihály Koncz,[1,2,30] Tamás Stirling,[1,2,3,30] Hiba Hadj Mehdi,[1,2,3,30] Orsolya Méhi,[1,30] Bálint Eszenyi,[1] András Asbóth,[1,2,4] Gábor Apjok,[1] Ákos Tóth,[5] László Orosz,[6] Bálint Márk Vásárhelyi,[1] Eszter Ari,[1,4,7] Lejla Daruka,[1] Tamás Ferenc Polgár,[8,9] György Schneider,[10] Sif Aldin Zalokh,[1] Mónika Számel,[1] Gergely Fekete,[1,7] Balázs Bohár,[1,11] Karolina Nagy Varga,[1] Ádám Visnyovszki,[12,13] Edit Székely,[14,15] Monica-Sorina Licker,[16,17] Oana Izmendi,[16,17,18]

(Author list continued on next page)

[1]Synthetic and Systems Biology Unit, Institute of Biochemistry, National Laboratory of Biotechnology, HUN-REN Biological Research Centre, Temesvári Krt. 62, 6726 Szeged, Hungary
[2]HCEMM-BRC Translational Microbiology Research Group, Budapesti út 9, 6728 Szeged, Hungary
[3]Doctoral School of Biology, University of Szeged, Dugonics tér 13, 6720 Szeged, Hungary
[4]Department of Genetics, ELTE Eötvös Loránd University, Pázmány Péter stny. 1/C, 1117 Budapest, Hungary
[5]National Center for Public Health and Pharmacy, Albert Flórián út 2–6, 1097 Budapest, Hungary
[6]Department of Medical Microbiology, University of Szeged, Szent-Györgyi Albert Medical School, Dom tér 10, 6720 Szeged, Hungary
[7]HCEMM-BRC Metabolic Systems Biology Group, Temesvári Krt. 62, 6726 Szeged, Hungary
[8]Institute of Biophysics, HUN-REN Biological Research Centre, Temesvári Krt. 62, 6726 Szeged, Hungary
[9]Theoretical Medicine Doctoral School, University of Szeged, Dugonics tér 13, 6720 Szeged, Hungary
[10]Department of Medical Microbiology and Immunology, Medical School, University of Pécs, Szigeti út 12, 7624 Pécs, Hungary
[11]Faculty of Medicine, Department of Metabolism, Digestion and Reproduction, Imperial College London, 10th Floor Commonwealth Building Hammersmith Campus, Du Cane Road, London W12 0NN, UK
[12]South-Pest Central Hospital National Institute of Hematology and Infectious Diseases, Nagyvárad tér 1, 1097 Budapest, Hungary
[13]Doctoral School of Interdisciplinary Medical Sciences, University of Szeged, Dugonics tér 13, 6720 Szeged, Hungary
[14]George Emil Palade University of Medicine, Pharmacy, Science and Technology of Targu Mures, Str. Gheorghe Marinescu 38, 540142 Targu Mures, Romania
[15]County Emergency Clinical Hospital of Targu Mures, Str. Dr. Gh. Marinescu 50, 540136 Targu Mures, Romania
[16]Microbiology Department, Multidisciplinary Research Center on Antimicrobial Resistance, "Victor Babes" University of Medicine and Pharmacy, Str. Eftimie Murgu 2, 300041 Timisoara, Romania
[17]Microbiology Laboratory, "Pius Branzeu" Emergency Clinical County Hospital, Str. Liviu Rebreanu 156, 300723 Timisoara, Romania
[18]Doctoral School, "Victor Babes" University of Medicine and Pharmacy, Str. Eftimie Murgu 2, 300041 Timisoara, Romania

(Affiliations continued on next page)

SUMMARY

Phage therapy is gaining increasing interest in the fight against critically antibiotic-resistant nosocomial pathogens. However, the narrow host range of bacteriophages hampers the development of broadly effective phage therapeutics and demands precision approaches. Here, we combine large-scale phylogeographic analysis with high-throughput phage typing to guide the development of precision phage cocktails targeting carbapenem-resistant *Acinetobacter baumannii*, a top-priority pathogen. Our analysis reveals that a few strain types dominate infections in each world region, with their geographical distribution remaining stable within 6 years. As we demonstrate in Eastern Europe, this spatiotemporal distribution enables preemptive preparation of region-specific phage collections that target most local infections. Finally, we showcase the efficacy of phage cocktails against prevalent strain types using *in vitro* and animal infection models. Ultimately, genomic surveillance identifies patients benefiting from the same phages across geographical scales, thus providing a scalable framework for precision phage therapy.

INTRODUCTION

The uncontrollable rise of antibiotic resistance will become the leading cause of human mortality by 2050 unless proactive measures are implemented.[1] Of particular concern is the widespread presence of antibiotic-resistant bacteria in healthcare settings.[2] Due to the limited number of effective antibiotic options, these infections often produce severe clinical outcomes.[3] Moreover, as

CellPress
OPEN ACCESS

Cell
Article

Carmen Costache,[19] Ina Gajic,[20] Bojana Lukovic,[21] Szabolcs Molnár,[22] Uzonka Orsolya Szőcs-Gazdi,[23] Csilla Bozai,[24] Marina Indreas,[25] Katalin Kristóf,[26] Charles Van der Henst,[27,28] Anke Breine,[27,28] Csaba Pál,[1] Balázs Papp,[1,7,29,*] and Bálint Kintses[1,2,31,*]

[19]Department of Microbiology, University of Medicine and Pharmacy "Iuliu Hatieganu" Cluj-Napoca, Str. Victor Babes 8, 400347 Cluj-Napoca, Romania
[20]Institute of Microbiology and Immunology, Faculty of Medicine, University of Belgrade, Dr Subotica 8, 11000 Belgrade, Serbia
[21]Academy of Applied Studies Belgrade, College of Health Sciences, Bulevar Zorana Djindjica 152a, Belgrade, Serbia
[22]Emergency County Hospital Miercurea-Ciuc, Str. Doctor Dénes László 2, 530173 Miercurea Ciuc, Romania
[23]County Hospital Odorheiu-Secuiesc, Str. Bethlen Gábor nr. 72, 535600 Odorheiu-Secuiesc, Romania
[24]County Emergency Hospital Satu Mare, Str. Ravensburg 1-3, 440192 Satu Mare, Romania
[25]Bacau County Emergency Hospital, Str. Haret Spiru 2-4, 600114 Bacau, Romania
[26]Institute of Laboratory Medicine, Semmelweis University, Üllői út 78/b, 1083 Budapest, Hungary
[27]Microbial Resistance and Drug Discovery, VIB-VUB Center for Structural Biology, VIB, Flanders Institute for Biotechnology, Pleinlaan 2, Building E-3, 1050 Brussels, Belgium
[28]Structural Biology Brussels, Vrije Universiteit Brussel (VUB), Pleinlaan 2, Elsene, 1050 Brussels, Belgium
[29]National Laboratory for Health Security, HUN-REN Biological Research Centre, Temesvári Krt. 62, 6726 Szeged, Hungary
[30]These authors contributed equally
[31]Lead contact
*Correspondence: papp.balazs@brc.hu (B.P.), kintses.balint@brc.hu (B.K.)
https://doi.org/10.1016/j.cell.2024.09.009

the conventional antibiotic development pipeline is drained,[4,5] finding alternative therapeutic approaches is crucial, with phage therapy emerging as a prominent candidate.[6]

Although numerous compassionate use cases have showcased phages successfully tackling infections resistant to conventional antibiotics,[7–12] the translation of this potential into positive patient outcomes on a broader scale has been progressing slowly.[13,14] This limitation stems from the narrow host range of bacteriophages, hindering their broad therapeutic application.[15] Specifically, many resistant bacterial species consist of hundreds of strain types, each characterized by distinct cell surface structures and defense mechanisms that restrict the host range of bacteriophages to a subset of bacterial strain types.[16,17] In response, two primary approaches have emerged.[14] The first combines multiple phages into a fixed composition for broader bacterial coverage, followed by the initiation of clinical trials for marketing authorisation.[18,19] While several such attempts are currently in progress, as of now, no registered medicinal phage products have reached the market.[20] The second strategy is personalized treatment, where the patient's bacterial sample is screened to identify effective phages from collections of bacteriophages.[14,15] While this approach has demonstrated promising effectiveness,[21] it comes with its own set of challenges, such as limited throughput due to time-consuming phage production and regulatory hurdles post-diagnosis of the infection.[22] Overall, irrespective of the chosen strategy, moving forward will largely depend on systematic procedures that identify patients requiring the same bacteriophages on a large scale.[23]

Genomic surveillance has emerged as an efficient tool for tracking pathogens at an unprecedented scale.[24] Advances in sequencing technologies have revealed the genomes of hundreds of thousands of bacterial isolates,[25] offering valuable insights into the distribution and transmission patterns of top-priority antibiotic-resistant pathogens flagged by the World Health Organization (WHO).[26] In fact, genomic surveillance has established that such infections can originate within healthcare facilities.[27–30] This mode of transmission raises the prospect of forecasting the likely causative agents of forthcoming infections and preemptively tailoring phages to combat them. This proactive approach could dramatically reduce the time required for administering personalized therapy. Moreover, understanding the geographic distribution of top-priority pathogens is crucial for study recruitment to achieve clinical validation and cost-effectiveness of phage therapy. Despite this immense potential, genomic surveillance remains largely untapped in phage therapy.[23]

We propose that genomic surveillance can lay the groundwork for scalable precision phage therapy (Figure 1). In support of this, we conducted a systematic analysis with >15,000 *Acinetobacter baumannii* (*A. baumannii*) genome sequences from around the world. We focused on this particular bacterial species as carbapenem-resistant *A. baumannii* (CRAB) is identified by the WHO as a critical priority pathogen urgently requiring innovative therapies,[26,31] with an alarming mortality rate of 25%–60% and over 100,000 deaths globally in 2019.[3,32,33] Additionally, CRAB has an especially narrow phage host range, potentially requiring a phage library of over 300 phages to effectively cover most clinical isolates.[34] To investigate this issue, we used large-scale phylogeographic analysis combined with experimental phage discovery and high-throughput phage typing to demonstrate that 90% of infections can be attributed to a limited number of strain types in each world region, addressable by a small set of bacteriophages. Furthermore, we found that prevailing CRAB strains can be predicted within a 6-year time frame for individual countries, and countries sharing identical CRAB strain types can be rapidly identified. These findings enable proactive measures, such as developing region-specific phage collections and formulating phage cocktails to target specific strain types in a highly precise manner.

RESULTS

A systematic view on the distribution of CRAB types

To assess the geographical distribution of CRAB strains at regional and continental scales, we retrieved all publicly available *A. baumannii* genomes from the NCBI database,

Please cite this article in press as: Koncz et al., Genomic surveillance as a scalable framework for precision phage therapy against antibiotic-resistant pathogens, Cell (2024), https://doi.org/10.1016/j.cell.2024.09.009

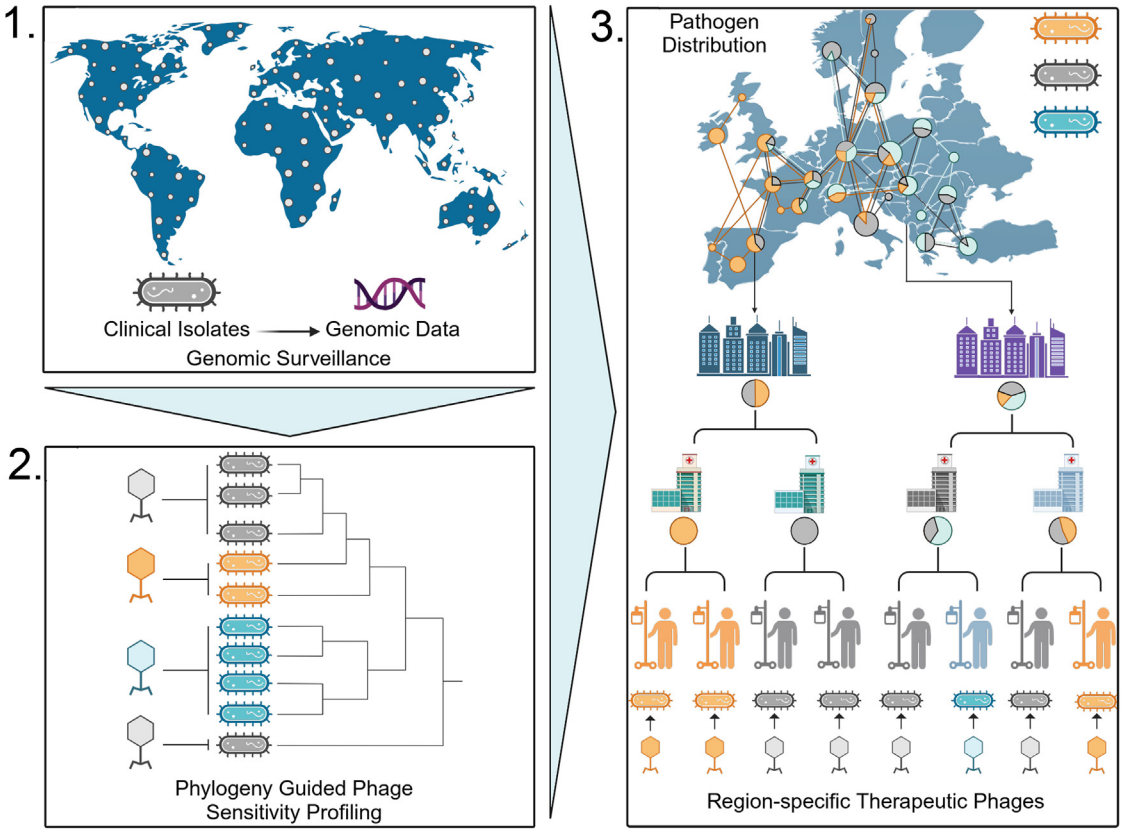

Figure 1. A pathogen genomic surveillance framework to inform precision phage therapy

(1) Collecting target pathogen isolates from surveillance programs and laboratory networks and using the information on the genome sequence, location, and time of isolation; (2) identifying dominant strain types requiring distinct bacteriophages based on pathogen genomics and phage sensitivity profiling; and (3) utilizing the spatiotemporal distribution of the strain types to design region-specific phage therapy interventions, maximizing the number of patients for therapy across geographical scales.

originating from 85 countries across five continents (15,410 genomes as of 09/2022; see Table S1). Given the limited representation of genomes from Eastern and Southern Europe, regions with high CRAB infection rates,[35] we additionally sequenced 419 *A. baumannii* clinical isolates collected between 2011 and 2022 from 44 healthcare facilities located in 34 cities across five neighboring countries, called focal countries (Hungary [*n* = 253], Romania [*n* = 120], Serbia [*n* = 28], Montenegro [*n* = 9], and Bosnia and Herzegovina [*n* = 9]; Table S1). After filtering the sequences for high quality, human origin, and specified information regarding the place and time of isolation, the initial 15,829 genomes narrowed down to a set of 11,129 genomes (Figure S1A; STAR Methods). Subsequently, we screened them for genetic determinants characteristic of CRAB, including resistance genes to carbapenems and other commonly used antibiotic classes (STAR Methods). Our analysis revealed that 80.1% of the 11,129 genomes can be considered CRAB (Figure 2A), with a noticeable increase in relative proportion observed between 2000 and 2022 (Figure 2B).

Next, we grouped the CRAB genomes using a dual genetic typing approach, combining multilocus sequence typing (MLST) and cell surface capsular polysaccharide (CPS) typing.[36,37] MLST typing clusters evolutionary-related genomes into sequence types (STs) based on sequence similarity of multiple housekeeping genes.[38] By contrast, CPS typing identifies specific genomic determinants responsible for synthesizing structurally different CPSs, which can serve as receptors for phages with different host specificities.[39] It is important to highlight that CPS evolves independently from ST due to frequent horizontal gene transfers.[16] To address sampling differences inherent in public databases, we implemented a stratified downsampling of the genomes based on geographical location and time (STAR Methods).[40,41] Then, we conducted additional subsampling, ensuring that the number of analyzed genomes reflects the population size of each country (Table S1). With this final dataset, we analyzed the distribution of currently (2016–2022) circulating CRAB types as defined by the combined MLST-CPS typing of the 1,334 retained genomes from 53 countries across nine major world regions (West, East, and South Europe; North and South America; and West, East, South, and South East Asia), where our sampling was sufficient to capture the majority of CRAB diversity (Figure S1B; STAR Methods).

In the nine world regions studied, contemporary CRAB diversity is characterized by a small number of prevalent MLST-CPS types and a large number of rare ones (Figure 2C). Typically, 3–5 MLST-CPS types collectively account for 50% of isolates in a

Please cite this article in press as: Koncz et al., Genomic surveillance as a scalable framework for precision phage therapy against antibiotic-resistant pathogens, Cell (2024), https://doi.org/10.1016/j.cell.2024.09.009

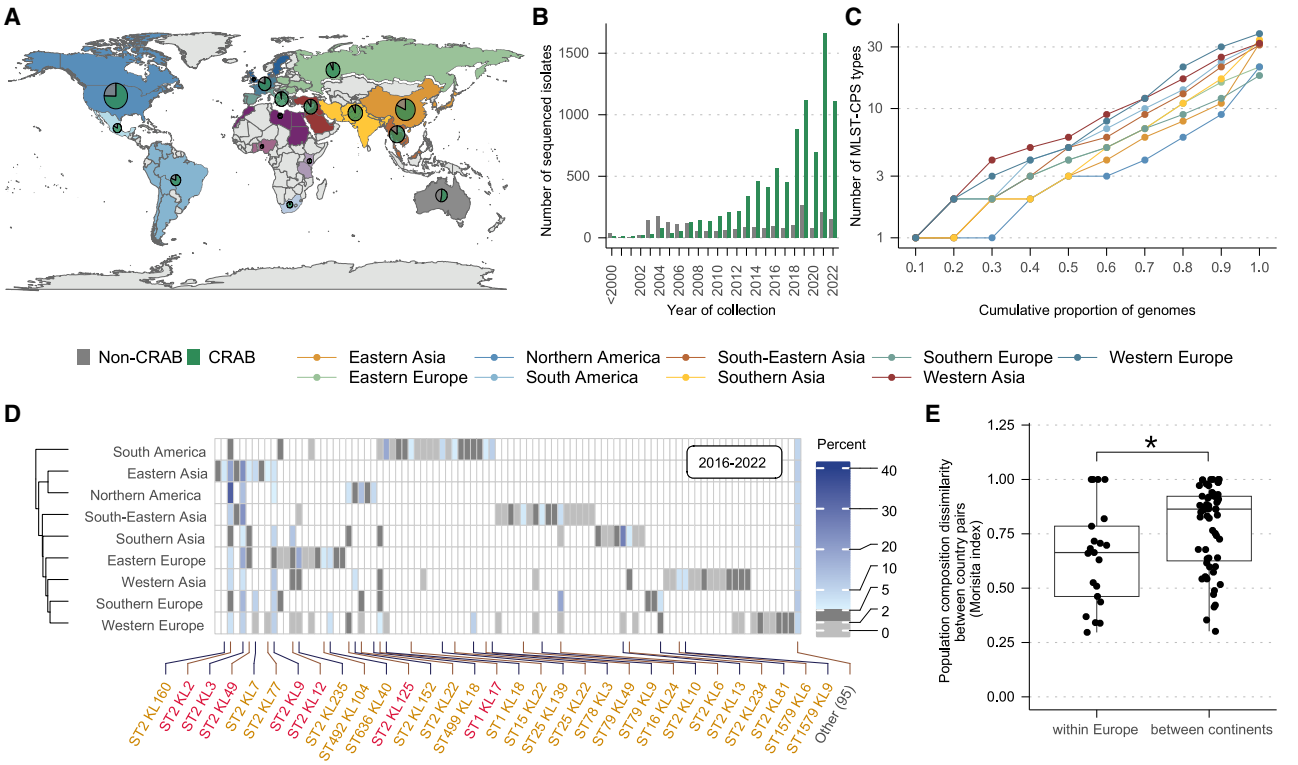

Figure 2. The geographic distribution of CRAB types

(A) Geographical distribution of 11,129 human-derived *A. baumannii* isolates with whole genome sequences. The size of each pie chart indicates the number of sequenced isolates, with green and gray denoting CRAB and non-CRAB isolates, respectively (Table S1; STAR Methods).

(B) Number of sequenced *A. baumannii* isolates over time.

(C) Cumulative proportion of sequenced isolates (x-axis) assigned to the most prevalent MLST-CPS types (y-axis) in the nine world regions, based on 1,334 contemporary (2016–2022) CRAB isolates after accounting for sampling bias (Figure S1B; STAR Methods). Each dot represents the number of most prevalent MLST-CPS types (y axis), cumulatively accounting for a certain proportion of isolates collected in a given world region (x axis; Table S1).

(D) Relative prevalences of CRAB MLST-CPS types across the nine world regions. The least prevalent 10% of strain types are pooled in each region (other). Colors indicate the relative prevalence ranges in percentage. MLST-CPS types classified as prevalent and global are labeled orange and red, respectively (STAR Methods).

(E) CRAB type composition is more similar between pairs of countries in Europe compared with country pairs across continents (two-sided two-sample Wilcoxon rank-sum test, $n_{within} = 21$, $n_{between} = 63$, $p = 0.018$; Table S1; STAR Methods). Boxes depict the interquartile range (IQR), the solid black line shows the median, and the whiskers extend to 1.5 IQR.

See also Figure S1.

given world region, while ~17 MLST-CPS types make up 90% (Figure 2C). Altogether, we identified 31 "prevalent" MLST-CPS types, with a relative prevalence above 5% in at least one world region (Figure 2D). Nevertheless, there is substantial variation in CRAB type composition across world regions. Specifically, among these 31 prevalent types, only 7 exhibit a relative prevalence exceeding 2% in three or more world regions, spanning at least two continents (Figures 2D and S1C), indicating global dispersion. In contrast to the large cumulative fraction of the CRAB population covered by the prevalent types, the remaining ~10% of isolates from the nine world regions can be attributed to 95 MLST-CPS types (Figure 2D).

Then, we investigated whether countries in close geographical proximity and unrestricted cross-country movements share a more similar composition of CRAB populations than countries on different continents with presumably lower travel volumes. Focusing on seven closely situated European and seven geographically distant non-European countries with sufficient genomic sampling (Figures S1D and S1E; STAR Methods), we found that CRAB populations between pairs of European countries tend to exhibit higher similarity compared with pairs of countries on different continents (Figure 2E). The high similarity between European countries is primarily attributed to the presence of 4 prevalent types shared by at least three of the seven European countries, collectively representing ~39% of isolates. Additionally, the set of 25 country-specific MLST-CPS types constitutes only ~22% of isolates in these countries (Figure S1F; Table S1).

To summarize, CRAB diversity in each world region features a few dominant types causing most infections alongside a long tail of rare types. While regional variations exist, geographically close and interconnected countries tend to share more similar CRAB compositions. Finally, we note that leveraging CRAB genomes from 53 countries across nine world regions (Table S1), our study explores a substantial portion of the global landscape.

Please cite this article in press as: Koncz et al., Genomic surveillance as a scalable framework for precision phage therapy against antibiotic-resistant pathogens, Cell (2024), https://doi.org/10.1016/j.cell.2024.09.009

CellPress
OPEN ACCESS

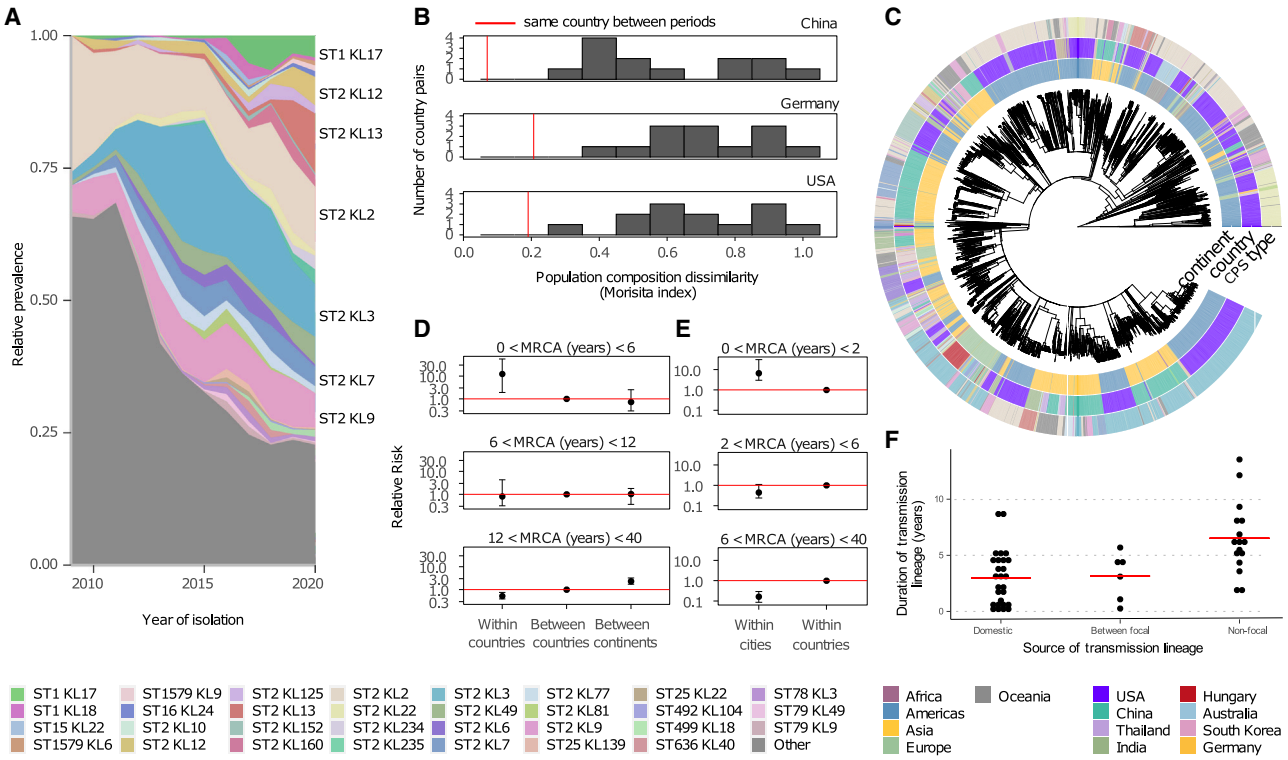

Figure 3. Temporal stability of CRAB populations

(A) The relative prevalence of MLST-CPS types between 2009 and 2020 (2-year moving average) based on 2,304 CRAB isolates (STAR Methods). Plot shows the 31 currently prevalent types (distinct colors) and the rest as pooled (gray).

(B) The MLST-CPS type composition of a specific country between 2009 and 2015 is more similar to its current (2016–2022) strain composition than that of other countries. Red lines show population composition dissimilarity (Morisita index) comparisons of the same country between the two time periods (n = 13).

(C) Phylogenetic tree of 7,720 ST2 *A. baumannii* isolates worldwide. Heatmaps indicate MLST-CPS type, country, and continent of origin. Only countries with at least 100 isolates are color-coded.

(D) Relative risk that pairs of genetically related ST2 isolates were collected in a certain geographic location (same country, different country but same continent) compared with the reference category (different country and different continent). Each facet describes pairs of samples within a certain genetic distance range (time to the most recent common ancestor [MRCA], years).

(E) Relative risks calculated by comparing within-city pairs with within-country pairs for the 5 European focal countries as in (D). In both (D) and (E), error bars represent 90% confidence intervals (Table S1; STAR Methods).

(F) Duration of ST2 transmission lineages within the 5 focal European countries. Transmission lineages are classified based on their geographical source, i.e., outside the 5 focal countries (non-focal), another focal country (between focal), and another city within the same country (domestic), respectively. Red line depicts the average duration for each category.

See also Figures S2 and S3.

However, achieving a fully comprehensive understanding requires expanding the data collection to include additional countries and improving coverage where it is limited, including in Europe (Table S1).

Existing CRAB variants dominate infections within countries over 6 years

We next investigated the temporal dynamics of CRAB populations. Initially, we analyzed temporal changes in the global frequencies of the 31 currently prevalent (2016–2022) MLST-CPS types (Figure 3A). Statistical modeling identified significant expansion in 7 of the 31 prevalent strains over the past 12 years on at least one continent (Figure S2A; Table S1; STAR Methods). The largest expansion was exhibited by the ST2-KL3 type (Figure 3A), which gradually increased from 2009 onward to become one of the top three most prevalent CRAB types in six out of the nine studied world regions (Figure S1C). This expansion across multiple geographical regions implies a potential fitness advantage of ST2-KL3 over other types.

Despite the temporal expansions of specific prevalent MLST-CPS types, ~68% of these types were already present in the preceding period (2009–2015), with a prevalence exceeding 2% in most world regions where they are currently prevalent (i.e., >5%; Table S1). This observation suggests local stability in CRAB population compositions over this time frame. To further assess temporal stability, we examined MLST-CPS type composition changes in three countries (China, Germany, and the US) with sufficient sequenced isolates from the two distinct periods (2009–2015 and 2016–2022). In each country, we observed that the previous MLST-CPS type composition was more similar to its contemporary counterpart than to the contemporary composition of other countries worldwide, confirming the

Please cite this article in press as: Koncz et al., Genomic surveillance as a scalable framework for precision phage therapy against antibiotic-resistant pathogens, Cell (2024), https://doi.org/10.1016/j.cell.2024.09.009

temporal stability of CRAB populations in these countries (Figure 3B).

To delve deeper into the spatiotemporal dynamics of CRAB types, we conducted a phylogeographical analysis of the dominant ST2 clade, providing insights into this pathogen's transmission dynamics at an unprecedented scale. Specifically, we built a time-calibrated phylogenetic tree using the core genomes of 7,720 ST2 global isolates, covering ~70% of the available 11,129 *A. baumannii* genomes (Figure 3C; STAR Methods). A strong temporal signal was evident in the phylogenetic tree, indicating that it accurately captures chronological information (Figure S2B). This is further supported by the estimated root date (1973), aligning with epidemiological data regarding the emergence of ST2.[42,43]

We then used the geographically and temporally stratified subsample of isolates from the time-calibrated phylogenetic tree to assess the time frame needed for CRAB lineages to spread across different geographical scales using an established method[44] (STAR Methods). We observed strong phylogeographic clustering, with genetically closely related isolates primarily circulating within the same country over a short period. Specifically, two contemporary CRAB isolates that diverged within the past 6 years were ~12 times more likely to originate from the same country rather than different countries (Figure 3D; Table S1), in agreement with the above analysis on the stability of the strain compositions of specific countries (Figure 3B). This local spatial clustering was also evident in Europe, a region of multiple small countries (Figure S2C). Nevertheless, over a longer period (6–12 years), the country-level spatial clustering disappears, indicating substantial transmission of isolates across countries (Figures 3D and S2C). As further support, we analyzed the spatial dispersal of CRAB isolates based on continuous geographic coordinates (instead of countries) using phylogenetic autocorrelation of the locations (STAR Methods). We found strong geographic clustering among recently diverged isolates that gradually decays as isolates diverge genetically, suggesting extensive global dispersal by ~20 years (Figure S2D; Table S1).

The dominance of local transmissions over a short period of time is also evident on a smaller geographic scale, such as cities. This analysis focused on the five neighboring Eastern and Southern European countries covered by our CRAB collection (Hungary, Romania, Serbia, Bosnia and Herzegovina, and Montenegro, referred to as focal countries) where fine-scale geographic data is available (STAR Methods). When considering two contemporary CRAB isolates that diverged in the past 2 years, there was a ~6-fold higher likelihood that they originated from the same city rather than different cities within the country (Figure 3E; Table S1). This pattern indicates that locally circulating strains in specific cities are poised to account for the majority of the CRAB infections within a 2-year time frame.

To gain a more granular understanding of CRAB transmission dynamics, we reconstructed transmission routes in these five focal countries. Specifically, we estimated the timing of introductions and traced the transmission events between 36 cities by estimating the likely geographical states of ancestral nodes on the time-calibrated tree (Figure S3A; STAR Methods).[45] The 365 ST2 CRAB isolates from the five focal countries belonged to 16 major transmission lineages circulating within this region for an average of at least 6.5 years (Figure 3F; Table S1). During this period, these major lineages underwent further spread, with a strong bias toward domestic transmission compared with the spread between different focal countries (27 vs. 6 events; Figure 3F). Within cities, domestically acquired transmission lineages persisted for an average of ~3 years (Figure 3F). Due to their central role and higher connectivity, capitals and cities with regional medical centers likely play a major role in epidemic dissemination. Indeed, these cities exhibit a markedly higher ratio of outward to inward transmission events compared with others (Figure S3B; Table S1), highlighting the importance of prioritizing CRAB isolates from capitals and cities hosting regional medical centers when evaluating the risk of future outbreaks spreading within a country.

Overall, our findings indicate the dominance of local transmissions for this nosocomial pathogen. Established CRAB lineages within a country are likely responsible for most infections for at least 6 years. Furthermore, our analysis suggests the possibility of predicting specific CRAB variants causing infections within a city, especially for shorter time frames.

Phylogeny-guided phage hunting and phage sensitivity profiling

Next, we demonstrated the potential of bacterial genomic surveillance in identifying an effective phage collection against the CRAB types responsible for the majority of infections within a specific region. Focusing again on the five focal Eastern and Southern European countries, we selected eleven prevalent MLST-CPS types, covering 90.7% of the 546 samples in this region between 2016 and 2022 (Table S1). Using representative clinical isolates from each of the 11 MLST-CPS types (Table S2), we conducted a phage hunt, isolating 15 phages from raw communal wastewater collected in five Hungarian cities (STAR Methods). All isolated phages exhibited potent lytic activity (>10^6 plaque-forming units [PFU]/mL) against at least one target clinical isolate. Next, we quantified the efficacy of the isolated phages on a larger collection of 92 CRAB clinical isolates from the 11 MLST-CPS types (Figure 4A). Each MLST-CPS type exhibited a unique phage susceptibility profile. Remarkably, phages effectively targeted over 95% of isolates within nine MLST-CPS types. For example, phage Highwayman potently targeted 28 out of the 29 tested isolates belonging to the most prevalent type (ST2-KL3) in Eastern Europe.

To further evaluate the broader relevance of the discovered phages, we tested them against an additional set of 107 *A. baumannii* clinical isolates using a simplified binary phage susceptibility profiling method (Table S2; STAR Methods). These isolates included further clinical isolates from Eastern and Southern Europe, as well as distant locations like Western Europe and North America, representing an even broader genetic diversity for the eleven MLST-CPS types and 15 additional ST backgrounds (Table S2). A systematic comparison of these binary phage susceptibilities across the entire dataset (i.e., 92 + 107 *A. baumannii* isolates) revealed that variations in phage susceptibility profiles are mainly determined by CPS type, with altered ST background and large geographic distance also playing a significant, albeit weaker role (Figure 4B). The impact of

Please cite this article in press as: Koncz et al., Genomic surveillance as a scalable framework for precision phage therapy against antibiotic-resistant pathogens, Cell (2024), https://doi.org/10.1016/j.cell.2024.09.009

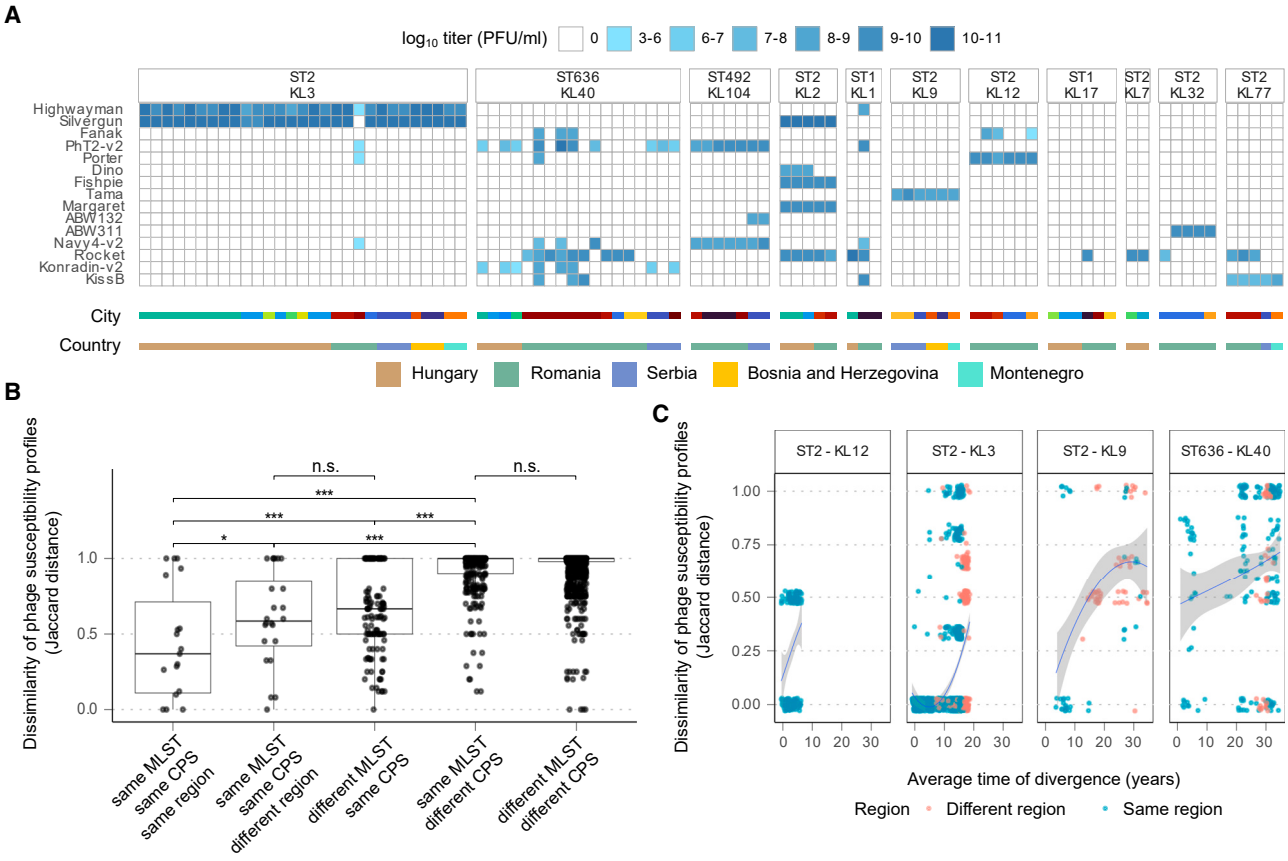

Figure 4. Phylogeny-guided phage hunting and phage sensitivity profiling

(A) Phage sensitivity profiles of 92 CRAB isolates (columns) representing the most abundant 11 MLST-CPS types in the studied Eastern and Southern European countries. MLST-CPS types are presented in descending order of their prevalence from left to right. Blue color intensity indicates the average $\log_{10}$ phage titer (PFU/mL) of three replicates for each of the 15 isolated phages. CRAB isolate origin (country and city) is color-coded at the bottom of each column (Table S2).

(B) Pairwise comparisons of binary phage sensitivity profiles of 199 *A. baumannii* isolates classified based on MLST, CPS, and geographical locations. Jaccard distances of 0 and 1 indicate identical and 100% dissimilar profiles, respectively. Each dot represents the average Jaccard distance of all pairwise comparisons between two isolate categories as specified by MLST, CPS, and geographical region categories. Number of isolate categories/pairs from left to right: 23, 28, 150, 340, and 1,462. Groups of categories (boxes) were compared using one-sided permutation tests (n.s., not significant, $^{*}p < 0.05$, and $^{***}p < 0.001$). Boxes depict the interquartile range (IQR), the solid black line shows the median, and the whiskers extend to 1.5 IQR.

(C) Pairwise phage sensitivity profile dissimilarities correlate with genetic distances for MLST-CPS types with at least 10 profiled CRAB isolates. Correlations were assessed by Mantel tests (p values from left to right: 0.008, 0.002, 0.018, and 0.009; $n = 153$, 1,431, 91, and 231, respectively). The fitted line is smoothed using a loess method (Table S2).

See also Figure S4.

geographical distance hints that genetic divergence within MLST-CPS types might influence phage susceptibility. Indeed, pairs of isolates that diverged earlier display less similar phage susceptibility profiles (Figure 4C). Further analysis of genome characteristics, including the presence or absence of specific plasmids, prophages, and phage defense mechanisms (Table S2; STAR Methods), revealed that these genomic features partly explain the association between genetic divergence and variations in phage susceptibility within specific MLST-CPS types (Table S2). Notably, for ST636-KL40, variations in phage susceptibility were observed even among genetically very similar isolates (Figure 4C). Analysis of surface properties using infrared spectroscopy revealed a significant correlation between cell surface variation and phage susceptibility profile dissimilarity, suggesting that cell surface variation not captured by CPS prediction can also influence phage susceptibility (Figures S4A–S4C; STAR Methods). While genetic divergence is generally associated with altered phage susceptibility, some phages retain efficacy across genetically diverse isolates of the same MLST-CPS type. For example, Silvergun is effective against all 23 tested ST2-KL2 isolates, despite their 30+ year genetic divergence (Figure S4D). This resilience to genetic divergence makes these phages promising candidates for therapeutic applications.

In summary, we have built a potent phage library effective against most CRAB clinical isolates in the focal European region. While bacterial susceptibility to phages is primarily dictated by CPS type, additional genetic variations acquired during the pathogen's geographic spread also play a role. This underscores the importance of tailoring phage collections to match the local genetic diversity of the pathogen.

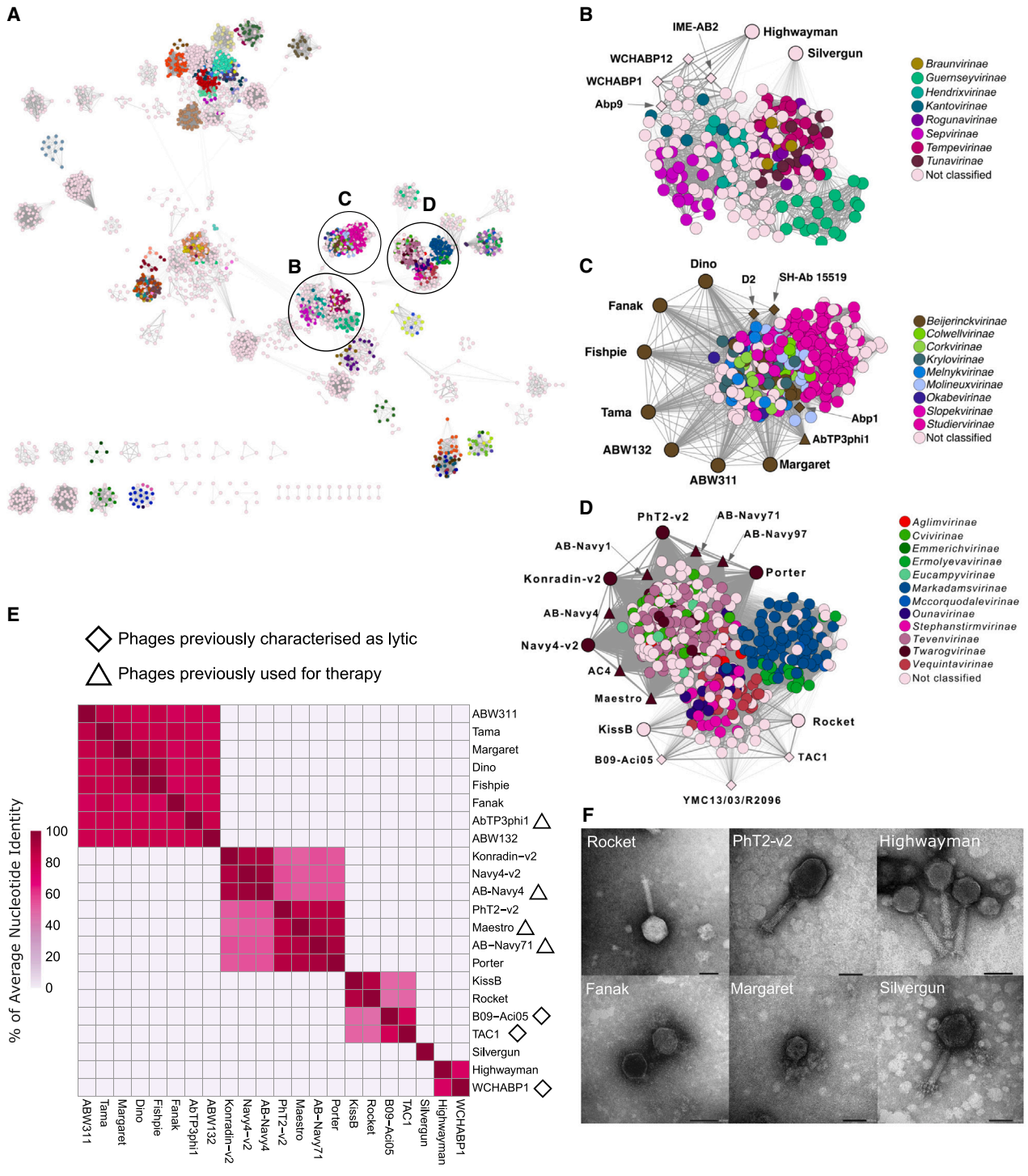

Figure 5. Sequence-based relationship of the 15 discovered phages and known phage species

(A) Protein orthogroup-based relationship network of 3,562 *Caudoviricetes* phages representing all species in the International Committee on Taxonomy of Viruses (ICTV) taxonomy, plus the 15 discovered phages generated using vContact2 (STAR Methods; Table S2). Node color codes represent subfamily membership. Edge thickness is proportional to the number of shared orthogroups between two phages. The three circled clusters are enlarged in (B)–(D) (Table S2).

(B–D) Enlarged protein orthogroup-based clusters containing the 15 phages. The closest previously characterized lytic or therapeutic phages are represented as rhombus or triangle, respectively. Nodes are color-coded based on subfamily membership. The nodes of the 15 phages discovered here are enlarged.

(legend continued on next page)

Known therapeutic phages with new targets

Next, we sequenced the genomes of the 15 isolated phages to determine their suitability for clinical use by employing established safety criteria, including a functionally well-annotated genome, an obligate lytic life cycle, and the absence of harmful genes.[46,47] To this end, first, we analyzed their protein sequence-based relationship with 3,562 known species of tailed double-stranded DNA (dsDNA) phages (*Caudoviricetes*).[48,49] This allowed us to characterize their higher-order taxonomy and genetic relatedness to phages that had been utilized for therapeutic purposes or had been previously characterized as lytic (Table S2).

Of the 15 phages we discovered, spanning 5 taxonomic groups, 14 exhibit extensive sequence similarity to previously used therapeutic or well-characterized lytic phages (Figure 5; Table S2). For example, seven phages from the *Autographoviridae* family share 80%–84% DNA sequence identity with the therapeutic phage AbTP3phi1 (Figure 5E). Furthermore, two-two myophage morphotype phages in the *Twarogvirinae* subfamily show 87%–95% DNA sequence identity with two other previously used therapeutic phages, AB-Navy-4 and AB-Navy-71, respectively (Figure 5E). Despite high sequence similarities stemming from conserved core gene sets, critical genetic determinants of host specificity, such as depolymerase-carrying tail proteins—responsible for CPS decomposition—differ from the corresponding components of previously reported phages in almost every case (Figure S5; Table S2). These relatively modest genetic variations compared with previously established lytic and therapeutic phages simplify the comprehensive characterization necessary for clinical application.

In contrast to the above patterns, Silvergun stands out from known phages due to its unique genetic composition, sharing few orthogroups with any other known phages, suggesting it could represent a new bacteriophage family (Figure 5B). Importantly, Silvergun is able to target the two most prevalent globally spreading strains belonging to ST2-KL3 and ST2-KL2 types (Figure 4A), which collectively account for ~46% of the 6,461 CRAB types isolated since 2016 (Figure 3A; STAR Methods). It is possible that the presence of two predicted depolymerase regions in the tail spike and fiber proteins of this phage explains its uniquely relevant host specificity.

None of the 15 isolated phages harbored toxins, antibiotic resistance genes, or temperate markers, which could potentially hinder therapeutic use (Table S2; Data S1). All studied phages with similarity to well-characterized lytic phages were predicted lytic using PhageAI,[50] except for Highwayman, for which lifestyle determination was inconclusive (Table S2; STAR Methods). Therefore, lysogenic behavior was experimentally confirmed to be absent from Highwayman, Silvergun, and PhT2-v2 on their corresponding hosts[51] (Figure S6; STAR Methods). Further details on genomic and morphological analyses of each phage are included in Data S1.

Precision phage cocktail against the ST2-KL3 strain type in Europe

The first clinical case study of *Acinetobacter* phage therapy revealed a key challenge: the emergence of resistance leading to treatment failure.[7,48] Therefore, our goal was to develop a phage cocktail—a commonly used strategy to tackle phage resistance[52]—against the European ST2-KL3 CRAB lineage (Figure 3C). This lineage was chosen due to its widespread prevalence across the continent (Figure 2D) and diverse representation among our isolates (Figure S7A), aiding the development of a widely applicable phage cocktail.

Initially, we focused on Highwayman and Silvergun, which together target 98% of a representative set of 56 ST2-KL3 clinical isolates (Table S2). When we co-incubated *in vitro* these two phages individually or in combination (cocktail HS) with the ST2-KL3 clinical isolates, resistance emerged after 10–12 h, regardless of whether the phages were applied individually or in combination (Figures 6A and S7B). Next, we examined whether Highwayman or Silvergun resistance induces sensitivity to other phages in the collection. All 22 tested Silvergun-resistant lines became collaterally sensitive to at least one of our five other phages (Fanak, PhT2-v2, Porter, Navy4-v2, and Konradin-v2; Table S2). Adding one or two of these five phages to the initial cocktail significantly suppressed target cell growth when measured up to 24 h (Figures 6B and S7B). This finding indicates that emerging collateral sensitivity to the newly added phages prevents the appearance of resistance. Even after 72 h, resistance against the best-performing four-phage cocktail composed of Highwayman, Silvergun, Fanak, and PhT2-v2, termed HSFPh, remained sporadic (Figure 6C; Table S2).

To elucidate the genetic basis of bacterial resistance, we sequenced the genomes of 19 phage-resistant bacterial lines, including those resistant to Highwayman, Silvergun, or their corresponding two-phage (HS), three-phage (HSF; Highwayman, Silvergun, and Fanak), or four-phage (HSFPh) cocktails (Table S2). Cell lines resistant exclusively to Highwayman contained loss-of-function mutations in a specific β-4-glucosyltransferase gene (Figure 6D; Table S2). By contrast, mutants resistant to Silvergun or the two other phages in the cocktail (i.e., Fanak and PhT2-v2) typically contained loss-of-function mutations in the genes involved in the CPS biosynthesis pathway (Figure 6D; Table S2). These patterns suggest that, in contrast to Highwayman, resistance to these three phages requires defective capsule production. This notion is confirmed by the abolished phage adsorptions to the cell surface (Figures 6E and 6F) and altered cell surface properties revealed by the combination of infrared spectroscopy and electron microscopy (Figures 6G and 6H). Overall, as decapsulation is a known phage-resistance mechanism among other MLST-CPS strain types of CRAB,[39,48] these results demonstrate that ST2-KL3 shares this feature with other CRAB types. Notably, however, the sensitivity of the Silvergun-resistant lines to Fanak and PhT2-v2 indicates that

(E) Pairwise average nucleotide identities (ANIs) for the 15 discovered phages and for their closest phage relatives previously used for therapy or characterized as lytic (STAR Methods; Table S2).

(F) Electron microscopic images of two phages from each subnetwork out of the 15 phages. Detailed morphological and genomic analyses of each phage are available in Data S1. Scale bar, 50 nm.

See also Figures S5 and S6.

Please cite this article in press as: Koncz et al., Genomic surveillance as a scalable framework for precision phage therapy against antibiotic-resistant pathogens, Cell (2024), https://doi.org/10.1016/j.cell.2024.09.009

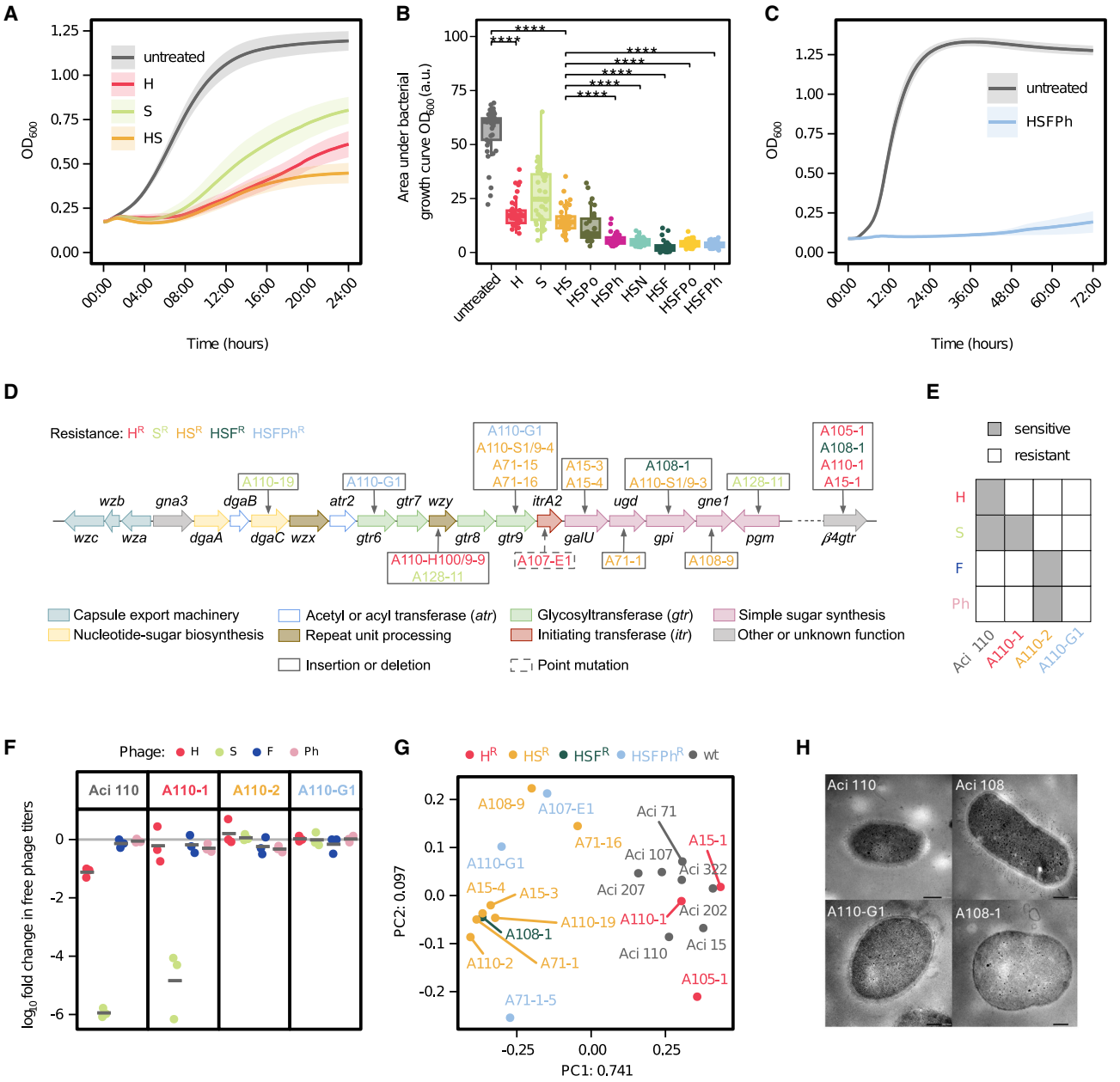

Figure 6. Constructing a precision phage cocktail against the dominant ST2-KL3 type in Europe

(A) Growth curves (OD_{600}) of 41 ST2-KL3 European isolates untreated or treated with Highwayman or Silvergun phages alone or in combination (HS). Plotted values represent the mean ± confidence interval (CI) 95% of 41 isolates, each having 3 biological replicates. Abbreviations: H, Highwayman; S, Silvergun.

(B) Area under the growth curve (arbitrary unit [a.u.]) either in the absence (untreated) or in the presence of different phages alone or in combinations ($n = 41$ distinct isolates, except for the 3-phage combinations, where $n = 27$). Each dot represents the average of three biological replicates of a given isolate. $^{*}p < 0.05$, $^{**}p < 0.01$, $^{***}p < 0.001$, $^{****}p < 0.0001$ from two-sided Kruskal-Wallis tests. Abbreviations: F, Fanak; Po, Porter; N, Navy-v2; Ph, PhT2-v2. Boxes depict the interquartile range (IQR), the solid black line shows the median, and the whiskers extend to 1.5 IQR.

(C) Growth curves (OD_{600}) for 25 ST2-KL3 isolates in the absence (untreated) or in the presence of the phage cocktail HSFPh measured for 72 h. Curves represent the mean ± CI 95% of 25 isolates, each having 3 biological replicates. Data for (A)–(C) are shown in Table S2.

(D) Schematic representation of the KL3 CPS biosynthetic gene cluster with color-coded functional categories and the β-4-glucosyltransferase gene (*β4gtr*, GenBank: WP_001033817.1), which is encoded *trans* to the CPS gene cluster. The vertical arrows point to genes harboring a loss-of-function deletion/insertion or a point mutation in different phage-resistant isolates listed within the frames. Text colors within the frames represent phage-resistance categories as follows: red, light green, yellow, dark green, and light blue corresponding to H, S, HS, HSF, and HSFPh resistance, respectively.

(E) Heatmap representing the phage susceptibility profile of Aci 110 and three phage-resistant derivatives of it: A110-1, A110-2, and A110-G1, which are resistant to H, HS, and HSFPh, respectively.

(legend continued on next page)

the decapsulated cell surface is different upon Silvergun resistance compared with HSFPh cocktail resistance. This notion is supported by the difference in the depleted genes (Figure 6D).

Given the capsule's crucial role in bacterial defense,[39,53,54] we hypothesized that resistance to phage cocktails may affect bacterial virulence and antibiotic susceptibility. To test this, we first measured the *in vivo* virulence of the cocktail-resistant isolates in the *Galleria mellonella* larvae infection model.[55,56] CPS-deficient strains exhibited significantly decreased virulence compared with the corresponding wild-type strain (Figures 7A, 7B, and S8A–S8E), while Highwayman-resistant lines, which have intact CPS, retained virulence (Figures 7C and S8F). Next, we measured the antibiotic susceptibility profiles of 34 phage-resistant lines against a panel of clinically relevant antibiotics (Figure S8H). Remarkably, 71% of the colistin-resistant lines became sensitive to colistin, and the two HSFPh-resistant lines regained sensitivity to meropenem, shifting from resistant to intermediate states (Figure 7D; STAR Methods).

Finally, we tested the efficacy of the phages in *in vivo* infection models (STAR Methods). Treatment with Highwayman or its cocktails HS and HSFPh significantly improved survival rates of *G. mellonella* larvae infected with an ST2-KL3 isolate (Figure 7E). In an intraperitoneal mouse infection model, Highwayman monotherapy and the HSFPh cocktail rescued 80% and 100% of the animals, respectively, whereas all untreated animals died 1-day post-infection (Figures 7F and S9E). While Highwayman monotherapy displayed similar efficacy to the cocktail in both *G. mellonella* and the mouse model, treatment failure due to the emergence of resistance in one mouse (Table S2; STAR Methods) underscores the advantage of the HSFPh cocktail.

In sum, resistance to HSFPh phage cocktail is relatively rare, and even when it does arise, it leads to decreased virulence and enhanced antibiotic sensitivity. Notably, as carbapenem resistance is associated with high mortality in patients infected with *Acinetobacter*,[57,58] meropenem resensitization by phage resistance can be clinically relevant and supports the use of the cocktail in combination with meropenem.[59,60]

Validating the region-specific treatment strategy

As a final objective, we validated the strategy of a geographically targeted treatment regimen. We designed new phage cocktails against each of the eight additional MLST-CPS types that our phages could comprehensively target (i.e., >95% of isolates; see Figure 4A). These types, along with ST2-KL3, collectively represent 85% of the 546 isolates within the focal region since 2016. The cocktail design mirrored that of the ST2-KL3: mixing 1–3 phages infecting the wild-type isolates with 1–3 phages targeting capsule-deficient CRAB variants to mitigate resistance (STAR Methods). Encouragingly, the obtained seven cocktails, and even a single phage in one instance, effectively suppressed the target isolates from the eight MLST-CPS types *in vitro*, with a few exceptions showing incomplete inhibition (Figure S10).

Finally, we sought to validate the ability of phage cocktails, designed based on 2016–2022 isolates, to target CRABs circulating in the same region at a later time point. We collected 157 previously unsampled CRAB isolates from 2023 and 2024 across 22 cities in four Eastern and Southern European countries (Hungary, Romania, Serbia, Kosovo; Table S2). As revealed by genome sequencing, 90% of these isolates represent nine CRAB types previously detected in this region, reinforcing the temporal stability of the local population (Table S1). Then, from each city, we randomly selected one isolate of each MLST-CPS type for which we could recommend a phage cocktail based on CPS typing (Figure S10). Among the resulting 32 isolates, belonging to seven MLST-CPS types, the corresponding phage cocktails effectively suppressed *in vitro* growth in 26 (81%) cases, with incomplete inhibition observed in the remaining 6 cases (19%; Table S2), demonstrating the feasibility of the strategy.

DISCUSSION

To combat the escalating crisis of antibiotic resistance, especially in the context of hospital-acquired multi-drug-resistant infections, this study explores the promise of precision phage therapy guided by genomic surveillance. Despite successful case studies of phage therapy,[7–12] the limited range of bacterial strains targeted by individual phages hinders its widespread application. We aim to overcome this limitation by demonstrating how genomic surveillance can guide phage therapy for CRAB, offering a scalable and cost-effective strategy. Instead of isolating individual phages for each patient's bacterial strain,[7] we proactively employ genomic surveillance to assemble region-specific phage collections that target the majority of CRAB infections within a particular geographical area.

The key findings of our study are as follows: first, we conducted a systematic analysis of about ten thousand CRAB genomes, identifying 31 prevalent CRAB types responsible for the majority of infections worldwide. Despite inter-regional variation, these types exhibit regional homogeneity, suggesting the potential effectiveness of region-specific phage collections for CRAB targeting. Second, our phylogeographical analysis revealed the temporal stability of CRAB populations within countries over a 6-year period, providing a crucial time frame for preemptively prepared region-specific phage collections. Third, in Eastern Europe, a region with high CRAB infection rates,[61] we performed a phylogeny-guided phage hunt, matching the 11 most prevalent

(F) Adsorption assay. Log_{10} reduction in free phage titers at a maximum adsorption time point as compared with the t_0 time point (light gray line) after mixing phages and hosts (Table S2; STAR Methods). The plots depict individual data points from biological replicates ($n = 3$) along with their average value.
(G) Principal coordinate analysis plot of cell surface similarity based on Fourier Transform Infrared Spectroscopy (Table S2; STAR Methods) distinguishes wild-type from phage-resistant ST2-KL3 isolates. Wild-type is shown in gray. Phage-resistance categories are H (red), HS (orange), HSF (green), and HSFPh (light blue).
(H) TEM images of HSFPh-resistant A110-G1 and HSF-resistant A108-1 isolates alongside their wild-type counterparts, Aci 110 and Aci 108, respectively. Scale bar, 200 nm.
See also Figures S7 and S10.

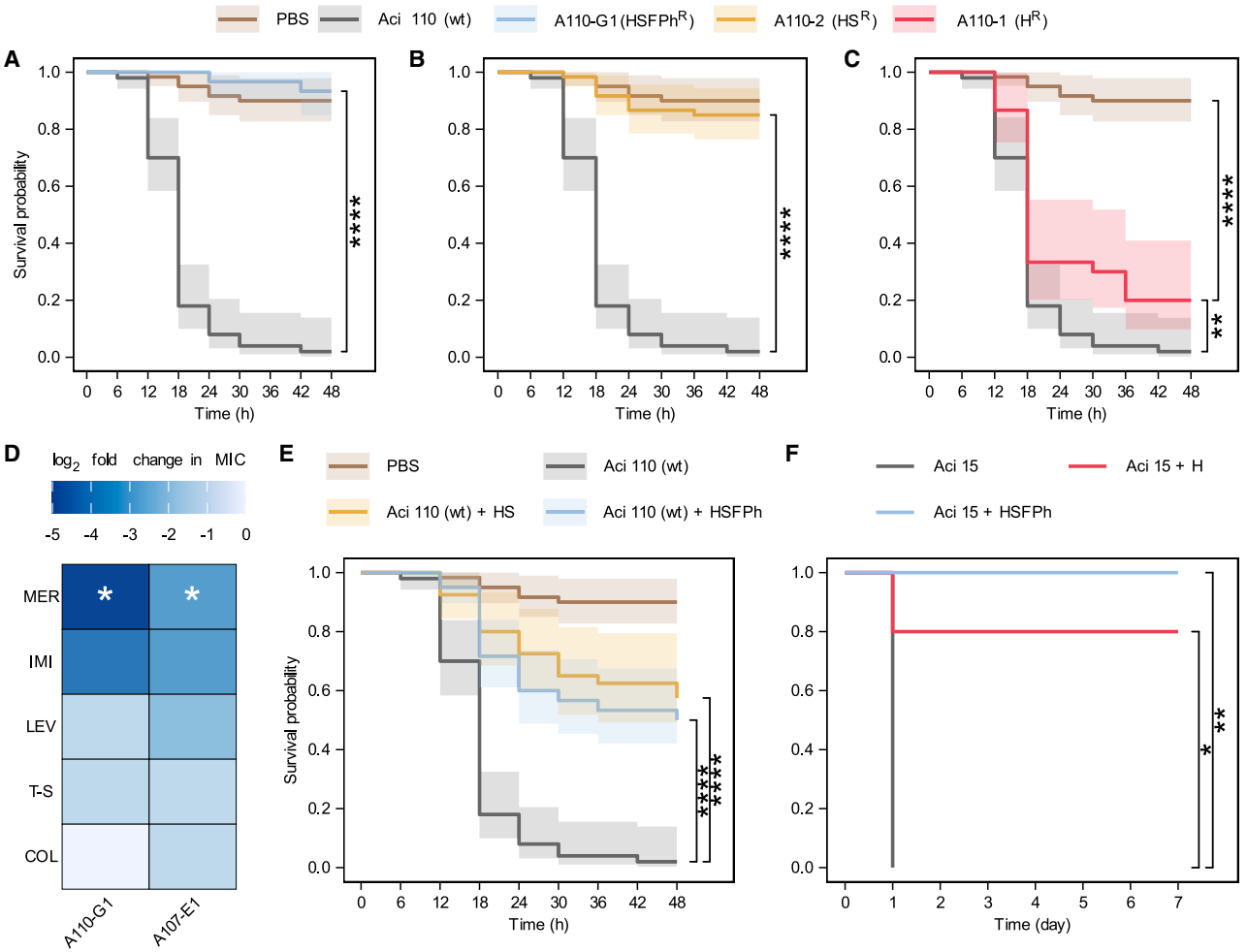

Figure 7. Cost of phage resistance and efficacy of Highwayman and its cocktails HS and HSFPh against ST2-KL3 CRAB isolates in *in vivo* infection models

(A–C) Kaplan-Meier curves showing the survival of *G. mellonella* larvae infected with phage-resistant or wild-type ST2-KL3 CRAB isolates. HSFPh- and HS-resistant lines (HSFPh^R and HS^R, A and B, respectively) display decreased virulence compared with their wild-type counterparts, while the H-resistant line retained virulence (H^R, C). ****$p < 0.0001$ from two-sided Log-rank test, $n = 10$ larvae/group, ≥ 3 biological replicates/group, PBS means larvae injected only with PBS, inoculum size = 9 * 10^6 colony-forming units (CFUs). Note that the Aci 110 and PBS control curves are the same in (A)–(C).

(D) Antibiotic sensitivity profile of the HSFPh cocktail-resistant lines. Blue intensity shows the median log$_2$ MIC change in cocktail-resistant vs. wild-type lines ($n \geq 3$ replicates; Table S2; STAR Methods). MER, meropenem; IMI, imipenem; COL, colistin; LEV, levofloxacin; T-S, trimethoprim + sulfamethoxazole. The star indicates a transition from the resistant state to the intermediate state according to the EUCAST clinical breakpoint.

(E) Kaplan-Meier curves show that significantly more *G. mellonella* larvae survive the infection with Aci 110 ST2-KL3 isolate when the larvae are treated with the cocktail HS (yellow) or HSFPh (light blue) as compared to larvae that were not treated with phages (gray). ****$p < 0.0001$ from a two-sided log-rank test.

(F) Kaplan-Meier curves showing that Highwayman alone (red) and the cocktail HSFPh (light blue) administered 1 h after infection with Aci 15 saved 80% and 100% of the mice, respectively, as opposed to the untreated animals (all died, gray) (CFU = 10^9, $n = 5$ mice/group). ***$p < 0.00027$ from the two-sided log-rank test. Optimization of the mice infection model is available in Figure S9. For (A)–(C), (E), and (F), see Table S2. Plotted values represent the mean ± confidence interval (CI) 95% of at least 3 biological replicates.

See also Figures S8 and S9.

CRAB types with 15 new phages with therapeutic potential. We systematically characterized the host range of these phages using 199 clinical isolates, assessing the scope of their geographic applicability. Finally, we formulated and validated precision phage cocktails with minimal emergence of resistance against a broad range of clinical isolates of the nine most prevalent MLST-CPS types in the focal Eastern and Southern European region. Four of these nine prevalent MLST-CPS types (ST2-KL2, ST2-KL3, ST2-KL9, and ST2-KL12) are also widely distributed globally, emphasizing the potential global applicability of these phage cocktails.

Overall, this study pioneers the use of bacterial phylogeography to scale up precision phage therapy. Genomic surveillance has been pivotal in elucidating pathogen evolution and transmission dynamics,[24] also informing vaccine design.[62,63] The proposed phage therapy framework aims to design phage

collections and cocktails benefiting the most patients across geographical scales, facilitating study recruitment, and expediting clinical trials for validation. Scaling up precision phage therapy will enhance its cost-effectiveness,[14] driving advancements in the field and ensuring its practical application in clinical settings. Furthermore, by creating targeted collections of off-the-shelf medicinal phage products against nosocomial pathogens, phage therapy becomes a viable adjunctive treatment for acute infections requiring immediate intervention. Similarly, a systematic approach has been recently applied for the development of a phage cocktail targeting specific *Escherichia coli* strain types causing fatal infections in hematological cancer patients.[19] Importantly, thanks to the growing availability of genome sequences, the genomic surveillance-based framework developed in this study is applicable beyond CRAB, offering effective strategies for combating a range of infectious diseases in healthcare settings.

Limitations of the study

Our study has limitations. Firstly, while we accounted for sampling bias in analyzing over 10,000 genomes, variations in sequencing efforts across countries and world regions may still introduce some residual bias. Secondly, most laboratory tests, including phage typing, were limited to isolates from four world regions due to limitations in global sample availability. Therefore, the testing of phage cocktails was confined to isolates sourced from just two to four global regions (East, West, and South Europe, along with North America), raising questions about the generalizability of our phage cocktails against the targeted strain types circulating in other world regions. Thirdly, limited animal lifespan due to rapid infection hindered our ability to assess efficacy differences in overcoming phage resistance between the four-phage cocktail and Highwayman.

RESOURCE AVAILABILITY

Lead contact

Further information and requests for resources and reagents should be directed to and will be fulfilled by the lead contact, Bálint Kintses (kintses.balint@brc.hu).

Materials availability

The CRAB clinical isolates collected and sequenced in this study are deposited in either the bacterial collection of HUN-REN Biological Research Centre (https://hun-ren.hu/en/research-network/research-centers/hun-ren-biological-research-centre-szeged), the National Center for Public Health and Pharmacy (NCPHP; https://www.nnk.gov.hu/), or in the Institute of Microbiology and Immunology, Faculty of Medicine, University of Belgrade (http://studiesinenglish.med.bg.ac.rs).

As specified in Material Transfer Agreements, these isolates and their derivatives cannot be transferred to a third party as they can be used "only at the recipient organizations and only in the recipient scientists' laboratories under the direction of the recipient scientists or others working under their direct supervisions."

A. baumannii bacteriophages isolated in this study are available, upon reasonable request, with a completed material transfer agreement.

Data and code availability

Processed next-generation sequencing data of the collected bacterial and phage genomes sequenced in this study have been deposited at the European Nucleotide Archive (ENA) under accession number PRJEB64245 (https://www.ebi.ac.uk/ena/browser/view/PRJEB64245; ENA: PRJEB64245). Phage-resistant *A. baumannii* mutants were deposited separately under accession number PRJEB64574 (https://www.ebi.ac.uk/ena/browser/view/PRJEB64574; ENA: PRJEB64574). Both are publicly available as of the date of publication. The identifiers and detailed information of *A. baumannii* bacteriophages and isolates are listed in the key resources table.

Original code for analyzing the geographic distribution of CRAB strains has been deposited at Zenodo (https://zenodo.org/doi/10.5281/zenodo.11098709) and is publicly available as of the date of publication. DOIs are listed in the key resources table. Any additional information required to reanalyze the data reported in this paper is available from the lead contact upon request.

ACKNOWLEDGMENTS

This work was supported by the National Laboratory of Biotechnology grant 2022-2.1.1-NL-2022-00008 (C.P., B.K., and B.P.); the National Laboratory for Health Security grant RRF-2.3.1-21-2022-00006 (B.P.); the European Union's Horizon 2020 Research and Innovation Programme no. 739593 (B.K. and B.P.); National Research Development and Innovation Office grants "Élvonal" Programme KKP 126506 (C.P.) and KKP 129814 (B.P.), FK-135245 (B.K.), FK-124254 (O.M.), and PD-131839 (E.A.); János Bolyai Research Fellowship BO/352/20 (B.K.) and BO/00303/19/8 (O.M.); New National Excellence Program of the Ministry of Human Capacities UNKP-20-5-SZTE-654 and UNKP-21-5-SZTE-579 (B.K.); Proof of Concept grant of the Eötvös Loránd Research Network ELKH-PoC-2022-034 (B.K.); the Ministry of Culture and Innovation of Hungary grant KDP-2023-C2285907, financed under the National Research, Development and Innovation Fund 2023-2.1.2-KDP-2023-00002 funding scheme (T.S.); and Ministry of Education, Science, and Technological Development of the Republic of Serbia grant no. 451-03-68/2022-14/200110 (I.G.). We thank Andrea Fejér for manuscript editing and proofreading and Gordana Mijovic and Aleksandra Smitran for providing clinical *A. baumannii* isolates from Montenegro and Bosnia and Herzegovina. Petra Szili's assistance with the larvae experiments is greatly appreciated. We also thank the providers of wastewater samples (Alföldvíz Zrt., Budapest Sewage Works Ltd., Debreceni Vízmű Zrt., and Szegedi Vízmű Zrt.). We thank Balázs Szirmai for performing white blood cell countings and Enviroinvest Zrt., Pécs for providing the animal facility for the mice experiments.

AUTHOR CONTRIBUTIONS

Conceptualization and methodology, B.K., B.P., M.K., T.S., H.H.M., and O.M.; investigation and validation, M.K., T.S., H.H.M., B.E., O.M., G.A., L.D., T.F.P., G.S., I.G., and S.A.Z.; software, formal analysis, and data curation, T.S., O.M., M.K., A.A., G.A., B.M.V., E.A., M.S., G.F., and K.N.V.; visualization, T.S., M.K., O.M., H.H.M., A.A., B.B., E.A., G.A., G.F., and M.S.; writing – original draft, B.K., B.P., M.K., T.S., H.H.M., O.M., G.A., and A.A.; writing – review and editing, B.K., B.P., and C.P.; resources, C.B., C.C., M.I., O.I., B.L., S.M., L.O., E.S., U.O.S.-G., Á.T., C.V.d.H., A.B., Á.V., K.K., and M.-S.L.; supervision, B.K. and B.P.

DECLARATION OF INTERESTS

M.K., T.S., H.H.M., O.M., G.A., B.E., B.P., and B.K. are inventors on a filed patent application of region-specific phage compositions (European Patent Office). B.K., T.S., M.K., B.E., and B.M.V. are employees of BRC-Bio Ltd. Hungary.

STAR★METHODS

Detailed methods are provided in the online version of this paper and include the following:

- KEY RESOURCES TABLE
- EXPERIMENTAL MODEL AND SUBJECT DETAILS
  - Microorganisms
  - Animals
- METHOD DETAILS
  - Establishing a collection of *Acinetobacter baumannii* isolates

SUPPLEMENTAL INFORMATION

Supplemental information can be found online at https://doi.org/10.1016/j.cell.2024.09.009.

Received: January 17, 2024
Revised: May 15, 2024
Accepted: September 4, 2024
Published: September 26, 2024

REFERENCES

1. The Review on Antimicrobial Resistance (2016). Tackling drug-resistant infection globally: final report and recommendations. https://amr-review.org/sites/default/files/160518_Final%20paper_with%20cover.pdf.
2. Baker, S., Thomson, N., Weill, F.X., and Holt, K.E. (2018). Genomic insights into the emergence and spread of antimicrobial-resistant bacterial pathogens. Science *360*, 733–738. https://doi.org/10.1126/SCIENCE.AAR3777.
3. Murray, C.J.L., Ikuta, K.S., Sharara, F., Swetschinski, L., Robles Aguilar, G., Gray, A., Han, C., Bisignano, C., Rao, P., and Wool, E. (2022). Global burden of bacterial antimicrobial resistance in 2019: a systematic analysis. Lancet *399*, 629–655. https://doi.org/10.1016/S0140-6736(21)02724-0.
4. Roope, L.S.J., Smith, R.D., Pouwels, K.B., Buchanan, J., Abel, L., Eibich, P., Butler, C.C., Tan, P.S., Walker, A.S., Robotham, J.V., et al. (2019). The challenge of antimicrobial resistance: what economics can contribute. Science *364*, eaau4679. https://doi.org/10.1126/science.aau4679.
5. Plackett, B. (2020). Why big pharma has abandoned antibiotics. Nature *586*, S50–S52. https://doi.org/10.1038/d41586-020-02884-3.
6. Gordillo Altamirano, F.L., and Barr, J.J. (2019). Phage therapy in the post-antibiotic era. Clin. Microbiol. Rev. *32*, e00066–e00018. https://doi.org/10.1128/CMR.00066-18.
7. Schooley, R.T., Biswas, B., Gill, J.J., Hernandez-Morales, A., Lancaster, J., Lessor, L., Barr, J.J., Reed, S.L., Rohwer, F., Benler, S., et al. (2017). Development and use of personalized bacteriophage-based therapeutic cocktails to treat a patient with a disseminated resistant Acinetobacter baumannii infection. Antimicrob. Agents Chemother. *61*, e00954–e00917. https://doi.org/10.1128/AAC.00954-17.
8. Dedrick, R.M., Smith, B.E., Cristinziano, M., Freeman, K.G., Jacobs-Sera, D., Belessis, Y., Whitney Brown, A.W., Cohen, K.A., Davidson, R.M., Van Duin, D., et al. (2023). Phage therapy of mycobacterium infections: compassionate use of phages in 20 patients with drug-resistant mycobacterial disease. Clin. Infect. Dis. *76*, 103–112. https://doi.org/10.1093/cid/ciac453.
9. Zhvania, P., Hoyle, N.S., Nadareishvili, L., Nizharadze, D., and Kutateladze, M. (2017). Phage therapy in a 16-year-old boy with netherton syndrome. Front. Med. *4*, 94. https://doi.org/10.3389/fmed.2017.00094.
10. Van Nieuwenhuyse, B., Van der Linden, D., Chatzis, O., Lood, C., Wagemans, J., Lavigne, R., Schroven, K., Paeshuyse, J., de Magnée, C., Sokal, E., et al. (2022). Bacteriophage-antibiotic combination therapy against extensively drug-resistant Pseudomonas aeruginosa infection to allow liver transplantation in a toddler. Nat. Commun. *13*, 5725. https://doi.org/10.1038/s41467-022-33294-w.
11. Fabijan, A.P., Lin, R.C.Y., Ho, J., Maddocks, S., Ben Zakour, N.L., and Iredell, J.R.; Westmead; Bacteriophage; Therapy Team (2020). Safety of bacteriophage therapy in severe Staphylococcus aureus infection. Nat. Microbiol. *5*, 465–472. https://doi.org/10.1038/s41564-019-0634-z.
12. Kortright, K.E., Chan, B.K., Koff, J.L., and Turner, P.E. (2019). Phage therapy: A renewed approach to combat antibiotic-resistant bacteria. Cell Host Microbe *25*, 219–232. https://doi.org/10.1016/j.chom.2019.01.014.
13. Pirnay, J.-P., and Kutter, E. (2021). Bacteriophages: it's a medicine, Jim, but not as we know it. Lancet Infect. Dis. *21*, 309–311. https://doi.org/10.1016/S1473-3099(20)30464-3.
14. Verbeken, G., and Pirnay, J.P. (2022). European regulatory aspects of phage therapy: magistral phage preparations. Curr. Opin. Virol. *52*, 24–29. https://doi.org/10.1016/j.coviro.2021.11.005.
15. Hatfull, G.F., Dedrick, R.M., and Schooley, R.T. (2022). Phage therapy for antibiotic-resistant bacterial infections. Annu. Rev. Med. *73*, 197–211. https://doi.org/10.1146/annurev-med-080219-122208.
16. Holt, K.E., Lassalle, F., Wyres, K.L., Wick, R., and Mostowy, R.J. (2020). Diversity and evolution of surface polysaccharide synthesis loci in Enterobacteriales. ISME J. *14*, 1713–1730. https://doi.org/10.1038/s41396-020-0628-0.
17. Georjon, H., and Bernheim, A. (2023). The highly diverse antiphage defence systems of bacteria. Nat. Rev. Microbiol. *21*, 686–700. https://doi.org/10.1038/s41579-023-00934-x.
18. Federici, S., Kredo-Russo, S., Valdés-Mas, R., Kviatcovsky, D., Weinstock, E., Matiuhin, Y., Silberberg, Y., Atarashi, K., Furuichi, M., Oka, A., et al. (2022). Targeted suppression of human IBD-associated gut microbiota commensals by phage consortia for treatment of intestinal inflammation. Cell *185*, 2879–2898.e24. https://doi.org/10.1016/j.cell.2022.07.003.
19. Gencay, Y.E., Jasinskytė, D., Robert, C., Semsey, S., Martínez, V., Petersen, A.Ø., Brunner, K., de Santiago Torio, A., Salazar, A., Turcu, I.C., et al. (2023). Engineered phage with antibacterial CRISPR–Cas selectively reduce E. coli burden in mice. Nat. Biotechnol. *42*, 265–274. https://doi.org/10.1038/s41587-023-01759-y.
20. Uyttebroek, S., Chen, B., Onsea, J., Ruythooren, F., Debaveye, Y., Devolder, D., Spriet, I., Depypere, M., Wagemans, J., Lavigne, R., et al. (2022). Safety and efficacy of phage therapy in difficult-to-treat infections: a systematic review. Lancet Infect. Dis. *22*, e208–e220. https://doi.org/10.1016/S1473-3099(21)00612-5.
21. Pirnay, J.-P., Djebara, S., Steurs, G., Griselain, J., Cochez, C., De Soir, S., Glonti, T., Spiessens, A., Vanden Berghe, E., Green, S., et al. (2024). Personalized bacteriophage therapy outcomes for 100 consecutive cases: a multicentre, multinational, retrospective observational study. Nat. Microbiol. *9*, 1434–1453. https://doi.org/10.1038/s41564-024-01705-x.
22. Green, S.I., Clark, J.R., Santos, H.H., Weesner, K.E., Salazar, K.C., Aslam, S., Campbell, J.W., Doernberg, S.B., Blodget, E., Morris, M.I., et al. (2023). A retrospective, observational study of 12 cases of expanded-access customized phage therapy: production, characteristics, and clinical outcomes. Clin. Infect. Dis. *77*, 1079–1091. https://doi.org/10.1093/cid/ciad335.
23. Mutalik, V.K., and Arkin, A.P. (2022). A phage foundry framework to systematically develop viral countermeasures to combat antibiotic-resistant bacterial pathogens. iScience *25*, 104121. https://doi.org/10.1016/j.isci.2022.104121.
24. Stockdale, J.E., Liu, P., and Colijn, C. (2022). The potential of genomics for infectious disease forecasting. Nat. Microbiol. *7*, 1736–1743. https://doi.org/10.1038/s41564-022-01233-6.
25. Fullam, A., Letunic, I., Schmidt, T.S.B., Ducarmon, Q.R., Karcher, N., Khedkar, S., Kuhn, M., Larralde, M., Maistrenko, O.M., Malfertheiner, L., et al. (2023). proGenomes3: approaching one million accurately and

consistently annotated high-quality prokaryotic genomes. Nucleic Acids Res. *51*, D760–D766. https://doi.org/10.1093/nar/gkac1078.

26. Tacconelli, E., Carrara, E., Savoldi, A., Harbarth, S., Mendelson, M., Monnet, D.L., Pulcini, C., Kahlmeter, G., Kluytmans, J., Carmeli, Y., et al. (2018). Discovery, research, and development of new antibiotics: the WHO priority list of antibiotic-resistant bacteria and tuberculosis. Lancet Infect. Dis. *18*, 318–327. https://doi.org/10.1016/S1473-3099(17)30753-3.
27. David, S., Reuter, S., Harris, S.R., Glasner, C., Feltwell, T., Argimon, S., Abudahab, K., Goater, R., Giani, T., Errico, G., et al. (2019). Epidemic of carbapenem-resistant Klebsiella pneumoniae in Europe is driven by nosocomial spread. Nat. Microbiol. *4*, 1919–1929. https://doi.org/10.1038/s41564-019-0492-8.
28. Ong, S.W.X., Rao, P., Khong, W.X., Ong, V.Y.F., Sridatta, P.S.R., Thevasagayam, N.M., Ho, B.C.H., Ang, B.S.P., De, P.P., Ng, O.T., et al. (2023). Genomic surveillance uncovers ongoing transmission of carbapenem-resistant Acinetobacter baumannii (CRAB) and identifies actionable routes of transmissions in an endemic setting. Infect. Control Hosp. Epidemiol. *44*, 460–466. https://doi.org/10.1017/ice.2022.115.
29. Marsh, J.W., Mustapha, M.M., Griffith, M.P., Evans, D.R., Ezeonwuka, C., Pasculle, A.W., Shutt, K.A., Sundermann, A., Ayres, A.M., Shields, R.K., et al. (2019). Evolution of outbreak-causing carbapenem-resistant Klebsiella pneumoniae ST258 at a tertiary Care Hospital over 8 years. mBio *10*, e01945–e01919. https://doi.org/10.1128/mBio.01945-19.
30. Snitkin, E.S., Won, S., Pirani, A., Lapp, Z., Weinstein, R.A., Lolans, K., and Hayden, M.K. (2017). Integrated genomic and interfacility patient-transfer data reveal the transmission pathways of multidrug-resistant Klebsiella pneumoniae in a regional outbreak. Sci. Transl. Med. *9*, eaan0093.
31. CDC (2019). Antibiotic Resistance Threats in the United States, 2019 (Atlanta, GA: U.S. Department of Health and Human Services, CDC). https://ndc.services.cdc.gov/wp-content/uploads/Antibiotic-Resistance-Threats-in-the-United-States-2019.pdf.
32. Appaneal, H.J., Lopes, V.V., LaPlante, K.L., and Caffrey, A.R. (2022). Treatment, clinical outcomes, and predictors of mortality among a national cohort of admitted patients with Acinetobacter baumannii infection. Antimicrob. Agents Chemother. *66*, e0197521. https://doi.org/10.1128/AAC.01975-21.
33. Du, X., Xu, X., Yao, J., Deng, K., Chen, S., Shen, Z., Yang, L., and Feng, G. (2019). Predictors of mortality in patients infected with carbapenem-resistant Acinetobacter baumannii: A systematic review and meta-analysis. Am. J. Infect. Control *47*, 1140–1145. https://doi.org/10.1016/j.ajic.2019.03.003.
34. Strathdee, S.A., Hatfull, G.F., Mutalik, V.K., and Schooley, R.T. (2023). Phage therapy: from biological mechanisms to future directions. Cell *186*, 17–31. https://doi.org/10.1016/j.cell.2022.11.017.
35. Kinross, P., Gagliotti, C., Merk, H., Plachouras, D., Monnet, D.L., Högberg, L.D., and Group, E.-N.S. (2022). Large increase in bloodstream infections with carbapenem-resistant Acinetobacter species during the first 2 years of the COVID-19 pandemic, EU/EEA, 2020 and 2021. Eurosurveillance *27*, 2200845. https://doi.org/10.2807/1560-7917.ES.2022.27.46.2200845.
36. Wyres, K.L., Cahill, S.M., Holt, K.E., Hall, R.M., and Kenyon, J.J. (2020). Identification of Acinetobacter baumannii loci for capsular polysaccharide (KL) and lipooligosaccharide outer core (OCL) synthesis in genome assemblies using curated reference databases compatible with Kaptive. Microb. Genomics *6*, e000339. https://doi.org/10.1099/mgen.0.000339.
37. Venditti, C., Vulcano, A., D'Arezzo, S., Gruber, C.E.M., Selleri, M., Antonini, M., Lanini, S., Marani, A., Puro, V., Nisii, C., et al. (2019). Epidemiological investigation of an Acinetobacter baumannii outbreak using core genome multilocus sequence typing. J. Glob. Antimicrob. Resist. *17*, 245–249. https://doi.org/10.1016/j.jgar.2018.11.027.
38. Maiden, M.C.J., Bygraves, J.A., Feil, E., Morelli, G., Russell, J.E., Urwin, R., Zhang, Q., Zhou, J., Zurth, K., Caugant, D.A., et al. (1998). Multilocus sequence typing: A portable approach to the identification of clones within populations of pathogenic microorganisms. Proc. Natl. Acad. Sci. USA *95*, 3140–3145. https://doi.org/10.1073/pnas.95.6.3140.
39. Gordillo Altamirano, F., Forsyth, J.H., Patwa, R., Kostoulias, X., Trim, M., Subedi, D., Archer, S.K., Morris, F.C., Oliveira, C., Kielty, L., et al. (2021). Bacteriophage-resistant Acinetobacter baumannii are resensitized to antimicrobials. Nat. Microbiol. *6*, 157–161. https://doi.org/10.1038/s41564-020-00830-7.
40. Hill, V., Ruis, C., Bajaj, S., Pybus, O.G., and Kraemer, M.U.G. (2021). Progress and challenges in virus genomic epidemiology. Trends Parasitol. *37*, 1038–1049. https://doi.org/10.1016/j.pt.2021.08.007.
41. Hodcroft, E.B., Zuber, M., Nadeau, S., Vaughan, T.G., Crawford, K.H.D., Althaus, C.L., Reichmuth, M.L., Bowen, J.E., Walls, A.C., Corti, D., et al. (2021). Spread of a SARS-CoV-2 variant through Europe in the summer of 2020. Nature *595*, 707–712. https://doi.org/10.1038/s41586-021-03677-y.
42. Diancourt, L., Passet, V., Nemec, A., Dijkshoorn, L., and Brisse, S. (2010). The population structure of Acinetobacter baumannii: expanding multiresistant clones from an ancestral susceptible genetic pool. PLoS One *5*, e10034. https://doi.org/10.1371/journal.pone.0010034.
43. Holt, K., Kenyon, J.J., Hamidian, M., Schultz, M.B., Pickard, D.J., Dougan, G., and Hall, R. (2016). Five decades of genome evolution in the globally distributed, extensively antibiotic-resistant Acinetobacter baumannii global clone 1. Microb. Genomics *2*, e000052. https://doi.org/10.1099/mgen.0.000052.
44. Moura, A., Lefrancq, N., Wirth, T., Leclercq, A., Borges, V., Gilpin, B., Dallman, T.J., Frey, J., Franz, E., Nielsen, E.M., et al. (2021). Emergence and global spread of Listeria monocytogenes main clinical clonal complex. Sci. Adv. *7*, eabj9805. https://doi.org/10.1126/sciadv.abj9805.
45. Chen, Z., Lemey, P., and Yu, H. (2024). Approaches and challenges to inferring the geographical source of infectious disease outbreaks using genomic data. Lancet Microbe *5*, e81–e92. https://doi.org/10.1016/S2666-5247(23)00296-3.
46. Philipson, C.W., Voegtly, L.J., Lueder, M.R., Long, K.A., Rice, G.K., Frey, K.G., Biswas, B., Cer, R.Z., Hamilton, T., and Bishop-Lilly, K.A. (2018). Characterizing phage genomes for therapeutic applications. Viruses *10*, 188. https://doi.org/10.3390/v10040188.
47. Yukgehnaish, K., Rajandas, H., Parimannan, S., Manickam, R., Marimuthu, K., Petersen, B., Clokie, M.R.J., Millard, A., and Sicheritz-Pontén, T. (2022). PhageLeads: rapid assessment of phage therapeutic suitability using an ensemble machine learning approach. Viruses *14*, 342. https://doi.org/10.3390/v14020342.
48. Liu, M., Hernandez-Morales, A., Clark, J., Le, T., Biswas, B., Bishop-Lilly, K.A., Henry, M., Quinones, J., Voegtly, L.J., Cer, R.Z., et al. (2022). Comparative genomics of Acinetobacter baumannii and therapeutic bacteriophages from a patient undergoing phage therapy. Nat. Commun. *13*, 3776. https://doi.org/10.1038/s41467-022-31455-5.
49. Lefkowitz, E.J., Dempsey, D.M., Hendrickson, R.C., Orton, R.J., Siddell, S.G., and Smith, D.B. (2018). Virus taxonomy: the database of the International Committee on Taxonomy of Viruses (ICTV). Nucleic Acids Res. *46*, D708–D717. https://doi.org/10.1093/nar/gkx932.
50. Tynecki, P., Guziński, A., Kazimierczak, J., Jadczuk, M., Dastych, J., and Onisko, A. (2020). PhageAI - bacteriophage life cycle recognition with machine learning and natural language processing. Preprint at bioRxiv. https://doi.org/10.1101/2020.07.11.198606.
51. Altamirano, F.L.G., and Barr, J.J. (2021). Screening for lysogen activity in therapeutically relevant bacteriophages. Bio Protoc. *11*, e3997. https://doi.org/10.21769/BioProtoc.3997.
52. Regeimbal, J.M., Jacobs, A.C., Corey, B.W., Henry, M.S., Thompson, M.G., Pavlicek, R.L., Quinones, J., Hannah, R.M., Ghebremedhin, M., Crane, N.J., et al. (2016). Personalized therapeutic cocktail of wild environmental phages rescues mice from Acinetobacter baumannii wound infections. Antimicrob. Agents Chemother. *60*, 5806–5816. https://doi.org/10.1128/AAC.02877-15.

53. Talyansky, Y., Nielsen, T.B., Yan, J., Carlino-Macdonald, U., Di Venanzio, G.D., Chakravorty, S., Ulhaq, A., Feldman, M.F., Russo, T.A., Vinogradov, E., et al. (2021). Capsule carbohydrate structure determines virulence in Acinetobacter baumannii. PLoS Pathog. *17*, e1009291. https://doi.org/10.1371/journal.ppat.1009291.

54. Geisinger, E., Huo, W., Hernandez-Bird, J., and Isberg, R.R. (2019). Acinetobacter baumannii: envelope Determinants That Control Drug Resistance, Virulence, and Surface Variability. Annu. Rev. Microbiol. *73*, 481–506. https://doi.org/10.1146/annurev-micro-020518-115714.

55. Tao, Y., Duma, L., and Rossez, Y. (2021). Galleria mellonella as a Good Model to Study Acinetobacter baumannii pathogenesis. Pathogens *10*, 1483. https://doi.org/10.3390/pathogens10111483.

56. Pereira, M.F., Rossi, C.C., da Silva, G.C., Rosa, J.N., and Bazzolli, D.M.S. (2020). Galleria mellonella as an infection model: an in-depth look at why it works and practical considerations for successful application. Pathog. Dis. *78*, ftaa056. https://doi.org/10.1093/femspd/ftaa056.

57. Lee, C.M., Kim, C.-J., Kim, S.E., Park, K.-H., Bae, J.Y., Choi, H.J., Jung, Y., Lee, S.S., Choe, P.G., Park, W.B., et al. (2022). Risk factors for early mortality in patients with carbapenem-resistant Acinetobacter baumannii bacteraemia. J. Glob. Antimicrob. Resist. *31*, 45–51. https://doi.org/10.1016/j.jgar.2022.08.010.

58. Lemos, E.V., de la Hoz, F.P., Einarson, T.R., McGhan, W.F., Quevedo, E., Castañeda, C., and Kawai, K. (2014). Carbapenem resistance and mortality in patients with Acinetobacter baumannii infection: systematic review and meta-analysis. Clin. Microbiol. Infect. *20*, 416–423. https://doi.org/10.1111/1469-0691.12363.

59. Gordillo Altamirano, F.L., Kostoulias, X., Subedi, D., Korneev, D., Peleg, A.Y., and Barr, J.J. (2022). Phage-antibiotic combination is a superior treatment against Acinetobacter baumannii in a preclinical study. EBiomedicine *80*, 104045. https://doi.org/10.1016/j.ebiom.2022.104045.

60. Eskenazi, A., Lood, C., Wubbolts, J., Hites, M., Balarjishvili, N., Leshkasheli, L., Askilashvili, L., Kvachadze, L., van Noort, V., Wagemans, J., et al. (2022). Combination of pre-adapted bacteriophage therapy and antibiotics for treatment of fracture-related infection due to pandrug-resistant Klebsiella pneumoniae. Nat. Commun. *13*, 302. https://doi.org/10.1038/s41467-021-27656-z.

61. Kinross, P., Gagliotti, C., Merk, H., Plachouras, D., Monnet, D.L., Högberg, L.D., Strauss, R., Mertens, K., Sabtcheva, S., Andrasevic, A.T., et al. (2022). Large increase in bloodstream infections with carbapenem-resistant Acinetobacter species during the first 2 years of the COVID-19 pandemic, EU/EEA, 2020 and 2021. Eurosurveillance *27*, 2200845. https://doi.org/10.2807/1560-7917.ES.2022.27.46.2200845.

62. Colijn, C., Corander, J., and Croucher, N.J. (2020). Designing ecologically optimized pneumococcal vaccines using population genomics. Nat. Microbiol. *5*, 473–485. https://doi.org/10.1038/s41564-019-0651-y.

63. Davies, M.R., McIntyre, L., Mutreja, A., Lacey, J.A., Lees, J.A., Towers, R.J., Duchêne, S., Smeesters, P.R., Frost, H.R., Price, D.J., et al. (2019). Atlas of group A streptococcal vaccine candidates compiled using large-scale comparative genomics. Nat. Genet. *51*, 1035–1043. https://doi.org/10.1038/s41588-019-0417-8.

64. Valcek, A., Collier, J., Botzki, A., and Van Der Henst, C. (2022). Acinetobase: the comprehensive database and repository of *Acinetobacter* strains. Database (Oxford) *2022*, baac099. https://doi.org/10.1093/database/baac099.

65. Martin, M. (2011). Cutadapt removes adapter sequences from high-throughput sequencing reads. EMBnet.journal *17*, 10–12. https://doi.org/10.14806/ej.17.1.200.

66. Kokot, M., Długosz, M., and Deorowicz, S. (2017). KMC 3: counting and manipulating *k* -mer statistics. Bioinformatics *33*, 2759–2761. https://doi.org/10.1093/bioinformatics/btx304.

67. Deorowicz, S., Debudaj-Grabysz, A., and Grabowski, S. (2013). Disk-based k-mer counting on a PC. BMC Bioinformatics *14*, 160. https://doi.org/10.1186/1471-2105-14-160.

68. Bankevich, A., Nurk, S., Antipov, D., Gurevich, A.A., Dvorkin, M., Kulikov, A.S., Lesin, V.M., Nikolenko, S.I., Pham, S., Prjibelski, A.D., et al. (2012). SPAdes: A new genome assembly algorithm and its applications to single-cell sequencing. J. Comput. Biol. *19*, 455–477. https://doi.org/10.1089/cmb.2012.0021.

69. Seemann, T. mlst GitHub https://github.com/tseemann/mlst.

70. Lam, M.M.C., Wick, R.R., Judd, L.M., Holt, K.E., and Wyres, K.L. (2022). Kaptive 2.0: updated capsule and lipopolysaccharide locus typing for the Klebsiella pneumoniae species complex. Microb. Genomics *8*, 000800. https://doi.org/10.1099/mgen.0.000800.

71. Hyatt, D., Chen, G.-L., LoCascio, P.F., Land, M.L., Larimer, F.W., and Hauser, L.J. (2010). Prodigal: prokaryotic gene recognition and translation initiation site identification. BMC Bioinformatics *11*, 119. https://doi.org/10.1186/1471-2105-11-119.

72. Buchfink, B., Reuter, K., and Drost, H.-G. (2021). Sensitive protein alignments at tree-of-life scale using DIAMOND. Nat. Methods *18*, 366–368. https://doi.org/10.1038/s41592-021-01101-x.

73. Camacho, C., Coulouris, G., Avagyan, V., Ma, N., Papadopoulos, J., Bealer, K., and Madden, T.L. (2009). BLAST+: architecture and applications. BMC Bioinformatics *10*, 421. https://doi.org/10.1186/1471-2105-10-421.

74. Manni, M., Berkeley, M.R., Seppey, M., Simão, F.A., and Zdobnov, E.M. (2021). BUSCO update: novel and streamlined workflows along with broader and deeper phylogenetic coverage for scoring of eukaryotic, prokaryotic, and viral genomes. Mol. Biol. Evol. *38*, 4647–4654. https://doi.org/10.1093/molbev/msab199.

75. Wood, D.E., Lu, J., and Langmead, B. (2019). Improved metagenomic analysis with Kraken 2. Genome Biol. *20*, 257. https://doi.org/10.1186/s13059-019-1891-0.

76. Bolger, A.M., Lohse, M., and Usadel, B. (2014). Trimmomatic: a flexible trimmer for Illumina sequence data. Bioinformatics *30*, 2114–2120. https://doi.org/10.1093/bioinformatics/btu170.

77. Li, D., Liu, C.-M., Luo, R., Sadakane, K., and Lam, T.-W. (2015). MEGAHIT: an ultra-fast single-node solution for large and complex metagenomics assembly via succinct de Bruijn graph. Bioinform. Oxf. Engl. *31*, 1674–1676. https://doi.org/10.1093/bioinformatics/btv033.

78. Nurk, S., Meleshko, D., Korobeynikov, A., and Pevzner, P.A. (2017). metaSPAdes: a new versatile metagenomic assembler. Genome Res. *27*, 824–834. https://doi.org/10.1101/gr.213959.116.

79. Siguier, P., Perochon, J., Lestrade, L., Mahillon, J., and Chandler, M. (2006). ISfinder: the reference centre for bacterial insertion sequences. Nucleic Acids Res. *34*, D32–D36. https://doi.org/10.1093/nar/gkj014.

80. Magill, D.J., and Skvortsov, T.A. (2023). DePolymerase Predictor (DePP): a machine learning tool for the targeted identification of phage depolymerases. BMC Bioinformatics *24*, 208. https://doi.org/10.1186/s12859-023-05341-w.

81. Nayfach, S., Camargo, A.P., Schulz, F., Eloe-Fadrosh, E., Roux, S., and Kyrpides, N.C. (2021). CheckV assesses the quality and completeness of metagenome-assembled viral genomes. Nat. Biotechnol. *39*, 578–585. https://doi.org/10.1038/s41587-020-00774-7.

82. Bin Jang, H., Bolduc, B., Zablocki, O., Kuhn, J.H., Roux, S., Adriaenssens, E.M., Brister, J.R., Kropinski, A.M., Krupovic, M., Lavigne, R., et al. (2019). Taxonomic assignment of uncultivated prokaryotic virus genomes is enabled by gene-sharing networks. Nat. Biotechnol. *37*, 632–639. https://doi.org/10.1038/s41587-019-0100-8.

83. Shannon, P., Markiel, A., Ozier, O., Baliga, N.S., Wang, J.T., Ramage, D., Amin, N., Schwikowski, B., and Ideker, T. (2003). Cytoscape: A software environment for integrated models of biomolecular interaction networks. Genome Res. *13*, 2498–2504. https://doi.org/10.1101/gr.1239303.

84. Gilchrist, C.L.M., and Chooi, Y.-H. (2021). clinker & clustermap.js: automatic generation of gene cluster comparison figures. Bioinformatics *37*, 2473–2475. https://doi.org/10.1093/bioinformatics/btab007.

85. Kelley, L.A., Mezulis, S., Yates, C.M., Wass, M.N., and Sternberg, M.J.E. (2015). The Phyre2 web portal for protein modeling, prediction and analysis. Nat. Protoc. *10*, 845–858. https://doi.org/10.1038/nprot.2015.053.

86. Katoh, K., and Standley, D.M. (2013). MAFFT Multiple Sequence Alignment Software Version 7: Improvements in Performance and Usability. Mol. Biol. Evol. *30*, 772–780. https://doi.org/10.1093/molbev/mst010.

87. Zankari, E., Hasman, H., Cosentino, S., Vestergaard, M., Rasmussen, S., Lund, O., Aarestrup, F.M., and Larsen, M.V. (2012). Identification of acquired antimicrobial resistance genes. J. Antimicrob. Chemother. *67*, 2640–2644. https://doi.org/10.1093/jac/dks261.

88. Joensen, K.G., Scheutz, F., Lund, O., Hasman, H., Kaas, R.S., Nielsen, E.M., and Aarestrup, F.M. (2014). Real-time whole-genome sequencing for routine typing, surveillance, and outbreak detection of verotoxigenic Escherichia coli. J. Clin. Microbiol. *52*, 1501–1510. https://doi.org/10.1128/JCM.03617-13.

89. Oksanen, J., Simpson, G.L., Blanchet, F.G., Kindt, R., Legendre, P., Minchin, P.R., O'Hara, R.B., Solymos, P., Stevens, M.H.H., Szoecs, E., et al. (2022). Vegan: Community Ecology Package. version 2.6-4. http://CRAN.R-project.org/package=vegan.

90. Croucher, N.J., Page, A.J., Connor, T.R., Delaney, A.J., Keane, J.A., Bentley, S.D., Parkhill, J., and Harris, S.R. (2015). Rapid phylogenetic analysis of large samples of recombinant bacterial whole genome sequences using Gubbins. Nucleic Acids Res. *43*, e15. https://doi.org/10.1093/nar/gku1196.

91. Mai, U., and Mirarab, S. (2018). TreeShrink: fast and accurate detection of outlier long branches in collections of phylogenetic trees. BMC Genomics *19*, 272. https://doi.org/10.1186/s12864-018-4620-2.

92. Volz, E.M., and Frost, S.D.W. (2017). Scalable relaxed clock phylogenetic dating. Virus Evol. *3*, vex025. https://doi.org/10.1093/ve/vex025.

93. Page, A.J., Taylor, B., Delaney, A.J., Soares, J., Seemann, T., Keane, J.A., and Harris, S.R. (2016). SNP-sites: rapid efficient extraction of SNPs from multi-FASTA alignments. Microb. Genomics *2*, e000056. https://doi.org/10.1099/mgen.0.000056.

94. Price, M.N., Dehal, P.S., and Arkin, A.P. (2009). FastTree: computing Large Minimum Evolution Trees with Profiles instead of a Distance Matrix. Mol. Biol. Evol. *26*, 1641–1650. https://doi.org/10.1093/molbev/msp077.

95. Seemann, T. (2023). Snippy: Fast Bacterial Variant Calling from ngs Reads. https://github.com/tseemann/snippy.

96. Louca, S., and Doebeli, M. (2018). Efficient comparative phylogenetics on large trees. Bioinformatics *34*, 1053–1055. https://doi.org/10.1093/bioinformatics/btx701.

97. Kremer, L.P.M., and Anders, S. (2019). ggpointdensity: a cross between a 2D density plot and a scatter plot. Version 0.1.0. https://cran.r-project.org/web/packages/ggpointdensity/ggpointdensity.pdf.

98. Di Tommaso, P., Chatzou, M., Floden, E.W., Barja, P.P., Palumbo, E., and Notredame, C. (2017). Nextflow enables reproducible computational workflows. Nat. Biotechnol. *35*, 316–319. https://doi.org/10.1038/nbt.3820.

99. Kurtzer, G.M., Sochat, V., and Bauer, M.W. (2017). Singularity: scientific containers for mobility of compute. PLoS One *12*, e0177459. https://doi.org/10.1371/journal.pone.0177459.

100. Pagès, H., Aboyoun, P., Gentleman, R., DebRoy, S., Carey, V., Delhomme, N., Ernst, F., Khan, H., Lakshman, A., O'Neill, K., et al. (2023). Biostrings: Efficient Manipulation of Biological Stringsversion 2.70.1. Bioconductor version: Release (3.18). https://doi.org/10.18129/B9.bioc.Biostrings.

101. Wickham, H., François, R., Henry, L., Müller, K., and Vaughan, D.; Software, P.; PBC (2023). dplyr: A Grammar of Data Manipulation. Version 1.1.4. https://dplyr.tidyverse.org/.

102. Charif, D., and Lobry, J.R. (2007). SeqinR 1.0-2: A Contributed Package to the R Project for Statistical Computing Devoted to Biological Sequences Retrieval and Analysis. In Structural Approaches to Sequence Evolution: Molecules, Networks, Populations Biological and Medical Physics, Biomedical Engineering, U. Bastolla, M. Porto, H.E. Roman, and M. Vendruscolo, eds. (Springer), pp. 207–232. https://doi.org/10.1007/978-3-540-35306-5_10.

103. Maechler, M., Rousseeuw, P., Struyf, A., Hubert, M., and Hornik, K. (2023). Cluster: cluster Analysis Basics and Extensions. R package version 2.1.6. https://CRAN.R-project.org/package=cluster.

104. Arel-Bundock, V., Enevoldsen, N., and Yetman, C.J. (2018). countrycode: an R package to convert country names and country codes. J. Open Source Softw. *3*, 848. https://doi.org/10.21105/JOSS.00848.

105. Paradis, E., and Schliep, K. (2019). ape 5.0: an environment for modern phylogenetics and evolutionary analyses in R. Bioinformatics *35*, 526–528. https://doi.org/10.1093/bioinformatics/bty633.

106. Quinlan, A.R., and Hall, I.M. (2010). BEDTools: a flexible suite of utilities for comparing genomic features. Bioinformatics *26*, 841–842. https://doi.org/10.1093/bioinformatics/btq033.

107. Luo, G., Spellberg, B., Gebremariam, T., Bolaris, M., Lee, H., Fu, Y., French, S.W., and Ibrahim, A.S. (2012). Diabetic murine models for Acinetobacter baumannii infection. J. Antimicrob. Chemother. *67*, 1439–1445. https://doi.org/10.1093/jac/dks050.

108. The European Committee on Antimicrobial Susceptibility Testing (2023). Breakpoint Tables for Interpretation of MICs and Zone Diameters, version 13.1. http://www.eucast.org.

109. Wellcome Open Research Open-access bacterial population genomics. https://wellcomeopenresearch.org/articles/3-124.

110. Evans, B.A., and Amyes, S.G.B. (2014). OXA β-lactamases. Clin. Microbiol. Rev. *27*, 241–263. https://doi.org/10.1128/CMR.00117-13.

111. Zander, E., Nemec, A., Seifert, H., and Higgins, P.G. (2012). Association between β-lactamase-Encoding bla OXA-51 Variants and DiversiLab Rep-PCR-Based Typing of Acinetobacter baumannii Isolates. J. Clin. Microbiol. *50*, 1900–1904. https://doi.org/10.1128/JCM.06462-11.

112. Li, S., Duan, X., Peng, Y., and Rui, Y. (2019). Molecular characteristics of carbapenem-resistant Acinetobacter spp. from clinical infection samples and fecal survey samples in Southern China. BMC Infect. Dis. *19*, 900. https://doi.org/10.1186/s12879-019-4423-3.

113. Turton, J.F., Ward, M.E., Woodford, N., Kaufmann, M.E., Pike, R., Livermore, D.M., and Pitt, T.L. (2006). The role of ISAba1 in expression of OXA carbapenemase genes in Acinetobacter baumannii. FEMS Microbiol. Lett. *258*, 72–77. https://doi.org/10.1111/j.1574-6968.2006.00195.x.

114. Segal, H., Jacobson, R.K., Garny, S., Bamford, C.M., and Elisha, B.G. (2007). Extended −10 promoter in ISAba-1 upstream of blaOXA-23 from Acinetobacter baumannii. Antimicrob. Agents Chemother. *51*, 3040–3041. https://doi.org/10.1128/AAC.00594-07.

115. Corvec, S., Poirel, L., Naas, T., Drugeon, H., and Nordmann, P. (2007). Genetics and expression of the carbapenem-hydrolyzing oxacillinase gene blaOXA-23 in Acinetobacter baumannii. Antimicrob. Agents Chemother. *51*, 1530–1533. https://doi.org/10.1128/AAC.01132-06.

116. Novovic, K., Mihajlovic, S., Vasiljevic, Z., Filipic, B., Begovic, J., and Jovcic, B. (2015). Carbapenem-resistant Acinetobacter baumannii from Serbia: revision of CarO classification. PLoS One *10*, e0122793. https://doi.org/10.1371/journal.pone.0122793.

117. Geisinger, E., Vargas-Cuebas, G., Mortman, N.J., Syal, S., Wainwright, E.L., Lazinski, D., Wood, S., Zhu, Z., Anthony, J., Opijnen, T.V., et al. (2018). The landscape of intrinsic and evolved fluoroquinolone resistance in *Acinetobacter baumannii* includes suppression of drug-induced prophage replication. Preprint at bioRxiv. https://doi.org/10.1101/442681.

118. Liu, C., Chen, K., Wu, Y., Huang, L., Fang, Y., Lu, J., Zeng, Y., Xie, M., Chan, E.W.C., Chen, S., et al. (2022). Epidemiological and genetic characteristics of clinical carbapenem-resistant Acinetobacter baumannii strains collected countrywide from hospital intensive care units (ICUs) in China. Emerg. Microbes Infect. *11*, 1730–1741. https://doi.org/10.1080/22221751.2022.2093134.

119. Leinonen, R., Akhtar, R., Birney, E., Bower, L., Cerdeno-Tárraga, A., Cheng, Y., Cleland, I., Faruque, N., Goodgame, N., Gibson, R., et al. (2011). The European nucleotide archive. Nucleic Acids Res. *39*, D28–D31. https://doi.org/10.1093/nar/gkq967.

120. Hawkey, J., Hamidian, M., Wick, R.R., Edwards, D.J., Billman-Jacobe, H., Hall, R.M., and Holt, K.E. (2015). ISMapper: identifying transposase insertion sites in bacterial genomes from short read sequence data. BMC Genomics *16*, 667. https://doi.org/10.1186/s12864-015-1860-2.

121. R Core Team (2021). R: A Language and Environment for Statistical Computing (R Foundation for Statistical Computing). https://www.R-project.org/.

122. Olson, R.D., Assaf, R., Brettin, T., Conrad, N., Cucinell, C., Davis, J.J., Dempsey, D.M., Dickerman, A., Dietrich, E.M., Kenyon, R.W., et al. (2023). Introducing the Bacterial and Viral Bioinformatics Resource Center (BV-BRC): a resource combining Patric, IRD and ViPR. Nucleic Acids Res. *51*, D678–D689. https://doi.org/10.1093/nar/gkac1003.

123. Tukey, J.W. (1977). Exploratory Data Analysis (Addison-Wesley Publishing Co.).

124. Ishikawa, S.A., Zhukova, A., Iwasaki, W., and Gascuel, O. A Fast Likelihood method to reconstruct and visualize ancestral scenarios. Mol. Biol. Evol. 36, 2069–2085. 10.1093/molbev/msz131.

125. Pupko, T., Pe'er, I., Shamir, R., and Graur, D. (2000). A fast algorithm for joint reconstruction of ancestral amino acid sequences. Mol. Biol. Evol. *17*, 890–896. https://doi.org/10.1093/OXFORDJOURNALS.MOLBEV.A026369.

126. Popova, A.V., Shneider, M.M., Arbatsky, N.P., Kasimova, A.A., Senchenkova, S.N., Shashkov, A.S., Dmitrenok, A.S., Chizhov, A.O., Mikhailova, Y.V., Shagin, D.A., et al. (2021). Specific interaction of novel Friunavirus phages encoding tailspike depolymerases with corresponding Acinetobacter baumannii capsular types. J. Virol. *95*, e01714–e01720. https://doi.org/10.1128/JVI.01714-20.

127. Anderson, B., Rashid, M.H., Carter, C., Pasternack, G., Rajanna, C., Revazishvili, T., Dean, T., Senecal, A., and Sulakvelidze, A. (2011). Enumeration of bacteriophage particles: comparative analysis of the traditional plaque assay and real-time QPCR- and nanosight-based assays. Bacteriophage *1*, 86–93. https://doi.org/10.4161/bact.1.2.15456.

128. Bonilla, N., Rojas, M.I., Netto Flores Cruz, G., Hung, S.-H., Rohwer, F., and Barr, J.J. (2016). Phage on tap-a quick and efficient protocol for the preparation of bacteriophage laboratory stocks. PeerJ *4*, e2261. https://doi.org/10.7717/peerj.2261.

129. Hietala, V., Horsma-Heikkinen, J., Carron, A., Skurnik, M., and Kiljunen, S. (2019). The removal of Endo- and enterotoxins from bacteriophage preparations. Front. Microbiol. *10*, 1674.

130. Reynolds, E.S. (1963). THE USE OF LEAD citrate AT HIGH pH AS AN ELECTRON-OPAQUE STAIN IN ELECTRON MICROSCOPY. J. Cell Biol. *17*, 208–212. https://doi.org/10.1083/jcb.17.1.208.

131. Kutter, E. (2009). Phage host range and efficiency of plating. Methods Mol. Biol. *501*, 141–149. https://doi.org/10.1007/978-1-60327-164-6_14.

132. Venturini, C., Petrovic Fabijan, A., Fajardo Lubian, A., Barbirz, S., and Iredell, J. (2022). Biological foundations of successful bacteriophage therapy. EMBO Mol. Med. *14*, e12435. https://doi.org/10.15252/emmm.202012435.

133. Timoshina, O.Y., Shneider, M.M., Evseev, P.V., Shchurova, A.S., Shelenkov, A.A., Mikhaylova, Y.V., Sokolova, O.S., Kasimova, A.A., Arbatsky, N.P., Dmitrenok, A.S., et al. (2021). Novel Acinetobacter baumannii bacteriophage Aristophanes encoding structural polysaccharide deacetylase. Viruses *13*, 1688. https://doi.org/10.3390/v13091688.

134. Latka, A., Leiman, P.G., Drulis-Kawa, Z., and Briers, Y. (2019). Modeling the architecture of depolymerase-containing receptor binding proteins in Klebsiella phages. Front. Microbiol. *10*, 2649. https://doi.org/10.3389/fmicb.2019.02649.

135. Camargo, A.P., Roux, S., Schulz, F., Babinski, M., Xu, Y., Hu, B., Chain, P.S.G., Nayfach, S., and Kyrpides, N.C. (2023). Identification of mobile genetic elements with geNomad. Nat. Biotechnol. *2023*, 1–10. https://doi.org/10.1038/s41587-023-01953-y.

136. Hauser, M., Steinegger, M., and Söding, J. (2016). MMseqs software suite for fast and deep clustering and searching of large protein sequence sets. Bioinformatics *32*, 1323–1330. https://doi.org/10.1093/bioinformatics/btw006.

137. Tesson, F., Hervé, A., Mordret, E., Touchon, M., d'Humières, C., Cury, J., and Bernheim, A. (2022). Systematic and quantitative view of the antiviral arsenal of prokaryotes. Nat. Commun. *13*, 2561. https://doi.org/10.1038/s41467-022-30269-9.

138. Altschul, S.F., Madden, T.L., Schäffer, A.A., Zhang, J., Zhang, Z., Miller, W., and Lipman, D.J. (1997). Gapped BLAST and PSI-BLAST: a new generation of protein database search programs. Nucleic Acids Res. *25*, 3389–3402. https://doi.org/10.1093/nar/25.17.3389.

139. Croxatto, A., Prod'Hom, G., and Greub, G. (2012). Applications of MALDI-TOF mass spectrometry in clinical diagnostic microbiology. FEMS Microbiol. Rev. *36*, 380–407. https://doi.org/10.1111/j.1574-6976.2011.00298.x.

140. Wiegand, I., Hilpert, K., and Hancock, R.E.W. (2008). Agar and broth dilution methods to determine the minimal inhibitory concentration (MIC) of antimicrobial substances. Nat. Protoc. *3*, 163–175. https://doi.org/10.1038/nprot.2007.521.

141. Teng, A.S.J., Habermehl, P.E., van Houdt, R., de Jong, M.D., van Mansfeld, R., Matamoros, S.P.F., Spijkerman, I.J.B., van Meer, M.P.A., and Visser, C.E. (2022). Comparison of fast Fourier transform infrared spectroscopy biotyping with whole genome sequencing-based genotyping in common nosocomial pathogens. Anal. Bioanal. Chem. *414*, 7179–7189. https://doi.org/10.1007/s00216-022-04270-6.

142. Schneider, G., Szentes, N., Horváth, M., Dorn, Á., Cox, A., Nagy, G., Doffkay, Z., Maróti, G., Rákhely, G., and Kovács, T. (2018). Kinetics of targeted phage rescue in a mouse model of systemic *Escherichia coli* K1. BioMed Res. Int. *2018*, 7569645. https://doi.org/10.1155/2018/7569645.

Please cite this article in press as: Koncz et al., Genomic surveillance as a scalable framework for precision phage therapy against antibiotic-resistant pathogens, Cell (2024), https://doi.org/10.1016/j.cell.2024.09.009

CellPress
OPEN ACCESS

STAR★METHODS

KEY RESOURCES TABLE

REAGENT or RESOURCE	SOURCE	IDENTIFIER
Bacterial and virus strains		
Collection of *A. baumannii* CRAB clinical isolates. See Table S1 (T1)	This study	https://www.ebi.ac.uk/ena/browser/view/PRJEB64245; ENA: PRJEB64245
External dataset used for the initial study: 16 CRAB isolates from BEI Resources	https://www.niaid.nih.gov/research/bei-resources-repository	Table S2 (T9); RRID: SCR_013698
External dataset used for the initial study: 47 CRAB isolates from the Belgian Acinetobase collection	Valcek et al.[64]	Table S2 (T9)
External dataset used for the initial study: 14 *A. baumannii* isolates provided by Alexandr Nemec	Alexandr Nemec	Table S2 (T9)
157 CRAB isolates collected in 2023 and 2024 to validate the region-specific treatment strategy	This study	Table S2 (T32); https://www.ebi.ac.uk/ena/browser/view/PRJEB64245; ENA: PRJEB64245
15 *A.baumannii* bacteriophages, see Table S2 (T12)	This study	https://www.ebi.ac.uk/ena/browser/view/PRJEB64245; ENA: PRJEB64245
A. baumannii mutant strains (n=19), see Table S2 (T21)	This study	https://www.ebi.ac.uk/ena/browser/view/PRJEB64574; ENA: PRJEB64574
Critical commercial assays		
GenElute™ Bacterial Genomic DNA Kit	Sigma-Aldrich (https://www.sigmaaldrich.com/HU/en/product/sigma/na2110	NA2110
MiSeq Reagent Kits v2	Illumina (https://www.illumina.com/products/by-type/sequencing-kits/cluster-gen-sequencing-reagents/miseq-reagent-kit-v2.html)	MS-102-2003
Nextera XT DNA Library Preparation Kit	Illumina (https://www.illumina.com/products/by-type/sequencing-kits/library-prep-kits/nextera-xt-dna.html)	FC-131-1096
Amicon® Ultra - 15 Centrifugal Filter	Millipore	UFC910024
Amicon® Ultra - 4 Centrifugal Filter	Millipore	UFC810024
Pierce™ High Capacity Endotoxin Removal Spin Columns, 1 ml	Thermo Scientific™	88276
Phage DNA Isolation Kit	NORGEN BIOTEK	SKU 46850
Deposited data		
Assembled genomes	This study	ENA: PRJEB64245; ENA: PRJEB64574
Experimental models: Organisms/strains		
Galleria mellonella larvae 2-3 cm (300-400 mg)	https://www.terraplaza.shop/	TP380081
Female BALB/c mice, 6-7 weeks old, 16-25 g	Envigo in the Netherlands	https://www.inotivco.com/
Software and algorithms		
cutadapt 4.3	Martin[65]	https://cutadapt.readthedocs.io/en/stable/; RRID: SCR_011841
kmc 3.2.1	Kokot et al.[66]; Deorowicz et al.[67]	https://github.com/refresh-bio/KMC; RRID: SCR_001245
SPAdes 3.15.5	Bankevich et al.[68]	https://github.com/ablab/spades; RRID: SCR_000131
mlst v2.23.0	Jolley et al.[69]	https://github.com/tseemann/mlst

(*Continued on next page*)

Continued

REAGENT or RESOURCE	SOURCE	IDENTIFIER
Kaptive 2.0.3	Lam et al.[70]	https://github.com/klebgenomics/Kaptive; RRID: SCR_024046
Prodigal v2.6.3	Hyatt et al.[71]	https://github.com/hyattpd/Prodigal; RRID: SCR_011936
Diamond v2.0.15	Buchfink et al.[72]	https://github.com/bbuchfink/diamond; RRID: SCR_016071
NCBI blast v2.13.0	Camacho et al.[73]	https://ftp.ncbi.nlm.nih.gov/blast/executables/blast+/; RRID: SCR_004870
busco v5.4.4	Manni et al.[74]	https://busco.ezlab.org/; RRID: SCR_015008
kraken2 v2.1.2	Wood et al.[75]	https://github.com/DerrickWood/kraken2; RRID: SCR_005484
Trimmomatic v0.36	Bolger et al.[76]	https://github.com/usadellab/Trimmomatic; RRID: SCR_011848
MEGAHIT	Li et al.[77]	https://github.com/voutcn/megahit; RRID: SCR_018551
MetaSpades v3.13.0	Nurk et al.[78]	https://github.com/ablab/spades; RRID: SCR_000131
ISfinder	Siguier et al.[79]	https://www-is.biotoul.fr/search.php; RRID: SCR_003020
PhageAI	Tynecki et al.[50]	https://phage.ai/
Phageleads	Yukgehnaish et al.[47]	https://phageleads.ku.dk/
Depolymerase Predictor	Magill and Skvortsov[80]	https://github.com/DamianJM/Depolymerase-Predictor
CheckV	Nayfach et al.[81]	https://bitbucket.org/berkeleylab/checkv/src/master/
vConTACT2	Bin Jang et al.[82]	https://bitbucket.org/MAVERICLab/vcontact2/src/master/
Cytoscape	Shannon et al.[83]	https://cytoscape.org/; RRID: SCR_003032
Clinker	Gilchrist and Chooi[84]	https://github.com/gamcil/clinker; RRID: SCR_016140
Phyre2 v2.0	Kelley et al.[85]	http://www.sbg.bio.ic.ac.uk/~phyre2/html/page.cgi?id=index; RRID: SCR_010270
mafft v7.520	Katoh and Standley[86]	https://mafft.cbrc.jp/alignment/server/index.html; RRID: SCR_011811
IR Biotyper Software V4.0.8 (2022-11-21T1119Z)	https://store.bruker.com/products/software-package-ir-biotyper	Software package IR Biotyper 4.0, Bruker Daltonics, Part No:1895589
Opus Software V8.2.28	https://store.bruker.com/products/software-package-ir-biotyper	Software package IR Biotyper 4.0, Bruker Daltonics, Part No:1895589
ResFinder v2.0.0	Zankari et al.[87]	https://bitbucket.org/genomicepidemiology/resfinder_db/src/master/; RRID: SCR_024314
VirulenceFinder v1.5	Joensen et al.[88]	https://cge.food.dtu.dk/services/VirulenceFinder/; RRID: SCR_024371
R package vegan v2.6-4	Oksanen et al.[89]	https://CRAN.R-project.org/package=vegan; RRID: SCR_011950
gubbins v3.3.0	Croucher et al.[90]	https://github.com/nickjcroucher/gubbins; RRID: SCR_016131
TreeShrink v1.3.9	Mai and Mirarab[91]	https://github.com/uym2/TreeShrink
treedater	Volz and Frost[92]	https://github.com/emvolz/treedater?tab=readme-ov-file
SNP-sites v2.5.1	Page et al.[93]	http://sanger-pathogens.github.io/snp-sites/; RRID: SCR_022265

(*Continued on next page*)

Continued

REAGENT or RESOURCE	SOURCE	IDENTIFIER
FastTree v2.1.11 SSE3	Price et al.[94]	http://www.microbesonline.org/fasttree/; RRID: SCR_015501
snippy v4.6.0	Seemann[95]	https://github.com/tseemann/snippy; RRID: SCR_023572
castor R package v1.8.0	Louca and Doebeli[96]	https://cran.r-project.org/web/packages/castor/index.html
ggpointdensity R package v0.1.0	Kremer and Anders[97]	https://CRAN.R-project.org/package=ggpointdensity
Nextflow v22.10.1	Di Tommaso et al.[98]	https://github.com/nextflow-io/nextflow/releases; RRID: SCR_024135
Singularity v3.9.0	Kurtzer et al.[99]	https://github.com/singularityhub/singularity-docker
Biostrings v2.70.1	Pagès et al.[100]	https://bioconductor.org/packages/release/bioc/html/Biostrings.html; RRID: SCR_016949
dplyr v1.1.4	Wickham et al.[101]	https://cran.r-project.org/web/packages/dplyr/index.html; RRID: SCR_016708
seqinr v1.0-2	Charif and Lobry[102]	https://cran.r-project.org/web/packages/seqinr/index.html; RRID: SCR_022678
cluster R package v2.1.6	Rousseeuw et al.[103]	https://CRAN.R-project.org/package=cluster; RRID: SCR_013505
R package countrycode v1.3.0.	Arel-Bundock et al.[104]	https://github.com/vincentarelbundock/countrycode/releases
Custom code and scripts	This study	https://zenodo.org/records/1109871
ape 5.0 R package	Paradis and Schliep[105]	https://academic.oup.com/bioinformatics/article/35/3/526/5055127; RRID: SCR_001245
bedtools v2.30.0	Quinlan and Hall[106]	https://bedtools.readthedocs.io/en/latest/index.html; RRID: SCR_006646

EXPERIMENTAL MODEL AND SUBJECT DETAILS

Microorganisms

Bacterial strains

The received clinical isolates were always verified by streaking them onto Acinetobacter-specific chrome agar (CHROMagarTM Acinetobacter, CheBio) and finally by genome sequencing. Some of them were verified by matrix-assisted laser desorption ionization-time of flight mass spectrometry (MALDI-TOF MS) analysis as well. *A. baumannii* isolates were routinely cultured on LB broth (LB, 5 g of tryptone, 2.5 g of yeast extract, 5 g of NaCl, and 500 ml of distilled water) or LB agar (LB plus 1.5% Bacto agar, w/v) at 37°C, unless otherwise specified. When grown in liquid medium, the cultures were aerated by shaking. The overnight cultures were started from glycerin stocks prepared by inoculating 3 ml LB broth with a single colony from a fresh streak plate, grown overnight, and stored at -80 °C with glycerol (25% final concentration). For antimicrobial susceptibility testing and *G. mellonella* larvae experiments, bacterial cells were grown in Mueller Hinton Broth 2 (MHB2) from Millipore. For all plaque assays, a 0.5% LB agar overlay (LB and 0.5% Bacto agar w/v) was inoculated with 0.1 ml of a fresh overnight LB culture of the host and poured over LB agar plates.

Phages

The phages used in this study were isolated in a phage hunt as part of this study. In all cases, phages were isolated from raw sewage water harvested from communal waste-water treatment plants from five Hungarian cities (Szeged, Budapest, Hódmezővásárhely, Debrecen, and Békéscsaba).

Animals

This research complies with all relevant ethical regulations and was approved by the Scientific and Research Ethics Committee of the Hungarian Health Science Council (BMEÜ/271-3/2022/EKU). Animal experiments were approved by the Animal Experimentation Scientific Ethical Council: Investigation of the Effectiveness of Bacteriophage Strains with Therapeutic Potential in Animal Experimental Model Systems with an authorization number: KA-3429.

Galleria mellonella larvae model

For the *G. mellonella in vivo* experiments, we used larvae in the final instar developmental stage. After receiving them in bulk, each larva was cleaned with a cotton swab dipped in 70% ethanol and stored at 15°C, in the absence of food, in plastic boxes with breathable lids, filled with sterile wood shavings to allow the larvae to burrow into. Only healthy-looking larvae, exhibiting a uniform cream colour, without pigmentation and weighing between 300-400 mg, were used for the experiments. They were not used if they were older than one week after being obtained from the distributor. The treatment solutions, containing bacteria or phage were prepared in 10 μl 1X Phosphate-Buffered Saline (PBS) and injected into the hemocoels of the larvae via the first left proleg (bacteria) or the first right proleg (phage) using 10 μl Hamilton syringes (Reno, Nevada, U.S.A.). Larvae were incubated at 37°C for 48 h in Petri dishes lined with filter paper and survival was monitored every 6 hours. Larvae were considered dead if they failed to respond to touch. The surviving larvae were euthanized by rapid cooling, placing them to -80°C.

Intraperitoneal mouse model

Female BALB/c mice, 6-7 weeks old and weighing 16-25 g, were obtained from Envigo, Netherlands. All animal care and handling procedures adhered to the European Federation for Laboratory Animal Science Association (FELASA) guidelines, and the Enviroinvest Co., Hungary's Animal Welfare committee approved the protocols (permit number: BA02/2000-12/2022). Mice were housed in individually vented sterile cages at 22°C and 30-70% humidity and provided water and food ad libitum. The mouse chow pellets were LabDiet® JL Rat and Mouse/Auto 6F 5K67 complete life-cycle diet that was autoclaved to sterilize.

They were separated into groups (each containing 5-5 animals) based on the experimental conditions. The treatment solutions (bacteria or phage) prepared in 200 μl PBS were administered intraperitoneally. The mouse was placed on its back, and the bacterial suspension was injected into its left side, while phages were injected into the right side. Death rates and body weights were recorded daily for seven days after the treatments.

Neutropenic mouse model

A neutropenic mouse model was performed as described earlier.[107] Specifically, the immune system of the mice was suppressed with cyclophosphamide (200 mg/kg) and cortisone acetate (250 mg/kg) by administering them subcutaneously. Blood samples were taken on days 0, 4, 7, and 10 and white blood cell (WBC) counts were determined from 3 treated and 3 untreated animals.

METHOD DETAILS

Establishing a collection of *Acinetobacter baumannii* isolates

Due to the underrepresentation of genomic samples from the Eastern and Southern European region, we collected and sequenced 419 carbapenem-resistant *Acinetobacter baumannii* (CRAB) clinical isolates from 5 countries from this region (Hungary (*n*=253), Romania (*n*=120), Serbia (*n*=28), Montenegro (*n*=9), and Bosnia and Herzegovina (n=9)) between 2011 and 2022 from 44 healthcare facilities in 34 cities (Table S1). These isolates were categorised as CRAB strains after performing the standard antimicrobial susceptibility tests according to the methods of the European Committee on Antimicrobial Susceptibility Testing (EUCAST). Nine antimicrobial agents were tested regularly including amikacin, gentamycin, tobramycin, ciprofloxacin, levofloxacin, imipenem, meropenem, trimethoprim-sulfamethoxazole, and colistin. The minimum inhibitory concentrations (MICs) were determined by *E*-test for carbapenems and by broth microdilution in the case of colistin. The susceptibility to the remaining antibiotics was determined by the disc diffusion method. The susceptibility test results were interpreted based on the EUCAST breakpoints[108] (Table S2). CRAB isolates were defined with both imipenem (MIC > 4 mg/L) and meropenem resistance (MIC > 8 mg/L). To study the host range of the isolated bacteriophages on an extended set of CRAB isolates, 16 additional CRAB isolates were obtained from BEI Resources (https://www.niaid.nih.gov/research/bei-resources-repository), 47 isolates from the Belgian Acinetobase collection,[64] and 14 isolates from Alexandr Nemec' collection. The identity of these strains is available in Table S2. Finally, we collected 157 CRAB isolates in 2023 and 2024, across 22 cities in four Eastern and Southern European countries (Hungary, Romania, Serbia, and Kosovo) to obtain an external dataset (Table S1) for the validation of the pipeline (Table S2).

Genome sequencing

For the isolation of the genomic DNA, all *A. baumannii* isolates were routinely cultured at 37°C, in LB broth (LB, 5 g of tryptone, 2.5 g of yeast extract, 5 g of NaCl, and 500 ml of distilled water) and inoculated from single colonies from LB agar plates (LB plus 1.5% Bacto agar, w/v). Genomic DNA was extracted using the GenElute™ Bacterial Genomic DNA Kit (Sigma-Aldrich) and sequenced by Illumina sequencing. Sequencing libraries were prepared by using either the MiSeq or the NexteraXT library preparation kit from Illumina according to the manufacturer protocol.

When using the MiSeq library preparation kit, pooled sequencing libraries were denatured with 0.1 M NaOH, diluted to 12 pM with HT1 hybridization buffer (Illumina) and mixed with 40% PhiX Control v3 (Illumina) sequencing control library. Denatured sequencing pools were loaded onto MiSeq Reagent kit V2-300 (Illumina) and 2 × 70 bp sequence reads were generated with an Illumina MiSeq instrument with paired-end sequencing and index 1 sequencing primers spiked in the appropriate cartridge positions (12, 14, and 13, respectively) at a final concentration of 0.5 μM.

When using the NexteraXT library preparation kit, genomic DNA has been fragmented to approx. 300 nt fragments and Illumina sequencing adaptors have been added by using tagmentation, then sample-specific indexes were added to each sample by PCR. Pooled libraries have been sequenced by Illumina NextSeq 500 using 2x150 PE sequencing chemistry in multiple sequencing runs.

Sequencing-ready libraries were quality control checked by BioAnalyzer2100 instrument using High Sensitivity DNA Chip (Agilent Technologies USA, Cat. No. 5067-4626). Sequencing was carried out on the NextSeq 500 sequencing system with NextSeq 500/550 Mid Output Kit v2.5 (300 Cycles) chemistry (Illumina, Inc. USA, Cat. No. 20024905).

Bioinformatics analysis of *A. baumannii* genome sequences

Genomes from public databases

We downloaded all publicly available 15,410 *A. baumannii* genomes from the NCBI database as of 09/2022 (Table S1).

Assembly of genomes sequenced in this study

The raw reads were trimmed using the cutadapt 4.3 program[65] (min quality 33, max N 0.5, min read length 30). An optimal reference genome for the reference-guided *de novo* assembly was chosen from the 5,271 NCBI genomes that were available on 19/04/2021. The reference genome was selected by comparing *k*-mer counts using the kmc 3.2.1 software.[66,67] We determined the number of shared *k*-mers between the raw reads and the 5,271 available genomes and selected the one with the highest shared *k*-mer value as a reference genome for the reference-guided *de novo* assembly.

The assemblies were performed with the SPAdes genome assembler 3.15.5[68] selecting only those contigs with lengths of at least 1,000 and coverage of at least 10x. Assembly fasta files that were at least an order of magnitude larger or smaller than the median file size were dropped from further analysis.

In silico molecular typing

Whole-genome assemblies were subsequently used for molecular typing. Multi Locus Sequence Typing (MLST) was performed according to the Pasteur scheme,[42] using the mlst v2.23.0 software[69] which incorporates components of the PubMLST database.[109] In addition, Kaptive v2.0.3 software[70] was used for identifying polysaccharide capsule and outer lipopolysaccharide loci and for classifying assemblies into CPS and O-types, using the K and OC locus primary reference databases within the software, respectively.

Detection of antibiotic resistance determinants

We detected antibiotic resistance determinants in all *A. baumannii* whole-genome sequences as follows. First, we predicted open reading frames (ORFs) using the Prodigal v2.6.3 software[71] and then identified resistance genes based on sequence similarity to literature-curated resistance genes compiled in the ResFinder database v2.0.0.[87] Specifically, we performed protein sequence similarity searches with DIAMOND v2.0.15[72] using a 10^{-5} *E*-value threshold, 80% identity and coverage thresholds, and keeping the best hit for each ORF. Beta-lactamase genes were assigned to gene families using two relevant publications.[110,111] Resistance determinants that were outside the scope of ResFinder were examined separately. These included the presence of the insertion sequence ISAba1, which can be required by some genes to confer resistance against carbapenems,[112–115] The absence of the *carO* gene which encodes a porin channel,[112,116] and three point mutations indicative of fluoroquinolone resistance, *gyrA*S81L, *gyrB*A414T, and *parC*S84L. For ISAba1,[117,118] we compiled a list of ISAba1 sequences using the European Nucleotide Archive[119] and ISMapper.[120] Then, we manually filtered this list selecting only the relevant sequences based on their descriptions. Most genomes contained both the insertion sequence and one or more genes or gene fragments, but LC136852 and LC136853 seemed to only contain ISAba1. LC136852 was used to trim the rest of the sequences and acquire variations for the sequence of ISAba1. Finally, a list of 53 non-redundant ISAba1 sequences was used to search ISAba1 in whole genomes using NCBI BLAST v.2.13.0[73] with a 10^{-5} *E*-value threshold. For the rest of the resistance determinants, we assembled a list of sequences including *carO*, *gyrA*, *gyrB*, and *parC* and searched for these using NCBI BLAST v.2.13.0 with a 10^{-5} *E*-value threshold. For point mutations, we then used a custom script written in R[121] and R packages Biostrings v2.70.1,[100] dplyr v1.1.4,[101] and seqinr v1.0-2,[102] for identifying genomes which carry the required amino acid substitutions.

Identifying CRAB isolates

For the purposes of this study, an *A. baumannii* isolate is considered CRAB if its genome contains resistance determinants against carbapenems as well as against aminoglycosides and fluoroquinolones. Our goal with this strict definition was to identify high-risk isolates that may be resistant towards a wider range of antibiotics in addition to carbapenems.

Aminoglycoside resistance was determined directly from ResFinder results. If at least one aminoglycoside resistance gene was found, the isolate was considered resistant. While ResFinder contains beta-lactam resistance genes, it does not distinguish between carbapenems and non-carbapenem beta-lactams, therefore a custom approach was applied to predict carbapenem resistance. Specifically, we downloaded all available *A. baumannii* antibiotic resistance test results from the Bacterial and Viral Bioinformatics Resource Center[122] (accessed 2023-02-16) and checked whether any of the beta-lactam resistance genes, ISAba1, or *carO* could be associated with observed carbapenem resistance. We found 1,283 observations where test results were available for either imipenem, meropenem, ertapenem, or doripenem, and the results could be linked to genomic sequences in our data set. We then tested for a statistical association between the experimentally determined phenotypes and the resistance determinants using contingency tables and standard statistics (Table S1). An earlier study suggested that beta-lactam resistance genes $bla_{OXA\text{-}23\text{-}like}$, $bla_{OXA\text{-}24/40\text{-}like}$, $bla_{OXA\text{-}58\text{-}like}$, $bla_{OXA\text{-}143\text{-}like}$, $bla_{OXA\text{-}235\text{-}like}$, any bla_{NDM}, bla_{VIM}, bla_{IMP}, bla_{KPC}, bla_{GES} were all associated with carbapenem resistance.[112] Our analysis generally agreed with these findings, therefore the presence of these resistance genes formed the basis of

our classification. Furthermore, our analysis additionally suggested that *bla*$_{OXA-312}$ may also be associated with carbapenem resistance (16 true positives and 0 false positives, Fisher test p=0.0005016, Table S1), therefore *bla*$_{OXA-312}$ was also added to the list of resistance determinants. However, the presence of ISAba1 alone did not exhibit a high positive predictive value (0.554, Table S1) and the association between carbapenem resistance and the absence of *carO* was not significant ($p_{adjusted}$=0.164, Table S1). Therefore, these two genetic determinants were not added to the list. Finally, we considered an isolate fluoroquinolone-resistant if it carried at least one of the three point mutations defined above.

Analysis of population structure and phylogeography

Quality filtering of genomes

For all subsequent analysis, we only kept genome assemblies where a) assembly coverage was at least 25 times, b) MLST could be predicted; c) CPS type could be predicted with at least "Good" confidence (i.e. "The locus was found in a single piece or with $\geq$ 95% coverage, with $\leq$ 3 truncated/missing genes and $\leq$ 1 extra gene compared to the reference"); we eliminated genomes where d) GC content was extremely high or extremely low; e) number of contigs was extremely high; f) length of the longest contig, g) N50 (length of the shortest contig which, together with all longer contigs, represent 50% of the nucleotides), or h) N95 (same for 95% of the nucleotides) was extremely low, i) number of ambiguous nucleotides was extremely high, j) BUSCO v5.4.4[74] complete score was lower than 95, k) taxonomic classification using sequence data with Kraken 2 v2.1.2[75] suggested a species other than *A. baumannii* or l) the Kraken2 taxon frequency for the species was extremely low (based on Inter-Quartile Ranges, extreme outliers).[123] We retained only genomes with metadata indicating m) the country of origin for the isolate and n) at least the collection year of the isolate. Biosample metadata from NCBI was extensively curated to o) eliminate samples that were not human-associated, or p) to eliminate known duplicates. Following filtering, only genome assemblies of 11,129 *A. baumannii* isolates were analysed further from the 15,829 that were included in the study.

Mitigating sampling bias by downsampling CRAB isolates

The set of 11,129 isolates with genome sequences is likely to be inherently biased due to overrepresentation or underrepresentation of certain regions and time periods compared to others. Such biases could reflect regional and temporal differences in reporting, rather than genuine epidemiological differences, and could therefore distort analyses of population structure (*e.g.* assessment of MLST-CPS type diversity or regional dynamics of MLST-CPS type frequencies). To address this, the 11,129 isolates were stratified by geographical region and time, a subsampling strategy suited for large-scale phylogeographic analyses.[40] Specifically, we applied the following subsampling procedure: First, we only retained isolates that were classified as CRAB (8,915 isolates, 6,461 since 2016). Then, for isolates with known city information, a maximum of one sample per city per week was kept and isolates with only country information were limited to a maximum of two samples per country per week. This stratification resulted in 4,559 isolates (3,184 ST2 isolates), out of which 4,134 were collected after 2009, and 2,536 were collected since 2016. Out of these 2,536 isolates, 654 were European, 1,882 were non-European. This set, referred to as the *stratified* isolate set was used for selecting geographical regions and countries with sufficient sample sizes (Figures S1B, S1D, and S1E), analysing the temporal dynamics of the relative prevalence of MLST-CPS types (Figures 3B and S2A), analysing ST2 global and regional transmission dynamics (Figures 3D, 3E, and S2C), and analysing phylogenetic autocorrelation of geographic locations of CRAB isolates (Figure S2D). Furthermore, to mitigate potential biases introduced by uneven sampling intensity across countries, the data was further downsampled after stratification. Each country was limited to a maximum of one sample per million inhabitants. This further downsampling resulted in 2,577 isolates, out of which 2,304 were collected between 2009 and 2020, 969 between 2009 and 2015, and 1,455 since 2016. Out of these 969 and 1,455 isolates, 873 and 1,334 were collected from the 9 selected world regions, respectively, and out of the 1,455 isolates, 146 were collected from the 7 selected European countries. This downsampling achieved a strong positive correlation between population size and the number of isolates per country (Pearson correlation coefficient = 0.78 after logarithmic transformation). We employed the final dataset to investigate CRAB type diversity and how it has changed over time (Figures 2C–2E, 3A, S1C, and S1F).

Defining prevalent and global MLST-CPS types

An MLST-CPS type was defined as prevalent if it accounted for more than 5% of the isolates in at least one of the 9 selected world regions. The world regions were defined according to the World Bank Development Indicators database (legacy), accessed through the R package countrycode v1.3.0.[104] Furthermore, an MLST-CPS type was classified as global if (i) it was prevalent according to the above definition and (ii) it accounted for more than 2% of the isolates in at least 3 world regions spanning at least 2 continents. Prevalent or global MLST-CPS types were identified using the 2,577 downsampled CRAB isolates (downsampled by population size as well) and were identified separately for isolates collected between 2016-2022 (current period, using 1,334 isolates from the selected 9 world regions) and for isolates collected between 2009-2015 (preceding period, using 873 isolates from the selected 9 world regions) to address temporal dynamics.

Temporal dynamics of the relative prevalence of individual MLST-CPS types

We investigated the temporal dynamics of each MLST-CPS type that had been classified as prevalent (see above) for each continent. For this analysis, we used the dataset with 4,134 stratified CRAB isolates since 2009, but without performing population size-based downsampling as the analysis was carried out for each continent separately. For each MLST-CPS type, we (i) identified the year when the first isolate was documented since 2009, (ii) filtered the dataset to include observations since that date, (iii) classified each isolate as belonging to the particular MLST-CPS type or not, and (iv) applied logistic regression analysis to study trends in relative prevalence over time. We studied temporal trends both globally and at the level of individual continents. To account for potential biases

caused by geographical differences within the studied regions, we included the continent as a covariate when inferring temporal trends on a global scale. In a similar vein, we included world regions as a covariate when inferring temporal trends for continents. Note that we only focused on MLST-CPS types with at least 50 isolates available in a given region, e.g. a particular MLST-CPS type on a particular continent was only considered if at least 50 isolates of that MLST-CPS type were collected from that continent since 2009. We applied FDR correction through R[121] to account for multiple comparisons (Table S1). Finally, we plotted the 9 statistically significant MLST-CPS trends (out of which 7 were statistically significant expansions) calculated based on individual continents (Figure S2A).

Selecting regions with sufficient sample sizes

For analyses that require sufficient representation of local MLST-CPS diversity, we carried out rarefaction analyses. Specifically, we manually included world regions or countries based on rarefaction analysis indicating that sufficient numbers of isolates are available to represent the local diversity of MLST-CPS types. For the rarefaction analysis, we used the stratified set of 2,536 CRAB isolates (not downsampled based on population size) since 2016 and counted the number of isolates belonging to each MLST-CPS type in each world region (Figure S1B) or country (Figures S1D and S1E) and calculated the rarefaction curves from these count matrices using the R package vegan v2.6-4.[89] After plotting the rarefaction curves, we manually selected 9 out of 16 regions to study the global distribution of CRAB strains (Figures 2C, 2D, and S1C). Similarly, we selected 7 European and 7 non-European countries for comparisons between countries (Figures 2E, 3B, and S1F). The European countries included France, Germany, Greece, Hungary, Italy, Romania, and Serbia, while the non-European countries included Brazil, China, India, Saudi Arabia, South Africa, Thailand, and the USA. For the geographically distant group, only those comparisons were considered when the two countries were situated on different continents.

Building time-calibrated phylogenetic trees

All quality filtered ST2 and ST636 *A. baumannii* genomes were used to build 2 separate time-calibrated phylogenetic trees for 2 sequence types: ST2 and ST636. The ST2 covers the most prevalent MLST worldwide and the ST636 is the second most prevalent MLST in the 5 focal Eastern and Southern European countries of this study (Figure 3C). For each sequence type, a reference genome was selected first. For ST2, the reference genome was selected manually (GCF_003288775.1, a Complete Genome from the NCBI RefSeq database, sequenced using PacBio, 120 times coverage, assembled into two contigs, one of which is labelled as a chromosome), for the rest of the sequence types we selected the genome with the longest contig. In the case of ties, we selected the earliest genome. Then, each genome belonging to a particular sequence type was mapped to its reference genome using snippy v4.6.0[95] to produce pseudo-whole genomes. For isolates that were sequenced in the present study, we mapped the reads, while for the rest of the isolates we mapped the assembled genomes. We kept the longest contigs, removed any duplicates (either genuinely duplicate sequences or sequences that only became duplicates after pseudo-whole genome reconstruction) and constructed the phylogenetic tree using gubbins v3.3.0,[90] (model fitter: raxmlng, tree builder: fasttree, maximum number of iterations: 10) to account for recombinations. Abnormally long branches were subsequently removed with TreeShrink v1.3.9.[91] The resulting tree was dated in two steps: the tree was first rooted using root-to-tip regression with the lowest sum of the squared residuals and then the rooted tree was dated with treedater[92] without rerooting, using a strict molecular clock. After dating, tips that had been removed due to sequence duplication were added back to each tree with 0 branch lengths.

ST2 global and regional transmission dynamics

To study the phylogeographic patterns of the ST2 sequence type (Figures 3D, 3E, and S2C), we built on a previously published method[44] and analysed genetic similarity between pairs of isolates across different temporal and spatial scales. The general idea behind the analysis is that pairs of isolates may be geographically close or distant and also genetically close or distant, and the distribution of isolate pairs across geographic-genetic distance categories characterizes the transmission dynamics of the bacterium. For example, pairs that are both genetically and geographically close indicate local spread, while pairs that are genetically close but geographically distant indicate cross-border transmissions. Therefore, the distribution of pairs across these categories yields insights into the relative importance of local versus cross-border transmissions.

For the analysis, we used the time-calibrated ST2 tree reconstructed above. We included CRAB isolates and focused on the geographically and temporally stratified subsampled dataset to address sampling bias (3,184 tips). In the case of global transmission dynamics (Figure 3D; Table S1), we considered pairs of isolates on the tree that were collected at most 2 years apart and categorised these pairs by geographic location (same country, different country, etc.) and genetic distance (based on the most recent common ancestor, MRCA). Then we counted the number of pairs in each combination of spatial and temporal categories and calculated relative risks separately for each temporal category. Specifically, we calculated the relative likelihood of occurrence in a given spatial category as compared with the likelihood of occurrence in the control spatial category. For example, we found that when focusing on pairs with MRCA below 6 years, the relative risk is approximately 10 for pairs that originate from the same country as compared to those that originate from different countries on the same continent (reference category).

To account for uncertainties associated with this analysis (*e.g.* sampling of isolates and tree building), we took multiple subsamples from the set of 3,184 isolates constituting the ST2 phylogenetic tree above (100 subsamples with 500 isolates each). For each subsample, we reconstructed a separate phylogenetic tree and analysed it as described above. To reconstruct such a subsampled tree, we selected the respective recombination-free polymorphic sites from the Gubbins output, filtered the subsampled sites using SNP-sites v2.5.1,[93] built a phylogenetic tree using FastTree v2.1.11 SSE3,[94] and performed rooting and dating the same way as for the ST2 and ST636 trees. Then, we calculated relative risks for each tree and finally, using the 100 subsamples we calculated the mean values

and 90% confidence intervals for these risks. Using 90% instead of 95% reflects that the relationships we seek to infer require one-sided tests.

We followed a similar procedure for the phylogeographic analysis of CRAB in Europe (Figure S2C; Table S1), and for regional transmission dynamics (Figure 4E; Table S1). For the regional analysis, we looked at pairs that were collected at most half a year apart and drew 500 subsamples with 100 isolates each.

Phylogenetic autocorrelation of geographic locations of CRAB isolates

To investigate the spatial dispersal of CRAB isolates based on continuous geographic coordinates, instead of discrete countries, we analysed the phylogenetic autocorrelation of the locations of ST2 isolates based on the time-calibrated phylogenetic tree. To account for uneven sampling, we used the subset of isolates retained after spatial-temporal stratification of the dataset (see STAR Methods section "mitigating sampling bias by downsampling CRAB isolates"). Additionally, we excluded isolates lacking precise geolocation data (city, latitude, and longitude) required for the autocorrelation test. These filtering steps resulted in a subset of 1,409 ST2 isolates for analysis. Then, we extracted the resulting subset of tips from the ST2 phylogenetic tree using the keep.tip function from the ape R package v5.7-1.[105] To calculate the phylogenetic autocorrelation function of geographical locations, we utilised the geographic_acf function within the castor R package v1.8.0,[96] sampling 1,000,000 randomly chosen pairs of tips. The resulting plot displays these tip pairs as points coloured by their density using the geom_pointdensity function from the ggpointdensity R package v0.1.0.[97]

Inferring transmission events using ancestral geographic reconstruction

To study the spatiotemporal dynamics of CRAB at high resolution, we reconstructed transmission events in five neighbouring countries with dense geographic sampling (Hungary, Romania, Serbia, Bosnia and Herzegovina, and Montenegro, collectively referred to as focal countries). For this, we used the time-calibrated phylogenetic tree of ST2 isolates. Note that we included all available ST2 isolates from this region (N=365), without further downsampling, due to the largely uniform sampling across the region within a defined timeframe (2016-2022).

We estimated the timing of introductions into the focal countries and inferred the transmission events between 36 cities within the focal region by estimating the likely geographical states of ancestral nodes on the time-calibrated phylogeny. Our analysis employed discrete geographical states (i.e., cities). This approach is particularly well-suited for situations with a limited number of distinct locations, where the primary interest lies in understanding the spread between these specific geographic locations.[45] Ancestral geographic reconstruction was performed with PastML[124] using the joint reconstruction method[125] with the JC model. This method returns the most likely set of unique ancestral states, facilitating downstream analyses. Each isolate within the ST2 phylogenetic tree was assigned a geographical state corresponding to either one of 36 distinct cities located within the focal countries or a broader category designated as "non-focal". We defined transmission lineages as monophyletic clades belonging to a single focal city where the MRCA's immediate predecessor was inferred to be in another location. This other location could have been another city in the same country (domestically acquired transmission lineage), a city in a different focal country (transmission between focal countries), or a location in a non-focal country. In the latter case the introduction established a "major" transmission lineage in the focal region. Note that a major transmission lineage imported from a non-focal location into a focal city gives rise to a transmission lineage in that focal city and can also subsequently spread to other focal cities, giving rise to new transmission lineages in the same (domestic) or in another focal country. Each transmission lineage included at least two tips and therefore singletons were excluded. We calculated the duration of each transmission lineage as the inferred time span between the MRCA's estimated date and the date of the most recent isolate collected.

Characterization of *A. baumannii* bacteriophages

Phage isolation

Phages were isolated using the enrichment procedure described previously[126] with some modifications. The host strains were *A. baumannii* wild-type isolates belonging to different MLST-CPS types (Table S2).

In brief, the sewage water was cleared by centrifugation (4500 rpm for 10 min), followed by filtration through a 0.45-μm- membrane filter and aliquots of wastewater were mixed with an equal volume of 2× LB medium and 0.1% of overnight bacterial culture. Samples were incubated overnight at 37°C with shaking at 140 rpm followed by centrifugation for 10 min at 4,500 rpm, and then the supernatant was filtered through a 0.45 μm membrane filter twice to remove the residual bacteria and debris. Plaque assay was performed to screen for the presence of lytic phage activity using the double-layer agar method.[127] The plates were incubated overnight at 37°C and examined for zones of lysis or plaque formation. Single plaques formed on the lawns of *A. baumannii* strains were picked up and this process was repeated three times, in order to obtain pure phage stock.

The phage lysate was concentrated by the addition of 10% polyethylene glycol (PEG) M.W. 8000 and 1M NaCl and incubated overnight at 4 °C. After centrifugation at 4,600 rpm for 20 min, the pellet was suspended in 1 ml SM buffer (50 mM Tris-HCl [pH 7.7], 100 mM NaCl, 80 mM MgSO4). The phage titer was determined by the double-layer agar method and the titer was reported as a plaque-forming unit (PFU/ml).

For the *in vivo* experiments, phage stocks were prepared using the Phage-on-Tap protocol[128] with some modifications. The corresponding *A. baumannii* culture was grown in 100 ml LB at 37°C to an OD_{600} of 0.6-0.7 and infected with the phage. The phage lysate was concentrated (10X) using centrifugal filters (Amicon Ultra-15, Sigma 100 MDa cut off) and the concentrate was washed with 1X PBS at least 5 times. The phage concentrates were mixed with 0.7 volume of 1-octanol for additional endotoxin removal,[129] shaken

Please cite this article in press as: Koncz et al., Genomic surveillance as a scalable framework for precision phage therapy against antibiotic-resistant pathogens, Cell (2024), https://doi.org/10.1016/j.cell.2024.09.009

for one hour at room temperature following incubation at 4°C for 2 hours. The phage-containing phase (bottom phase) was collected with a syringe after centrifugation at 4,000 × g and 4°C for 10 min. The removal of octanol was enhanced by repeating the centrifugation step two additional times. This was followed by a few extra washing steps with PBS using Amicon filter (100 MWCO) devices. To ensure that the endotoxin concentration is low, an additional step was included using Pierce high-capacity endotoxin removal spin 1 ml column (Thermo Scientific) following the manufacturer's instructions.

Phage morphology

In order to obtain transmission electron microscopy images, 6 μl of the phage lysate was mounted on a TEM copper grid (300-mesh, Electron Microscopy Sciences) with carbon-coated ultrathin formvar film.[130] The samples were dried using filter paper after 1 minute. To obtain the negatively stained samples, the samples were contrasted with 6 μl uranyl acetate (2% w/v) in 50% ethanol for 2 min (this process was repeated 3 times). After the removal of the excessive staining solution, samples were dried under a Petri dish for 2 h before the electron microscopic evaluation. Negatively stained samples were systematically screened, and the grids were examined under a transmission electron microscope (JEM-1400 Flash transmission electron microscope) at 80kV with a 16 MP Matataki Flash scientific complementary metal–oxide–semiconductor (sCMOS) camera (JEOL) (Figure 5F).

Phage host specificity

The lytic activity of each phage was screened against multiple *A. baumannii* clinical isolates (Figure 4A; Table S2) with the standard plaque assay as previously described.[131] Briefly, serial dilution of phage lysate was plated on soft agar overlays of different bacterial isolates. After incubating the plates overnight at 37°C, the individual plaques were counted and the average of 3 biological replicates was calculated. For calculating the efficiency of plating (EOP), we compared the number of plaques on the original host of phage isolation and the isolate of interest as follows: average PFU on target bacteria / average PFU on original host bacteria (Table S2; Data S1).

Screening for lysogen activity in bacteriophages

As the absence of lysogenic activity is a requirement for phages to be used in traditional phage therapy,[132] we tested some of the isolated phages: Silvergun, Highwayman, and PhT2-v2 with therapeutic potential for lysogenic activity by adapting the protocol described before.[51] Briefly, after performing a spot assay with the phage in question (PFU scaling from 10^5 to 10^8) bacterial cells were isolated from mesas, zones of confluent bacterial or phage-resistant cell growth in the centre of the lysis spots. After applying the phage in two different concentrations, twenty colonies were isolated and tested in patch plate screens to see if the phages were capable to lysogenize the cells. This step was repeated twice to eliminate the chance of carry-over of phage particles between the steps. To ensure the absence of the lysogen activity of the phages tested, we performed the spontaneous phage release test and the immunity assay as well. Plates were incubated overnight, and phage infection was identified by lysis zones (Figure S6).

Phage adsorption assay

The adsorption assay of the phages was done as previously described[59,133] with slight modifications, 10 ml bacterial culture of wild-type isolates or induced phage-resistant isolates was pre-grown until exponential phase (OD_{600}=0.6-0.7) and mixed with the phage at Multiplicity Of Infection (MOI) 0,1. The cells were incubated at 37°C with aeration and at each time point 100 μL samples were taken every 5 or 10 min for 30 min. Samples were mixed with 850 μl of LB supplemented with 50 μl of chloroform, vortexed, and then centrifuged for 1 min at 13,000 rpm in a benchtop centrifuge. The supernatant was diluted in LB to determine the unadsorbed phages by the plaque assay using the double-layer method (Figure 6F; Table S2).

Constructing precision phage cocktails

Phage cocktails were designed based on growth inhibition efficiency. Specifically, growth suppression was measured in 96-well microtiter plates with a final volume of 200 μl in Mueller-Hinton broth 2 (MHB2) medium. The optical density at 600 nm (OD_{600}) of the wells was recorded every 20 minutes for a duration of 24 hours using an EPOCH 2 instrument from Biotech. The instrument was set to operate at 37°C with 10 seconds of shaking before each measurement. In each well, except for the control wells, 20 μl of bacterial culture with an initial OD_{600} of 0.6-0.8 was added along with 20 μl of phage(s) at a final concentration of 106 PFU per well. The phages were used either individually or in combination (Figures 6A–6C, S7B, and S10). A phage cocktail was considered efficient for a certain isolate, when the average area under curve (AUC) value (calculated from the bacterial growth curve (OD_{600})) plus its standard deviation was not higher than 13.2 arbitrary units, that is, 2 times the AUC of the media containing control well. Initially 1-3 phages infecting the wild-type isolates of the same MLST-CPS were combined until the growth of the maximum number of isolates could be suppressed. If phage resistance was observed (i.e. delayed growth), additional 1-3 phages targeting capsule-deficient CRAB variants were added to the cocktail to mitigate the growth of resistant variants. Phages targeting capsule-deficient CRAB variants were identified by standard spot assay using isolates derived from the end point of the 24h measurements. Data is provided in Table S2.

Sequencing and bioinformatics analysis of phage genomes

Whole-genome sequencing and assembly

Phage genomic DNA was extracted using a commercial phage DNA isolation kit (Norgen Biotek Corp.; 46850) following the manufacturer's instructions with the sole exception of applying sterile, distilled H_2O during the elution step instead of the provided elution buffer. Afterwards, samples were sequenced by Illumina sequencing. We used 1 ng of DNA as the input amount recommended in the Nextera XT Sample Preparation Guide. We followed the rest of the protocol as written. Sequencing-ready libraries were quality control checked by BioAnalyzer2100 instrument using High Sensitivity DNA Chip (Agilent Technologies USA, Cat. No. 5067-4626). NGS

was carried out on the NextSeq 500 sequencing system with NextSeq 500/550 Mid Output Kit v2.5 (300 Cycles) chemistry (Illumina, Inc. USA, Cat. No. 20024905). The applied read length was in the 150-300 bp range.

Processing of the sequencing data was started with quality control and trimming of reads using Trimmomatic v0.36.[76]

Assembly of the filtered reads into contigs was carried out by either MEGAHIT[77] or MetaSPAdes v.3.13.0[78] on a per-sample basis. Contigs of less than 10kb in length were then investigated to identify phages in the samples by BLAST+ v2.12.0 blastn alignment to NCBI RefSeq database.[73]

Gene content analysis

Bioinformatic prediction of ORFs and annotation of the phage contigs was done by a simple customary Python script. In brief, the code translated the whole input nucleotide sequence into an amino acid sequence in all six reading frames. Then, regions with a length longer than 50 from start to stop codon, were collected in a list along with the positional and start-end values and the assigned identifier of the candidate gene. The collected amino acid sequences were matched to the NCBI nr database then the name and taxonomic information of the best hits were added to the identifier of the candidate subject (if any). The above data was then collectively processed to generate GenBank files for the individual phage contigs. Further, genes of interest i.e. genes related to therapeutically important functions were listed in separate files. Genes of interest were extracted from the prediction data with regular expressions together with the positional information (see Data S1).

The therapeutic suitability and the possible life cycle of isolated phages were predicted with PhageAI software using default settings[50] and the Phageleads web service.[47] Endonucleases were identified by blastp alignment. The presence of antibiotic or virulence-conferring genes was checked by utilising the RESFINDER v2.0.0 and VIRULENCEFINDER v1.5 database respectively,[87,88] corroborated with PhageLeads results. Insertion sequences were screened using ISfinder.[79] Depolymerase prediction was done by Depolymerase Predictor. A tail fibre or spike protein was deemed as a carrier of a depolymerase region if the value of probability was 0,85<.[80] The completeness of assembled phage genomes was elucidated via CheckV software[81] (Table S2).

Phage pangenomic network construction

To visualise the location of our phages in the broad landscape of viruses, we used the classical approach of constructing an orthogroup-based network of viruses, where proteins of all participant phages are clustered, and the phages' level of connection is determined by the number of proteins they have in common viral clusters (VCs). The tool we found to best suit this task was vConTACT2,[82] which implements the above methods and outputs results largely adhering to the classifications of the ICTV database. To acquire the data for the network, we retrieved all phage genomes assigned to the Caudovirecetes order from the International Committee on Taxonomy of Viruses (ICTV) database[49] (version August 22, 2022).

We also conducted literature mining to identify Acinetobacter phages that have been used as therapeutic agents (Table S2). In addition, we included Acinetobacter phages from our collection.

We obtained taxonomy information for the accession IDs originating from the ICTV database, while for our own phages, we conducted a blast search to identify their tail fibres and spikes. Taxonomy information was obtained based on the closest relative's taxonomic position.

Prodigal[71] was used to predict ORFs for all phages, and these ORFs were used as input for vConTACT2's gene2genome module to generate a network file in Cytoscape format.[83] A custom R script was then used to merge additional metadata information for the nodes visible in the network.

The final network file was then created with vConTACT2's default settings, no reference database, the 'BLASTP' method, and c1 clustering. To ensure reproducibility and scalability, the entire process was implemented in a Nextflow pipeline.[98] The network subplots in Figure 5 were created in Cytoscape.

Phage pangenomic visualisation

Phage genome sequences were colinearised according to a reference point (an official lytic or therapeutic phage in each case) and then the GenBank files were supplied to Clinker.[84] The pangenomic comparisons of phages were done with a custom R script that compared each of our phage genome's genes against the corresponding one from the reference genes using blastn. Then from all compared tail coding sequences, we predicted depolymerase regions using the Phyre2 web platform,[85] where we selected the best hit among those that had above 0.4 confidence and contained the word 'hydrolase' and 'lyase', corresponding mostly to the methods described earlier.[134] For depolymerase comparisons (Figure S5; Table S2), we only used the depolymerase regions.

Average Nucleotide Identity (ANI) of phages

We compared the genomes of our phages with those considered therapeutically important or known to have a lytic life cycle (Figure 5E; Table S2). The alignments resulting from this comparison were handled as follows: for a specific section of the genome, if multiple alignments were possible, we chose the one with a higher identity. In cases where an alignment with lower identity covered a longer section, it was used for the entire section. In situations where one genome was longer than the other, we adjusted the ANI value by subtracting the length difference. For instance, if one genome was 90% the length of the other, even if the genomes exhibited 100% identity, the maximum ANI value achievable was 90%.

Correlating genetic distance, prophage-, plasmid- and defence island-content with phage susceptibility

Plasmids and prophages were identified using geNomad.[135] In the case of prophages, prophage genomes were filtered for above 90% completeness using CheckV software.[81] Both plasmids and prophages were clustered with MMseqs2[136] using the command "mmseqs easy-cluster <input>.fasta clusterRes tmp –min-seq-id 0.9 -c 0.9 –cov-mode 1". Then a distance matrix was constructed based on the matrices representing the presence or absence of each cluster in our bacterial strains, using the Jaccard distance

method of the vegdist function from R's vegan package.[89] Defense islands were identified with the DefenseFinder software,[137] using default settings. In this case, islands were not clustered, but the presence or absence of each island in each bacteria was used to construct the distance matrix. Then, we used Mantel correlation tests to probe whether sharing of the aforementioned genetic elements provide additional information beyond phylogenetic distance in explaining phage susceptibility profile dissimilarity. Specifically, we used the partial Mantel test function of the vegan package to calculate the partial correlations between phage susceptibility profile dissimilarity and Jaccard distance of the presence / absence of the aforementioned genetic elements while controlling for phylogenetic distance. This was performed for each MLST-CPS type: ST2-KL12, (N=153 pairs), ST2-KL3, N=1431 pairs), ST2 KL9, (N= 91 pairs), ST636 KL40, (N=231). The correlations were calculated using the Spearman method. The p values and rho coefficients of these analyses are provided in Table S2, along with the input distances in Table S2 and the raw data of plasmid prophage or defense islands in our strains in Table S2.

Isolating phage-resistant *A. baumannii* mutants

In vitro

Phage-resistance was induced in a 96-well microtiter plate in 200 μl final volume in LB medium. The OD_{600} values of the wells were measured every 20 min for 24 hrs in an EPOCH 2 (Biontech) instrument, at 37°C with 10 second shaking before each measurement. Each well, except the control wells, contained 100 μl from the bacterial culture with OD_{600}=0.7 and the phage(s) in 10^6 PFU/well concentration. Resistance was evolved to a single phage or a combination of 2, 3, or 4 different phages. If phage combinations were used, each phage was added in 10^6 PFU/well concentration (in a 1:1 ratio). Following a 24-hour incubation period, the wells that exhibited cell growth as indicated by OD_{600} values, samples were streaked onto plates containing chromogenic agar and incubated overnight at 37°C for each strain. The resulting individual colonies were restreaked at least 3 times to avoid phage contamination. The phage-resistant phenotypes were confirmed using phage susceptibility tests including the double-layer agar plate method or *in vitro* growth curves.

Mutations in the genomes of phage-resistant lines were analysed using the following procedure: First, we carried out reference mapping of the reads of the mutant strains to the genome sequence of their respective wild-type isolates (snippy v4.6.0), followed by the identification of point mutations, insertions and deletions (custom script based on bedtools 2.30.0).[106] wild-type genomes were annotated using diamond blastp and NCBI nr database to identify the mutated ORFs in the genomes. Additionally, genes of the K antigen biosynthetic pathway as well as β-4-glucosyltransferase (WP_001033817.1) were detected using blastn 2.13.0+,[138] in both the wild-type and the mutant lines. Finally, we identified point mutations in these detected genes, by aligning the blast hits to the respective reference genes with mafft v7.520,[86] and a custom Python script for calling the nucleotide and the amino acid variants (Figure 6D; Table S2).

In vivo

From *G. mellonella* larvae, the CRAB colonies were isolated 48 hours post-infection, either at the endpoint of the survival experiment or earlier if larvae died before this time point. On the larva's ventral side, an incision was made with a sterile blade, and then streaked from the body lumen onto Acinetobacter-specific chrome agar (CHROMagarTM Acinetobacter, CheBio). The resulting colonies were re-streaked at least 3 times to obtain a pure bacterial culture. The resistance phenotype was confirmed by phage typing against the phage(s) used in the treatment of the larvae and, in addition, we checked the susceptibility of the isolate against the other cocktail components, PhT2-v2 and Fanak as well (Table S2). If we detected an altered phage infection pattern compared to the wild-type, we sent the isolate for sequencing.

From mice, CRAB colonies were isolated from one deceased animal. Specifically, following dissection, the heart, lung, and spleen of the mice were individually removed and homogenised in 3mL of PBS using 50mL centrifuge tubes. The homogenised samples were then serially diluted tenfold, and colony-forming units (CFUs) from each organ were quantified on selective agar plates containing ceftazidime (2 μg/mL) and eosin methylene blue. Then, twenty random colonies were selected and subjected to identification using matrix-assisted laser desorption ionisation time-of-flight mass spectrometry (MALDI-TOF MS) with a Microflex instrument manufactured by Bruker Daltonics in the USA.[139] To achieve this, bacterial colonies were applied onto the sample plate of the instrument and treated with formic acid before analysis. Data is available in Table S2. Subsequently, colonies were tested for phage sensitivity using the double layered agar method as described in the "phage host specificity" section.

Antimicrobial susceptibility testing of phage-resistant isolates

Minimum inhibitory concentrations (MICs) of five clinically relevant antibiotics: Colistin (Pharma), Meropenem (Bioscience), Imipenem (MedChemExpress), Levofloxacin (MedChemExpress), Trimetoprim: Sulphametoxazole (1:5 ratio) (Sigma, MedChemExpress) were determined using the standard microbroth dilution protocol[140] and interpreted using the European Committee on Antimicrobial Susceptibility Testing (EUCAST) guidelines.[108] Cells were grown in Mueller Hinton Broth 2 (MHB2) (Millipore) and the inoculum size was set to 5 x 10^5 bacteria per ml. Among the tested antibiotics were two carbapenems (Meropenem and Imipenem) and the last-resort antibiotic Colistin. In order to maximise reproducibility and accuracy, we used a robotic liquid-handling system (Hamilton) to automatically prepare 7-step, two-fold serial dilutions in 384-well microtiter plates. After 18 h of incubation at 37°C, raw OD_{600} nm values were measured in a Biotek Synergy microplate reader. MIC was defined by a cutoff OD_{600} nm value (mean +2 s.d. of A600 nm values of bacteria-free wells containing only growth medium). MIC fold change was calculated as $MIC_{wild\text{-}type}$ strain / $MIC_{phage\text{-}resistant}$ strain (Figure S8H; Table S2).

Capsule visualisation of *A. baumannii* ST2-KL3 isolates

To visualise the capsule of different *A. baumannii* clinical isolates and induced phage-resistant isolates, we performed Transmission Electron Microscopy (TEM) imaging by following a previously described protocol.[130] Briefly, 0.5 ml of overnight culture from each bacterial isolate (n=4) was centrifuged for 2 min at 13000 rpm in a benchtop centrifuge and then fixed overnight at 4°C with Karnovsky fixative solution (pH 7.4). After fixation, samples were briefly rinsed in distilled water (pH 7.4) for 15 min and fixed furthermore in 1% osmium tetroxide in ddH2O (Sigma-Aldrich, St. Louis, MO, USA) for 1 h. After fixation, samples were briefly rinsed in distilled water for 10 min, then dehydrated gradually in ethanol. Afterwards, bacteria were polymerized through propylene oxide (Molar Chemicals) and then embedded in an epoxy-based resin (Durcupan ACM; Sigma-Aldrich) for 48 h at 56°C. From the resin blocks 50 nm thick ultrathin sections were cut using an Ultracut UCT ultramicrotome (Leica; Wetzlar, Germany) and were mounted on a single-hole, formvar-coated copper grid (Electron Microscopy Sciences; Hatfield, PA, USA). The contrast of the samples was enhanced by staining with 2% uranyl acetate in 50% ethanol (Molar Chemicals, Electron Microscopy Sciences) and 2% lead citrate in distilled water (Electron Microscopy Sciences) (Figure 6H).

Analysis of cell surface properties of *A. baumanii* isolates using Fourier-transform infrared spectroscopy (FTIR)

In order to compare the cell surface properties of wild-type and phage resistant isolates, we adapted the protocol described before[141] with minor modifications. Briefly, according to the manufacturer's instructions, bacterial biomass was collected from LB agar plates. The isolates were incubated for 24 h at 37°C. After incubation, bacterial suspensions were prepared by adding a full inoculation loop (1 μl) of bacteria in 1.5 ml Eppendorf tubes containing 50 μl of 70% ethanol and 2 mm metal beads provided by the supplier. The bacterial suspension was thoroughly vortexed after which 50μl of sterile H_2O was added. Then, 15μl of bacterial suspension was pipetted on a silicon plate (provided by Burker IR Biotyper equipment) in three biological replicates per isolate (Table S2). We prepared two standard suspensions (provided by the supplier) and 10μl was added as controls in two biological replicates. The plate was then dried for 20 minutes in the laminar hood at room temperature. Results were evaluated using Opus Software V8.2.28 and IR Biotyper Software V4.0.8 (2022-11-21T1119Z) with the default settings (32 scans per biological replicate; spectral resolution, 6 cm^{-1}; apodization function, Blackman-Harris 3-term; zero-filling factor 4). Following the manufacturer's instructions, the pre-processing steps of the acquired data were as follows: the FTIR spectra measurements of individual biological replicates that did not meet the default quality criteria ($0.4 < absorption < 2$, signal-to-noise-ratio < 40, biological replicate of an isolate was not clustering with the other replicates of that isolate) were manually removed from further analysis to prevent inclusion of wrongful data. The distance matrix provided by the IR Biotyper software was used for further analyses (i.e. cell surface property distance).

To investigate the associations between phage susceptibility profiles, cell surface properties, and phylogenetic distance, we also calculated the phage susceptibility profile distances and phylogenetic distances among the studied isolates. We performed a map-based visualisation of distances between isolates using principal coordinate analysis (PCoA, see Figure S12) with the ape 5.0 R package.[105] The nine isolates were clustered into four groups based on their phage susceptibility profiles using Partitioning Around Medoids (PAM) clustering calculated with the cluster R package v2.1.6.[103] To calculate the correlations between phage susceptibility distance vs cell surface property and phylogenetic distance, we performed Mantel tests using the vegan R package[89] on 9 samples and 10,000 permutations with the Pearson correlation method.

Efficacy of phage treatment in *in vivo* models

Galleria mellonella model

We used *Galleria mellonella* larvae as one animal model to evaluate the effectiveness of Highwayman and Silvergun phages alone and in combination with other phages against *A. baumannii* clinical isolates. For each experimental condition, 10 larvae were used and experiments were repeated independently at least 3 times. Survival of the larvae was monitored for 48 hr, every 6 hr.

As a first step, we determined the proper inoculum size to be used in further experiments. 6 different *A. baumannii* isolates and 5 different inoculum sizes for each isolate (CFU = $9x10^6$, $9x10^7$, $9x10^8$, $9x10^9$, $9x10^{10}$ per ml) were tested. Based on these preliminary results, the inoculum size of $9x10^8$ CFU/ml was chosen as the mortality rate of the larvae was 50% at 18 hr post-infection for half of the tested isolates at this inoculum size.

Prior to the infection of the larvae, the bacterial strain was grown overnight in MHB2 medium at 37°C with aeration. To remove the growth media, the bacterial culture was washed twice with 1X Phosphate-Buffered Saline (PBS) and the density was set to $9x10^8$ CFU/ml. From this, 10 μl was injected into the first proleg of the larva. Phage treatment was administered in the same volume in PBS, in the opposite proleg, 5 minutes after the bacterial infection. This time point was chosen based on the results of preliminary experiments where we compared the survival rate of the larvae that received the same phage treatment 5 minutes and 60 minutes post-infection and found that the survival rate of the larvae receiving the treatment 5 minutes post-infection was significantly higher. When the HS cocktail was administered, Highwayman and Silvergun phages were mixed in MOI 10:10 ratio, while when the cocktail HSFPh was administered, Highwayman, Silvergun, Fanak and PhT2-v2 phages were mixed in MOI 10 : 1 : 0.1 : 0.1 ratio (see Figure 7E).

To assess the *in vivo* fitness of the phage-resistant *A. baumannii* isolates in comparison to their wild-type counterparts, in the case of each isolate an inoculum size of $9x10^8$ CFU/ml was injected into the left proleg of the larvae (Figures S8A–S8G; Table S2).

Please cite this article in press as: Koncz et al., Genomic surveillance as a scalable framework for precision phage therapy against antibiotic-resistant pathogens, Cell (2024), https://doi.org/10.1016/j.cell.2024.09.009

Intraperitoneal mouse model

We created a mouse intraperitoneal model to study the infectivity of Aci 15 *A. baumannii* isolate. Female BALB/c mice, 6-7 weeks old and weighing 17-18 g, were obtained from Envigo in the Netherlands. All animal care and handling procedures adhered to the European Federation for Laboratory Animal Science Association (FELASA) guidelines, and the EnivoInvest Co., Hungary's Animal Welfare committee approved the protocols (permit number: BA02/2000-12/2022).

As a first step, for the Aci 15 isolate, we determined the proper inoculum size to be used in further experiments. For this, 5 different inoculum sizes (CFU = 10^5, 10^6, 10^7, 10^8 and 10^9) were tested. Prior to the experiment, one colony of the Aci 15 isolate from a one-day-old LB agar plate was transferred into a 5 mL LB liquid medium and was cultivated for 14 hours in a shaker thermostat (120 rpm, 37°C). The next day, the liquid culture was centrifuged (2 minutes, 10.000 g) and washed once with PBS. The gained bacterium suspension was serially diluted (10x) to obtain different inoculum sizes. From the dilutions, 200 μl was administered intraperitoneally to each mouse. Mice were separated into groups (each containing 5-5 animals) based on the infection doses. Weight and death rates of the infected and control animals were recorded in the subsequent 8 days (Figure S9). Based on these results, the inoculum size of 10^9 was chosen for phage rescue experiments

Neutropenic mouse model

A neutropenic mouse model was performed as described earlier[107] in order to test the possibility to increase the sensitivity of the experimental animals against the Aci 15 *A. baumannii* isolate. For this reason, the immune system of the mice was suppressed with cyclophosphamide (200 mg/kg) and cortisone acetate (250 mg/kg) by administering them subcutaneously. Blood samples were taken on days 0, 4, 7, and 10 and white blood cell (WBC) counts were determined from 3 treated and 3 untreated animals. In parallel 15 neutropenic and 15 control mice were infected with different inoculum sizes ($5*10^8$, $5*10^9$ and $5*10^{10}$) of the Aci 15 strain (5 animals/inoculum size). Neutropenia was induced 2 days prior to the infection. Survival of animals was daily monitored for 8 days. In the case of the neutropenic animals, by the 4th day after the neutropenia treatment, a drastic decrease (60-80%) in the WBC counts was observed in comparison to the control animals, confirming the successful neutropenia treatment. These values showed a slight increase by the 7th day and eventually reached the normal WBC count (9.000-10.000 /μl) by the 10th day. Despite the sharp decrease of the WBC counts in the blood of the neutropenic animals, only a slight increase in their sensitivities to the infection could be observed. The survival of the neutropenic and control animals was similar (Figure S9B; Table S2) indicating that the induction of neutropenia is not necessary for further experiments.

To further test the suitability of the used intraperitoneal mouse model, we studied the infectivity of another isolate, Aci 111 belonging to the ST636-KL40 MLST-CPS type by using 5 different inoculum sizes (CFU = 10^4, 10^5, 10^6, 10^7 and 10^8). We observed an inoculum size-dependent mortality of the infected animals, proving the suitability of the model.

Therapeutic efficacies of single and combined purified bacteriophages (phage Highwayman alone and the HSFPh phage cocktail) against Aci 15 isolate were tested as described before,[142] with slight modifications. For this purpose, mice (30 animals) were divided into 6 groups (G1-G6). Members of the G1-G5 groups were infected with 10^9 CFU/mice. Mice in group G6 received only the HSFPh phage cocktail, serving as phage controls. Mice in G1 served as bacterium controls and did not receive phage treatment. Members of G2 and G3 received phage HWM at MOI 6, 10 min and 1 hr post infection, respectively. Members of G4 and G5 received the HSFPh phage cocktail 10 min and 1 hr post infection, respectively, where for HWM MOI was 6, while for the other 3 phage components, MOI was 1. Death rates and body weights of all animals were daily recorded for seven days after the treatments (Figures 7F and S9; Table S2).

QUANTIFICATION AND STATISTICAL ANALYSIS

Statistical analyses were performed using R (version 4). GraphPad Prism version 10.2.0 was used for the calculation of AUC values from OD600 growth curves.

For analysing temporal dynamics of the relative prevalence of individual MLST-CPS types (Figure S2A; Table S1), we performed logistic regression analyses and calculated the coefficients and p-values between MLST-CPS type frequency and collection date (year). *P*-values were corrected for multiple testing using FDR correction. Sample numbers, estimates, *p*-values and FDR corrected *p*-values are included in Table S1.

For comparing population composition dissimilarity between pairs of countries (Figure 2E; Table S1), we used a two-sided two-sample Wilcoxon rank-sum test. Sample sizes and *p*-value are included in the figure caption.

For ST2 global and regional transmission dynamics (Figures 3D, 3E, and S2C), the risk of a geographical category was considered significant if the 90% confidence interval of risks in that category did not overlap with the red horizontal line which indicated no effect. Sample sizes and further details of the analysis are included in the STAR Methods.

For analysing the phylogenetic autocorrelation of geographic locations (Figure S2D), we used the phylogenetic autocorrelation function (geographic_acf) of the castor R package v1.8.0,[96] sampling 1,000,000 randomly chosen pairs of tips. Further details of the analysis are included in the figure caption.

To compare the inward to outward transmission ratio between capitals and cities with regional medical centres vs other cities, we used Fisher's exact test.

For pairwise comparisons of binary phage sensitivity profiles (Figure 4B), we calculated Jaccard distances between pairs of isolates. Next, all isolates were categorised based on their MLST, CPS, and geographical regions and we calculated the average

Jaccard distances of all pairwise comparisons between two isolate categories. Jaccard distances between groups of isolate categories were compared using one-sided permutation tests (with 5,000 permutations of the isolates' MLST-CPS types). The number of category pairs and *p*-values are indicated in the figure caption.

For analysing the correlation between genetic distances and pairwise phage susceptibility profile dissimilarities (Figure 4C), we performed Mantel tests. Sample numbers and p-values are indicated in the figure caption.

Statistical associations between the experimentally determined resistance phenotypes and the presence / absence of specific genomic resistance determinants (Table S1) were calculated using contingency tables and Fisher's exact tests with FDR correction.

Most analytical pipelines were orchestrated using Nextflow v22.10.1.[98] Steps in these pipelines were containerised using Docker v24.0.7 and Singularity v3.9.0.[99]

The plotted bacterial growth curves represent the mean values with 95% confidence intervals (CI) based on different numbers of isolates that are indicated at each experiment with the letter N. The measurement with each isolate was repeated three times (biological replicates). To compare the growth of CRAB isolates in the absence and presence of different phages alone or in combinations, we calculated the area under the growth curve (AUC) as a proxy for bacterial growth for each isolate / treatment combination. Then we performed two-sided Kruskal-Wallis tests to compare treatments (Figure 6B).

Principal coordinate analysis was performed to distinguish between wild-type and phage-resistant isolates based on cell surface property similarities (Figure 6G). The nine isolates were clustered into four groups based on their phage susceptibility profiles using Partitioning Around Medoids (PAM) clustering calculated with the cluster R package v2.1.6. To calculate the correlations between phage susceptibility distance vs cell surface property and phylogenetic distance, we performed Mantel tests using the vegan R package[89] on 9 samples and 10,000 permutations with the Pearson correlation method.

Two-sided log-rank tests were used to compare the survival of larvae or mice under different treatment conditions, where Kaplan-Meier survival curves (average values) are plotted along with 95% confidence intervals (Figures 7A–7C, 7E, and S8A–S8G). Sample sizes are given in the corresponding figure captions. In the case of the mice experiments (Figures 7F and S9A–S9E), no confidence intervals are shown as for ethical reasons the experiments were performed only once.

CellPress
OPEN ACCESS

Supplemental figures

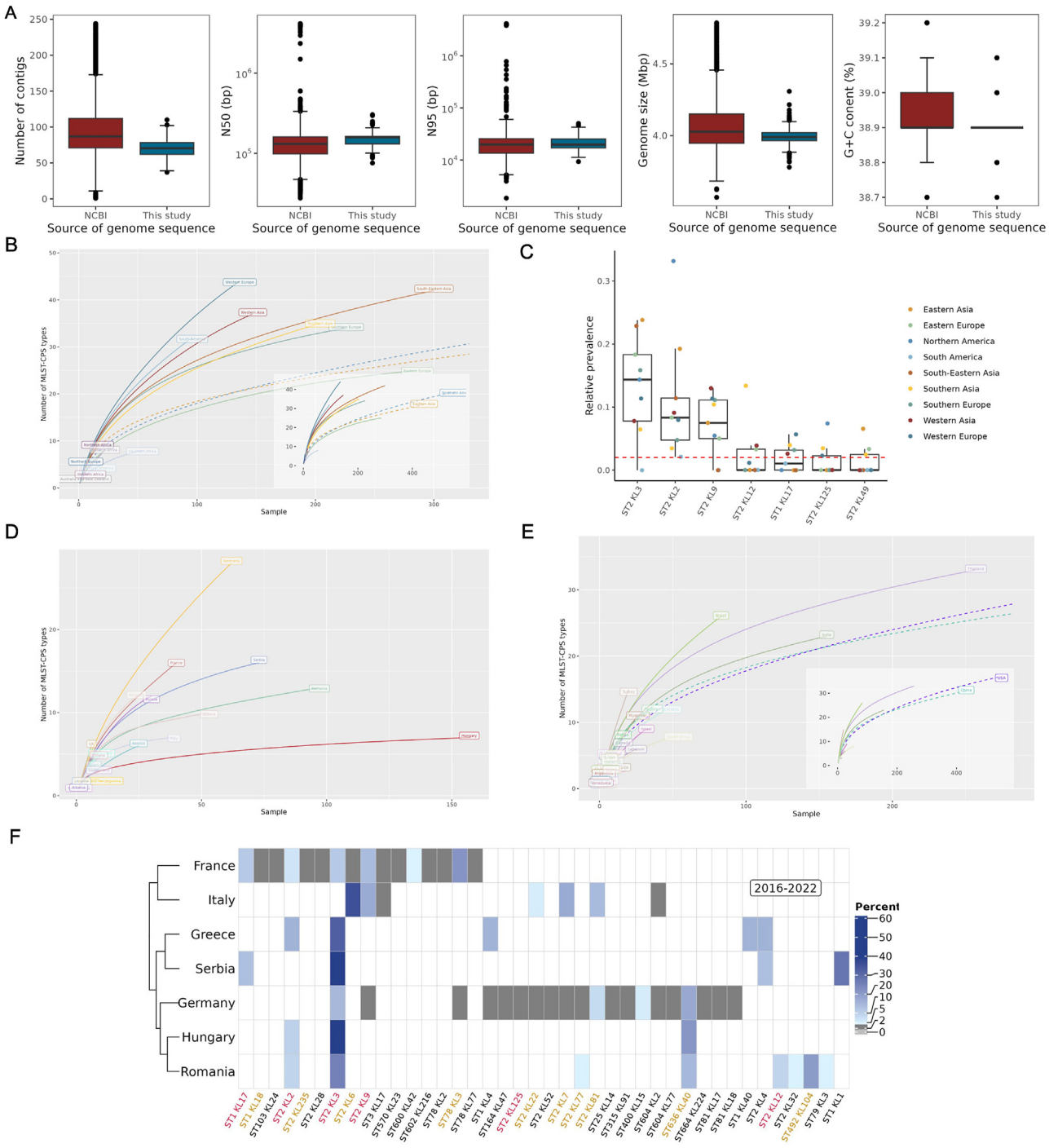

Figure S1. The geographic distribution of CRAB strains, related to Figure 2

(A) Assembly quality control metrics for genome assemblies included in this study.

(B) Rarefaction analysis of CRAB isolates for all geographical world regions between 2016 and 2022 (Figure 2C).

(legend continued on next page)

(C) Relative prevalence of the 7 global MLST-CPS types in 9 selected regions of the world (Figure 2D). Boxes depict the interquartile range (IQR), the solid black line shows the median, and whiskers extend to 1.5 IQR.
(D) Rarefaction analysis for European countries based on 654 downsampled European CRAB isolates from the period between 2016 and 2022.
(E) Rarefaction analysis for non-European CRAB isolates from the period between 2016 and 2022. Axis boundaries on the main plot were truncated to eliminate the distortion. The embedded figure shows the same plot with default axis boundaries.
(F) Relative prevalence of CRAB MLST-CPS types in 7 European countries between 2016 and 2022. The blue and gray color-coding represents the prevalence in percent of the MLST-CPS types in the countries. MLST-CPS types classified as prevalent or global are marked with orange and red labels, respectively.

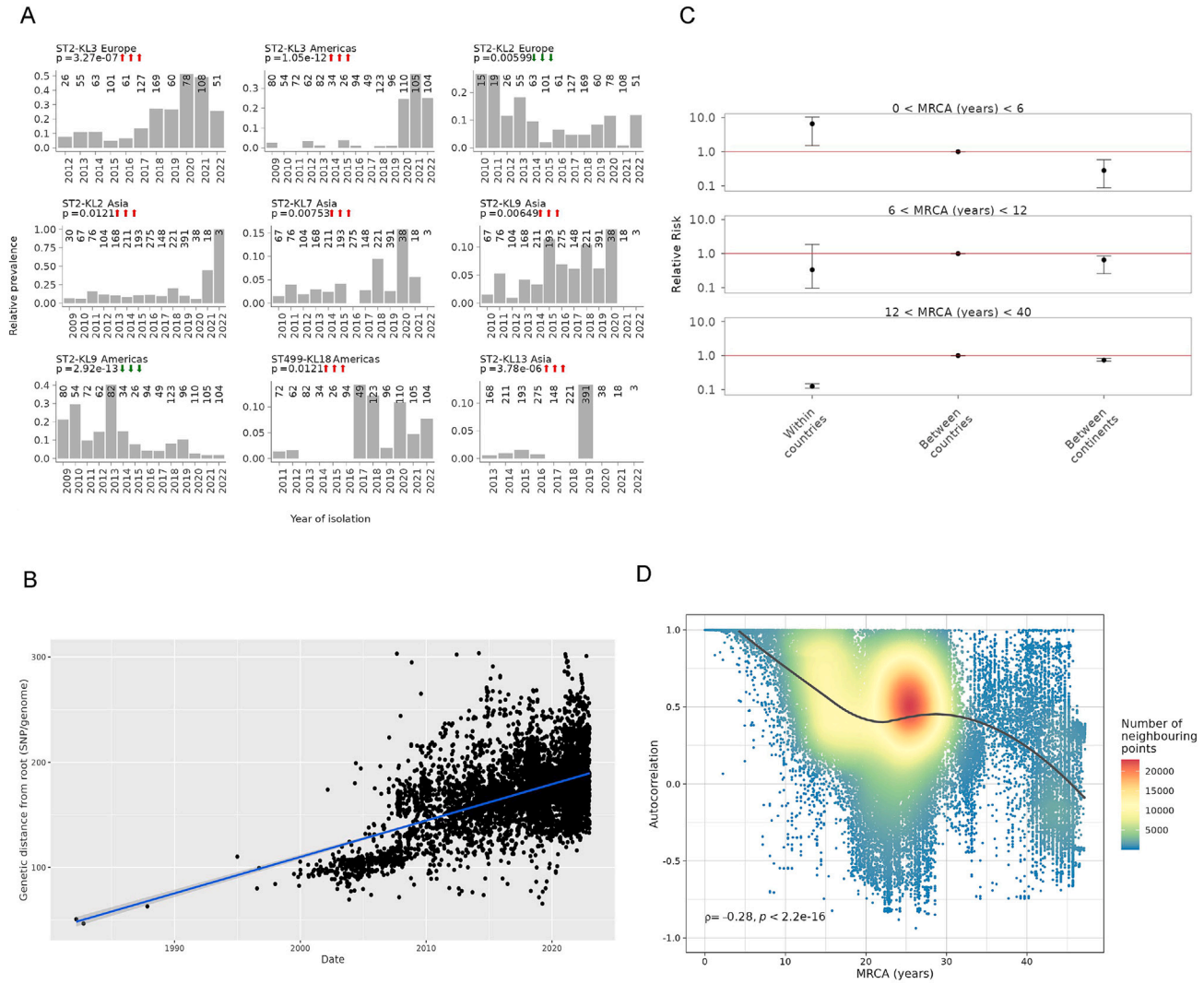

Figure S2. Temporal and spatial dynamics of CRAB, related to Figure 3

(A) Relative prevalence of CRAB MLST-CPS types over time. Relative prevalence was calculated by dividing the number of isolates from a specific MLST-CPS type by the total number of isolates in a given year. Each plot shows a single MLST-CPS type on a single continent. Columns indicate the overall number of CRAB isolates statistically significant increase or decrease over time (red and green arrows, respectively).

(B) Root-to-tip regression plot for the global dated ST2 tree. x axis shows the sampling date of isolates (years), while the y axis shows the root-to-tip genetic distance (SNPs/genome). Estimated time of most recent common ancestor (MRCA): 1,973, estimated rate of core genome substitution rate: 3.47 SNPs/genome/year. Blue line shows linear regression ($R^2 = 0.279$, $p = 0$).

(C) Phylogeographic analysis of CRAB in Europe (Figure 3D). The relative risk that pairs of isolates were collected in a certain geographic location compared with the reference (different European countries). Each facet describes pairs of samples within a certain genetic distance range MRCA (years). Error bars represent 90% CIs based on 100 downsampled time-calibrated trees (see STAR Methods).

(D) Spatial dispersal of ST2 isolates as revealed by phylogenetic autocorrelation of geographic locations. Plot shows the phylogenetic autocorrelation function of geographic locations of ST2 isolates with known source city ($n = 1,409$). Given a rooted phylogenetic tree and geographic coordinates (latitudes and longitudes) of each tip, the autocorrelation function (y axis) analyzes how similar the locations of pairs of isolates are considering their phylogenetic distance (x axis). Points represent tip pairs colored by density. The solid line shows loess regression.

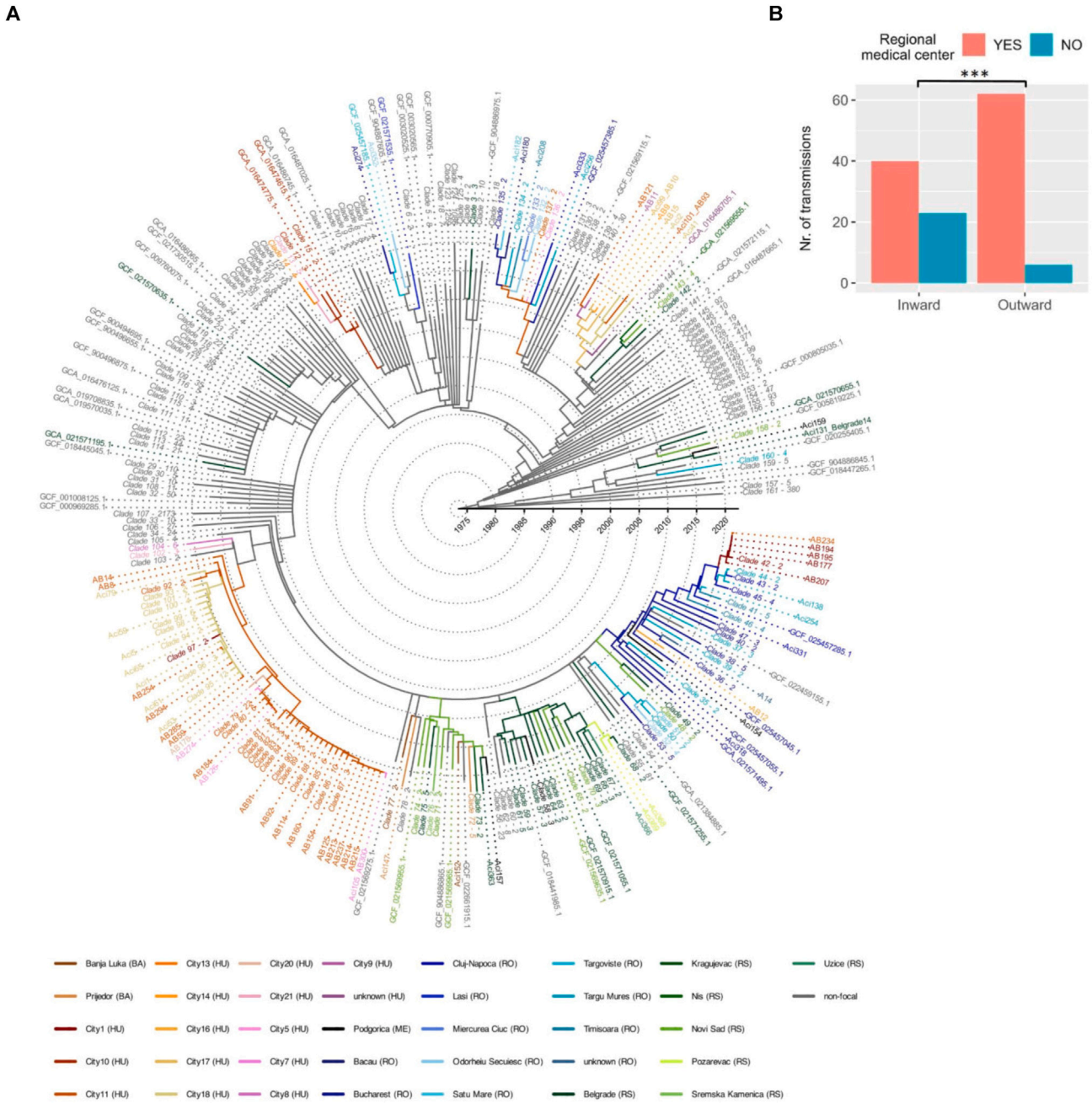

Figure S3. Reconstructed transmission events among 36 cities of five focal Eastern and Southern European countries, related to Figure 3

(A) Ancestral geographic locations were reconstructed on the time-calibrated phylogeny of ST2 isolates. Tip and edge colors denote observed and inferred geographical locations, respectively. Countries and cities are denoted by different shades: brown shades, Bosnia and Herzegovina; red, yellow, and pink shades, Hungary; black, Montenegro; blue shades, Romania; green shades, Serbia; and gray, locations outside the five focal countries. Samples belonging to a monophyletic clade from the same city or non-focal sources were collapsed into clades (arbitrary italicized numbers). The number of isolates within each merged clade is indicated after the hyphen in the clade name.

(B) Capitals and cities with regional medical centers (N = 12) display a higher ratio of outward to inward within-region transmission events than the rest of the cities (N = 20) in the region (p = 0.00007, odds ratio = 6.36, Fisher's exact test, two-sided).

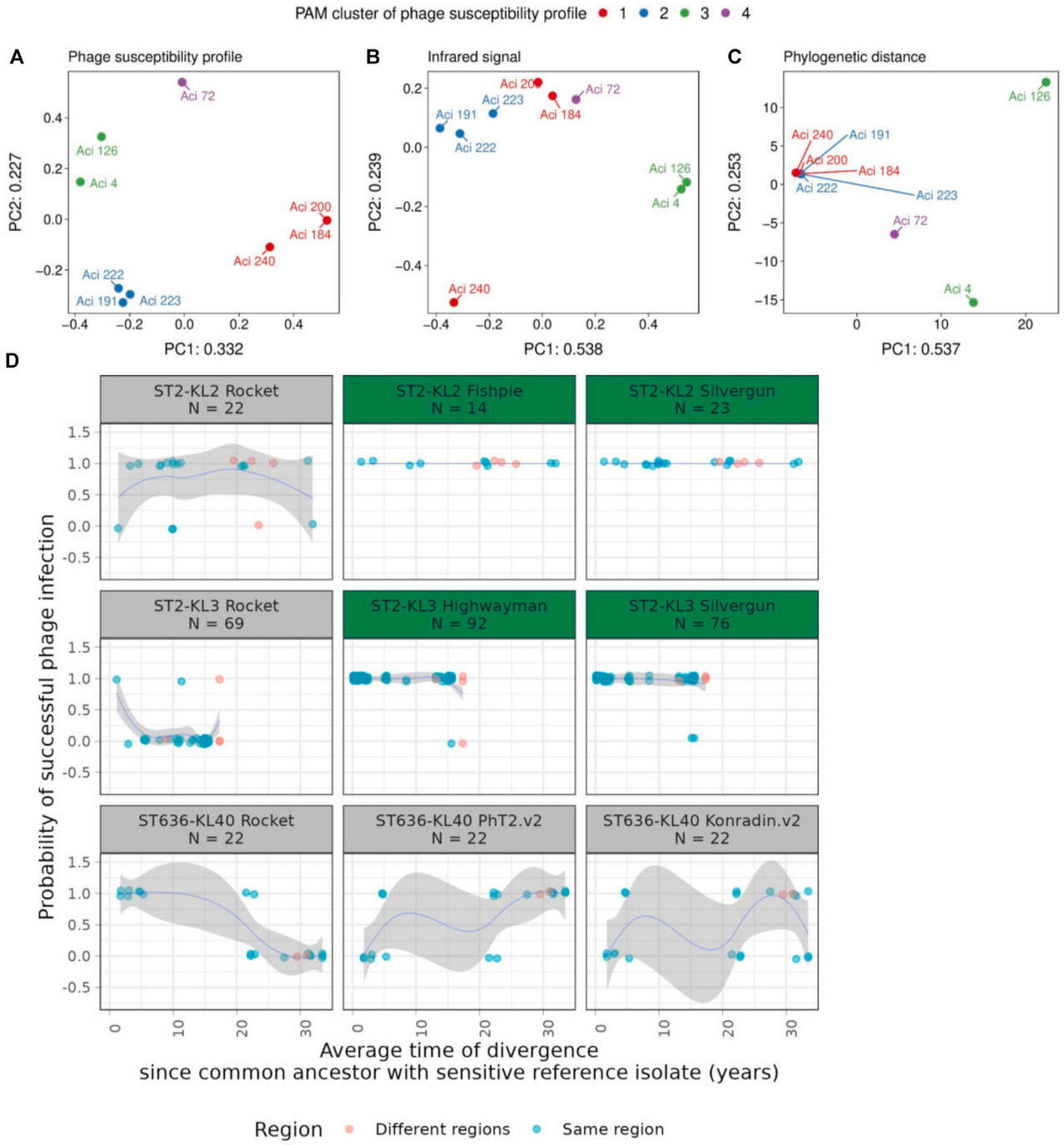

Figure S4. Phylogeny-guided phage sensitivity profiling, related to Figure 4

(A–C) Principal coordinate analysis (PCoA) of nine ST636-KL40 isolates based on their specific phenotypic and genomic properties, that is, (A) phage susceptibility profile distance, (B) cell surface property distance based on infrared measurements, and (C) phylogenetic distance. Phage susceptibility profile distance correlates with surface property distance (Mantel test, $r = 0.408$, $p = 0.012$), but not with phylogenetic distance (Mantel test, $r = 0.110$, $p = 0.272$). Isolates were clustered into four groups, indicated by color-coding, based on their phage susceptibility profiles using partitioning around medoids (PAMs) clustering. (D) Specific phages remain effective across most isolates of the same MLST-CPS type regardless of genetic divergence. Each panel shows the effectiveness of a phage against *A. baumannii* isolates that belong to an MLST-CPS type over various times of divergence. The x axis shows the divergence between an isolate and a reference isolate. Panels highlighted in green indicate promising MLST-CPS-phage combinations. The effectiveness of studied phages against ST636-KL40 isolates was sporadic, indicating that we could not find a broad-host range phage against ST636-KL40.

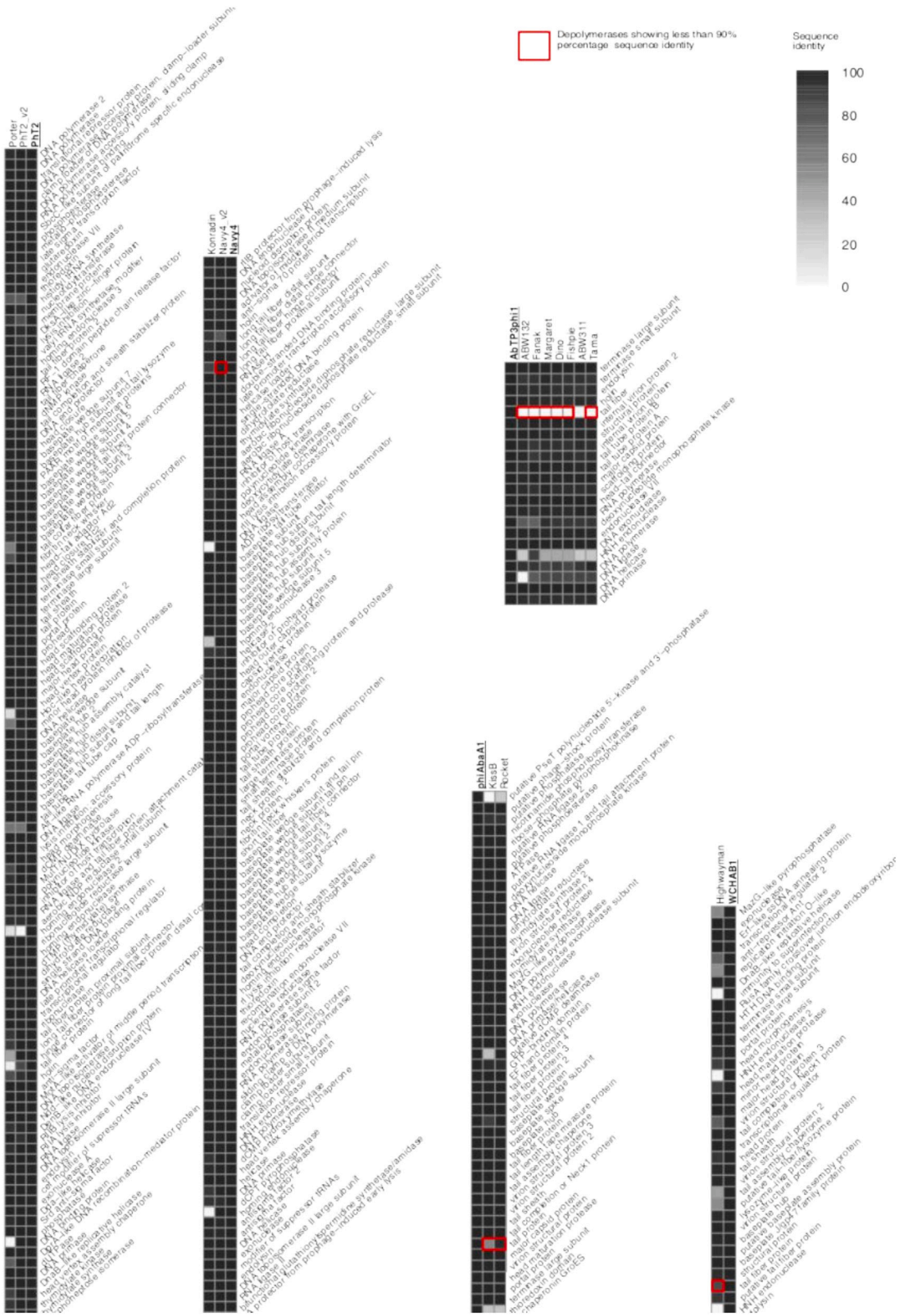

(legend on next page)

Figure S5. Pairwise protein sequence identities of shared orthogroups for 14 of the discovered phages and their closest therapeutic or lytic relatives, related to Figure 5

The therapeutic and lytic reference phages are shown alongside the discovered phages with their names underlined. Heatmap shading represents the degree of similarity between the translated ORFs from 0% to 100% percentage identity. Proteins with predicted depolymerases showing less than 90% sequence identity to the corresponding reference phage are framed in red. Note that only 14 phages were used for this analysis, as Silvergun exhibits low similarity to other known phages (see Table S2).

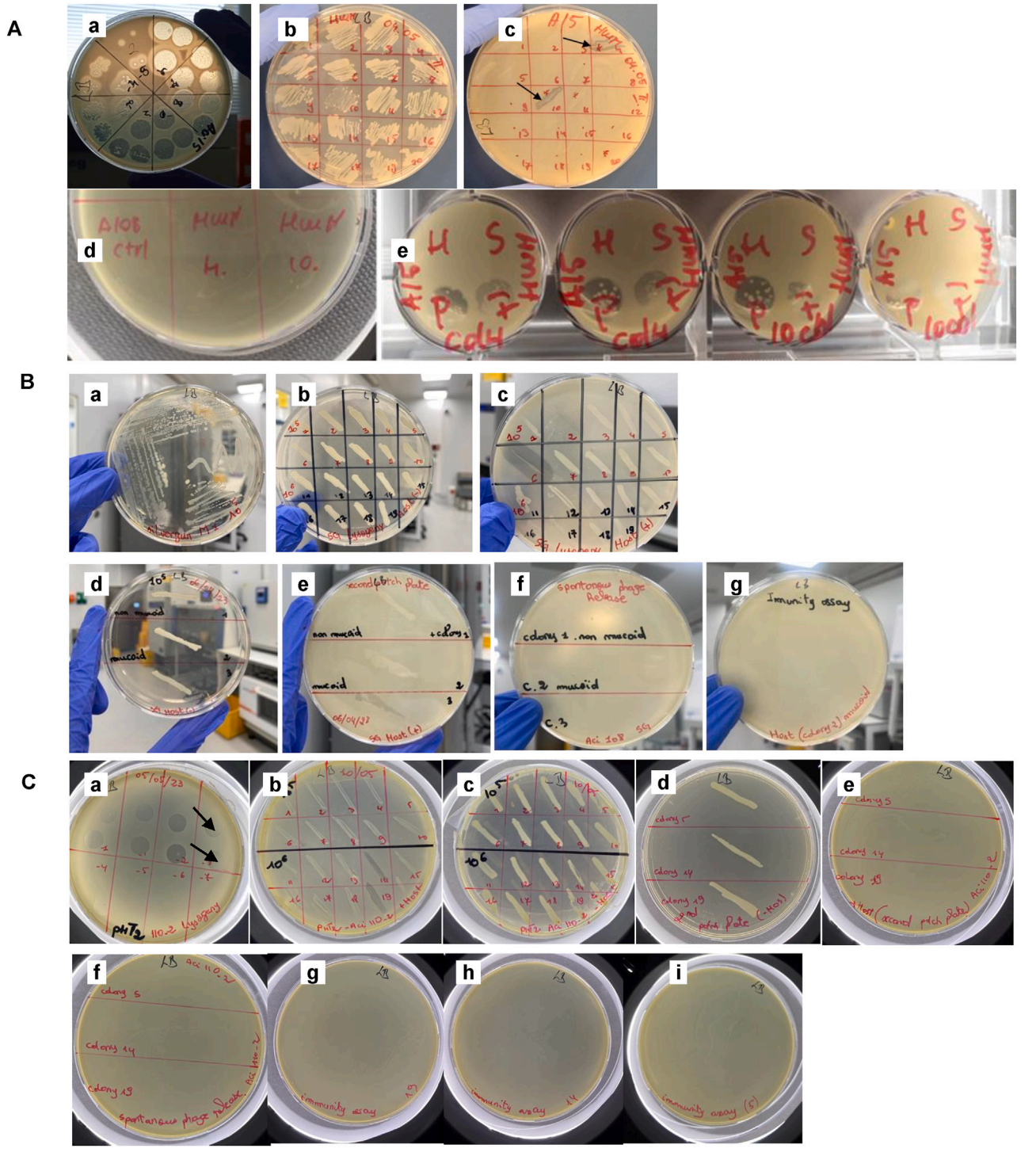

Figure S6. Absence of lysogenic behavior of Highwayman, Silvergun, and PhT2-v2, related to Figure 5

(A) Testing Highwayman for lysogenic life cycle on Aci 15 ST2-KL3 isolate. (Aa) Spot assay with Highwayman in serial dilution after 24 h incubation. Arrows denote the location of mesas. (Ab and Ac) Patch assay of identical colonies plated on an LB plate and LB plate with bacterial overlay, respectively. Arrows indicate bacterial cell lysis by the phage. (Ad) Phage release assay performed with the filtered supernatant from overnight cultures. (Ae) Phage susceptibility test, indicating altered phage infection profile.

(B) Testing Silvergun for lysogenic life cycle in Aci 108 ST2-KL3 isolate. (Ba) Single colony purification after the spot assay with Silvergun. (Bb–Be) Two rounds of patch assays of identical colonies plated on an LB plate and an LB plate with bacterial overlay, respectively. (Bf) Phage release assay performed with the filtered supernatant from overnight cultures. (Bg) Immunity assay of colonies, the test demonstrates resistance to the phage.

(legend continued on next page)

(C) Testing PhT2-v2 for lysogenic life cycle on one of the ST2-KL3 derivatives (A110-2-resistant to Highwayman and Silvergun). (Ca) Spot assay black arrows denote the location of cell isolation. (Cb and Cc) patch plates with and without lawn of the bacterial host, bacterial growth with surrounding lysis, indicating the presence of phage (cells 5, 14, 19). (Cd and Ce) Second patch plates. (Cf) Phage release assay performed with the filtered supernatant from overnight cultures. (Cg–Ci) Immunity assay, indicates the absence of lysis zones.

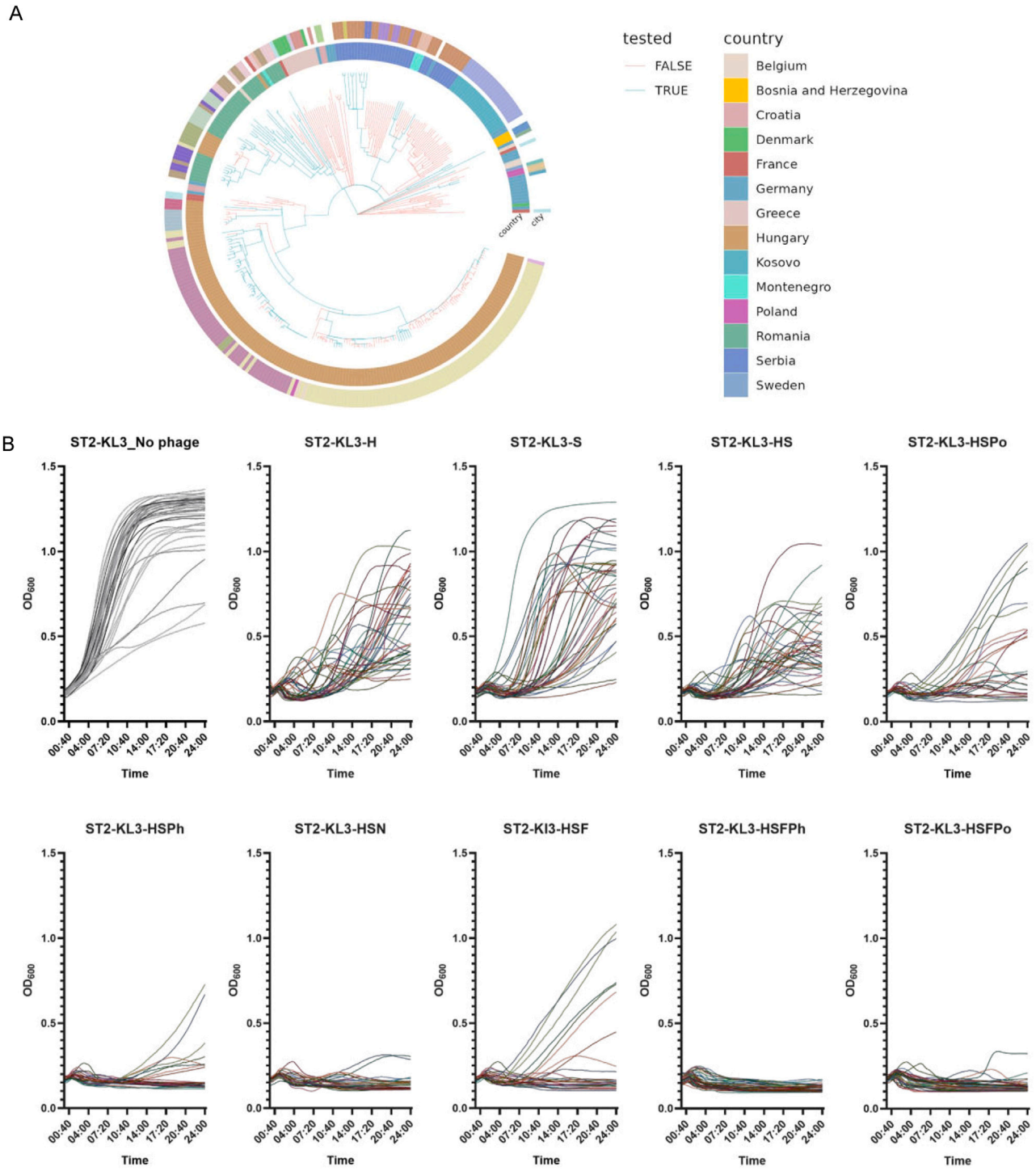

Figure S7. Precision phage cocktail against the ST2-KL3 strain type in Europe, related to Figure 6

(A) Phylogenetic tree of 316 European ST2-KL3 isolates, showing the representative set of isolates used for experimental testing as indicated by the color turquoise (TRUE). The phylogenetic tree was built using all 7,735 ST2 high-quality *A. baumannii* genome sequences included in this study (for details, see STAR Methods section "Building time-calibrated phylogenetic trees"). Subsequently, the tree was filtered to focus solely on ST2-KL3 European genomes for visualization. Country and city of origin are color-coded.

(B) Growth suppression by individual phages and by their combinations. Each growth curve represents individual ST2-KL3 CRAB isolates ($n = 41$, except the 3-phage combinations, where $n = 27$). Growth kinetics were measured for 24 h. Each figure represents a different phage treatment indicated at the top. Abbreviation of phages: H, Highwayman; S, Silvergun; F, Fanak; Po, Porter; N, Navy-v2; Ph, PhT2-v2; OD_{600}, optical density measured at 600 nm (for details, see Table S2).

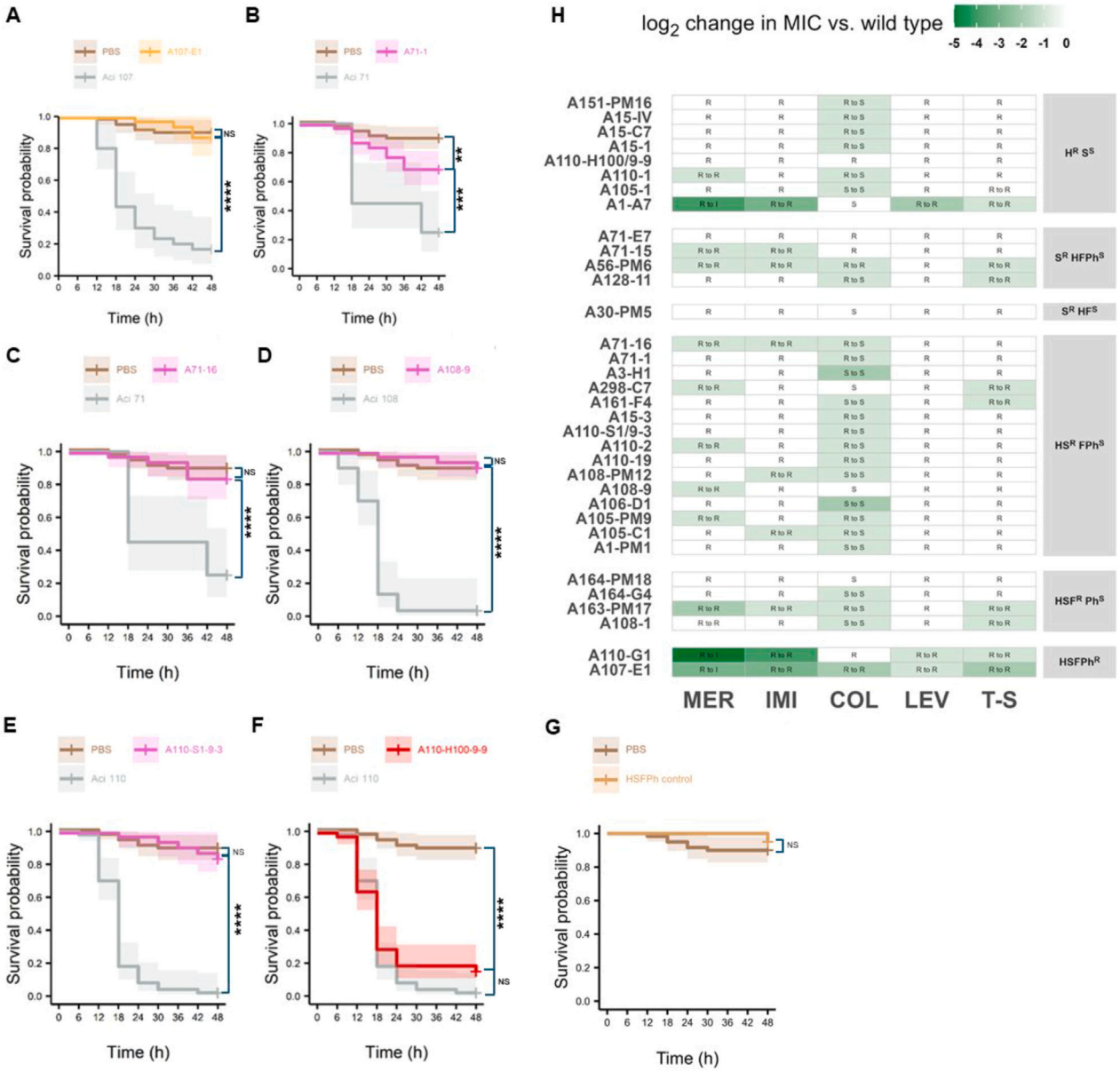

Figure S8. Cost of phage resistance, related to Figure 7

(A–F) The survival of *G. mellonella* larvae after infection with phage-resistant lines in comparison to their wild-type counterparts. HSFPh- (A, orange) and HS-resistant lines (B–E, purple) have decreased virulence compared with their wild-type counterparts (gray) (n = 10 larvae/group; ≥3 biological replicates/group; PBS, larvae injected only with PBS). H-resistant line (F, red) is still virulent.

(G) The survival of *G. mellonella* larvae when treated only with the HSFPh cocktail (n = 10 larvae/group). Stars indicate significance levels calculated from two-sided log-rank test. NS, not significant.

(H) Antibiotic sensitivity profile of phage-resistant strains (n = 34) against 5 antibiotics with clinical potential. Isolates are grouped based on their sensitivity profile to the four phages from the HSFPh cocktail. The intensity of the color green indicates the median ($n \geq 3$) of the $\log_2$ reduction in minimum inhibitory concentration (MIC) of the phage-resistant strains compared with their wild-type ancestor strain (the higher the reduction, the darker the intensity). Antibiotic susceptibility changes are also highlighted based on the MIC breakpoints from EUCAST. R, resistant; S, susceptible; I, intermediate (susceptible, increased exposure). In the case of colistin, 44% of the isolates transitioned from a low-level resistant state to a sensitive state (R to S), while 23% of the isolates became even more sensitive (S to S). MIC was measured using the microbroth dilution method. Abbreviations: MER, meropenem; IMI, imipenem; COL, colistin; LEV, levofloxacin; T-S, trimethoprim and sulfamethoxazole; H , Highwayman; S, Silvergun; F, Fanak; N, Navy-v2; Ph, PhT2-v2. For details, see Table S2 and STAR Methods.

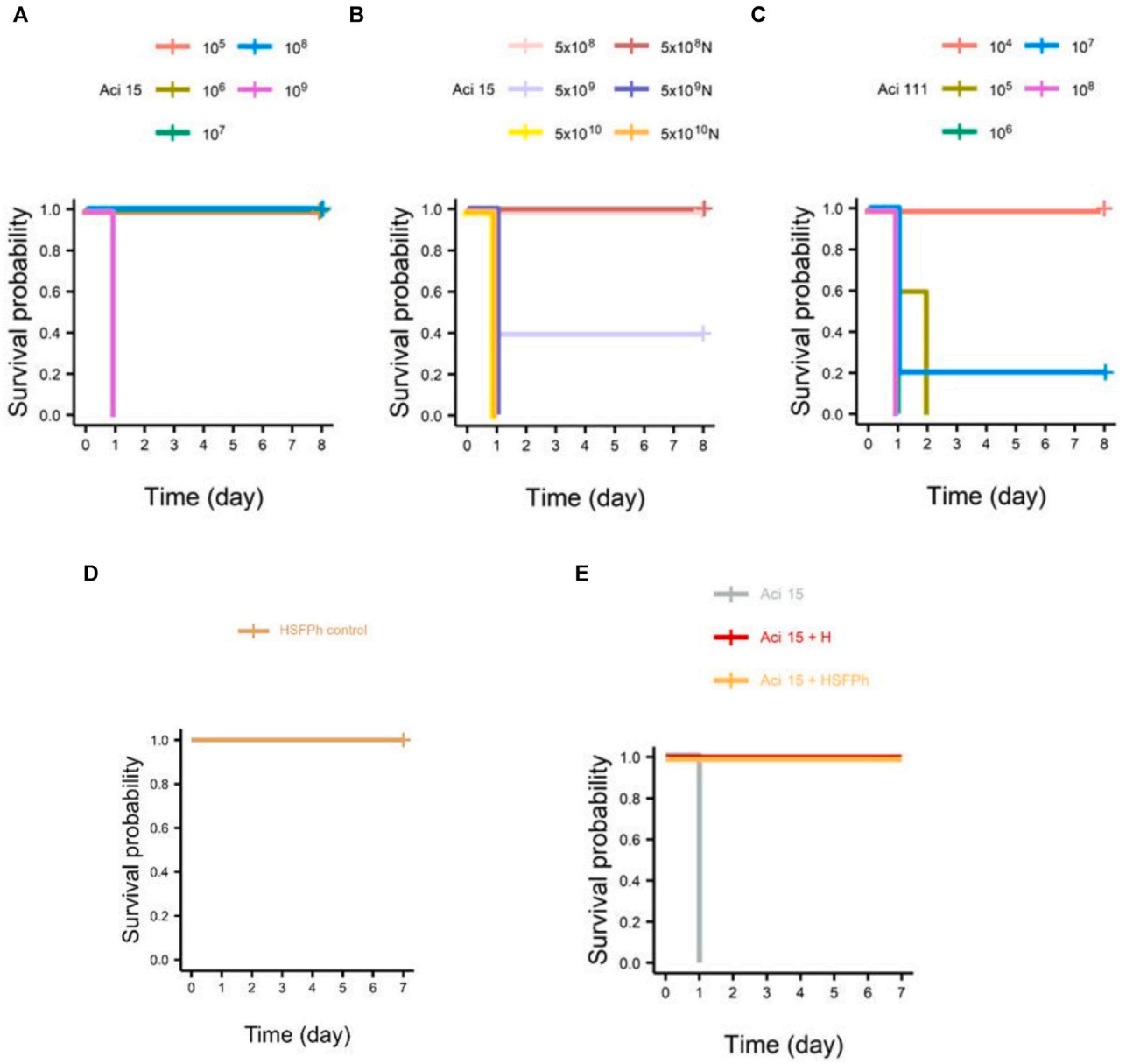

Figure S9. Mice *in vivo* infection model, related to Figure 7

(A) Assessing the impact of different colony-forming units on the survival rates of mice infected with the Aci 15 ST2-KL3 isolate.

(B) Comparing survival rates of neutropenic (N) and non-neutropenic mice after infection with different colony-forming units of the Aci 15 ST2-KL3 isolate.

(C) Assessing the impact of different colony-forming units on the survival rates of mice infected with the Aci 111 ST636-KL40 isolate.

(D) Survival of mice (n = 10 mice/group) after treatment with HSFPh cocktail without bacterial infection. The cocktail by itself does not have a negative effect on the survival of larvae or mice.

(E) Both the Highwayman phage alone and the cocktail HSFPh administered 10 min after infection with the Aci 15 ST2-KL3 isolate saved 100% of the mice compared with untreated animals, all of which died (gray) (CFU = 10^9, n = 5 mice/group) ($p < 0.0001$ from two-sided log-rank test). Data are available in Table S2.

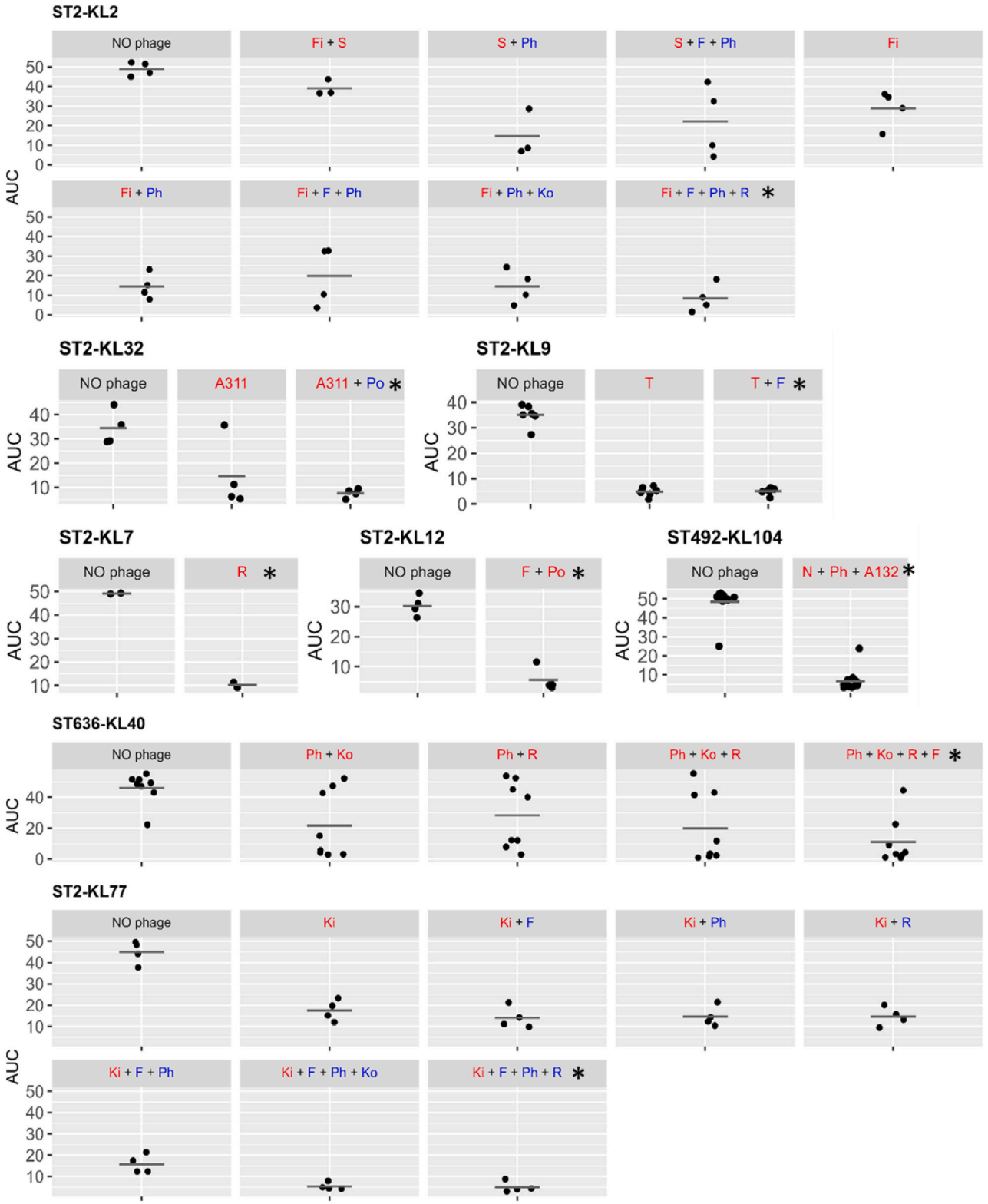

(legend on next page)

Figure S10. Selecting the most efficacious cocktails to target eight MLST-CPS types in the focal region, related to Figure 6 and "Validating the region-specific treatment strategy"

Each data point represents the average area under bacterial growth curve (OD_{600}, average area under curve [AUC]) value for individual isolates of specific MLST-CPS types collected between 2016 and 2022 (n = 3 biological replicates). For each of these MLST-CPS types, the final cocktail with the strongest growth suppression property was labeled with a black star. Dark gray line represents the average AUC value of different isolates. These cocktails were used for targeting CRAB isolates collected in the same region in 2023 and 2024. Phages infecting the wild-type isolates are labeled with red, while phages targeting capsule-deficient CRAB variants are labeled with blue. Abbreviations: A132, ABW132; A311, ABW311; F, Fanak; Fi, Fishpie; Ki, KissB; Ko, Konradin-v2; N, Navy4-v2; Ph, PhT2-v2; Po, Porter; R, Rocket; S, Silvergun; NO phage, no phage treatment. The number of isolates varies from 2 to 12 depending on the MLST-CPS type. AUC is provided in arbitrary units. For details, see Table S2 and STAR Methods.